

PDF hosted at the Radboud Repository of the Radboud University Nijmegen

The following full text is a publisher's version.

For additional information about this publication click this link.

<http://hdl.handle.net/2066/113118>

Please be advised that this information was generated on 2018-07-08 and may be subject to change.

**Magnetophotoluminescence on III-V semiconductors:
high-purity bulk materials and low-dimensional systems**

Frank Driessen

Magnetophotoluminescence on III-V semiconductors: high-purity bulk materials and low-dimensional systems

Frank Driessen

Driessen, Frank Arnoldus Johannes Maria

Magnetophotoluminescence on III-V semiconductors:
high-purity bulk materials and low-dimensional systems /
Frank Arnoldus Johannes Maria Driessen.-[S.l.:s.n.]-III.
Proefschrift Nijmegen.-Met lit. opg.
ISBN 90-9005830-3
Trefw.: halfgeleiders / fotoluminescentie

Magnetophotoluminescence on III-V semiconductors: high-purity bulk materials and low-dimensional systems

een wetenschappelijke proeve op het gebied van
de Natuurwetenschappen

Proefschrift

ter verkrijging van de graad van doctor aan
de Katholieke Universiteit Nijmegen,
volgens besluit van het College van Decanen
in het openbaar te verdedigen op
dinsdag 16 maart 1993,
des namiddags om 3.30 uur precies

door

Frank Arnoldus Johannes Maria Driessen

geboren op 13 april 1966
te Groesbeek

Promotor: Prof. Dr. L.J. Giling

The work described in this thesis is part of the research program of the
“Nederlandse Maatschappij voor Energie en Milieu B.V.” (NOVEM).

**voor Anke,
Ruben, Rincke en Moric**

Bij het tot stand komen van dit proefschrift wil ik een aantal mensen persoonlijk bedanken.

Allereerst John Giling voor zijn betrokkenheid en de mogelijkheden die ik heb gekregen om mijn onderzoek te verrichten.

Mijn dank aan Stef Olsthoorn is niet te verwoorden: Zijn onvoorwaardelijke hulp, gedrevenheid, bereidheid tot lang doorwerken, maar vooral ook de onderlinge 'big and smalltalk' hebben de afgelopen vier jaar tot een geweldige tijd gemaakt.

Verder dank ik alle andere collega's van de afdeling Experimentele Vaste Stof Fysica III. In het bijzonder Harry Lochs voor de zeer goede introductie in PL en als magneet-quencher, en ook de 'lumi'-studenten Hermen Pen, Astrid Eijkelenboom en René in 't Zandt (m.n. Hermen's prima computer programma's dreven de vaart van het onderzoek op). Paul van der Wel, Paul Hageman en Michel Anders dank ik voor hun computer-bijstand, Gerard Bauhuis voor alle transport hulp van elektrische of andere aard, Peter Schmidt en Hans te Nijenhuis voor inspirerende gesprekken en verder alle groeiers, m.n. André van Geelen en Paul Hageman voor de groei van de GaInP samples.

G.A.C. Jones, D.A. Ritchie, and J.E.F. Frost from the Clarendon Laboratory, Cambridge, are gratefully acknowledged for fabricating high-carrier-density heterojunctions.

Van de medewerkers van het Laboratorium voor Hoge Magneetvelden wil ik bedanken: Jos Perenboom voor de gastvrijheid, Peter van der Linden voor technische ondersteuning, en John Singleton en Prof. Jan Kees Maan voor inspirerende discussies. Voor dit laatste bedank ik ook Roel Kusters, Peter Christianen en Tos Berendschot van EVSF 2.

Bijzonder vruchtbaar en prettig was de samenwerking met Billiton Research en Billiton Precursors -in de personen van Dario Frigo, James Wilkie en Ton Gal- en, gekoppeld hieraan, de interactie met EPI, Cardiff. Especially, 'the huge bunch of free time' that Dario spent to improve the literary value of my work is irrepayable; not even with large amounts of 'Châteauneuf-du-Pape'.

Verder was het een plezier samen te werken met Peter Fontein, Peter Hendriks, Richard van Haren en Frans Blom van de TUE.

Dr. John Henning wil ik bedanken voor de metingen die we in zijn laboratorium mochten uitvoeren en voor zijn actieve interesse in ons werk.

De 'cool guys' Theo Geneste en Frits Janssen van de vloeibaar-Helium productie worden ook van harte bedankt.

Mijn ouders stonden altijd achter mij en voor mij klaar; hen dank ik hiervoor van harte.

Tenslotte dank ik Anke voor haar liefde, steun, belangstelling in mijn werk en begrip voor de zoveelste avond die zij zonder mij zou doorbrengen. Aan haar en onze zonen draag ik dit proefschrift daarom op.

Frank

Contents

1	General Introduction	1
	References	3
2	Optical transitions in semiconductors	5
2.1	Donor and acceptor states in semiconductors	5
2.2	Photoluminescence transitions	6
2.2.1	Excitons	6
2.2.2	Exciton-polaritons	7
2.2.3	Bound excitons	7
2.2.4	Two-electron satellites and resonant excitation	8
2.2.5	Two-hole satellites	9
2.2.6	(D^0, A^0) and (e, A^0)	9
2.3	Effects of magnetic fields	10
2.3.1	Relation with astrophysics	10
2.3.2	Donor identification	11
2.3.3	Landau levels in three dimensions	12
2.3.4	Landau levels in two dimensions	13
2.3.5	Spin splittings	14
2.3.6	Experimental arrangement for PL	14
2.4	Photoluminescence excitation spectroscopy	14
2.5	Photoreflectance	16
	References	18
3	An analysis of the two-electron satellite spectrum of GaAs in high magnetic fields	21
3.1	Introduction	22
3.2	Experimental Details	23
3.3	Theory	23
3.4	Experimental Results and Discussion	25
3.5	Conclusions	32
	References	32
4	Influence of magnetic fields on an extremely narrow exciton line in a high-carrier-density heterojunction	35
4.1	Introduction	36
4.2	Experimental Details	37
4.3	Results and Discussion	37

4.4	Conclusions	44
	References	45
5	Fermi-edge-induced magnetophotoluminescence in high-carrier-density single heterojunctions	47
5.1	Introduction	49
5.2	Experimental Details	50
5.3	Results and Discussion	51
5.3.1	Lowest carrier density	51
5.3.2	Intermediate carrier density	54
5.3.3	Highest carrier density	59
5.3.4	PL mechanism	60
5.3.5	Resonant Excitation	61
5.4	Conclusions	65
	References	66
6	Detection of two-dimensional electron gases in undoped heterojunctions with magnetophotoluminescence	69
	References	72
7	Effects of confined donor states on optical and transport properties of ordered GaInP₂ alloys	75
7.1	Introduction	76
7.2	Experimental Details	76
7.2.1	Experimental Techniques	76
7.2.2	Samples and their degree of ordering	77
7.3	Results and Discussion	78
7.3.1	Photoreflectance	78
7.3.2	Hall-van der Pauw measurements	79
7.3.3	Photoluminescence	82
7.4	Conclusions	87
	References	88
8	Photoluminescence on high quality Al_xGa_{1-x}As grown by metalorganic vapour phase epitaxy using alane bis(dimethylethylamine)	91
	References	96
9	Excitonic photoluminescence spectra of Al_xGa_{1-x}As grown by metalorganic vapour-phase epitaxy	97
	References	103
10	The influence of impurity concentration on exciton PL in GaAs and InP	105
10.1	Introduction	106
10.2	Experimental Details	107

10.3 Results and Discussion	108
10.4 Conclusions	116
References	118
Summary	121
Samenvatting	125
List of Publications	129
Curriculum Vitae	131

Chapter 1

General Introduction

The field of semiconductor physics is still rapidly expanding. The understanding of fundamental processes in this field has led to the development of semiconductor technology, which strongly influenced modern society. In contrast to the group IV semiconductors Si and Ge, certain group III-V compounds (such as GaAs and InP) have direct band gaps, which makes them far better suited for the generation of light. The demands for optoelectronic devices and high speeds of operation have led to strong interest in these III-V compound semiconductors.

Modern growth techniques such as metalorganic vapour-phase epitaxy (MOVPE) and molecular beam epitaxy (MBE) have rapidly developed: extremely pure III-V materials can be grown and the deposition can be controlled at monolayer resolution, which has opened the way to make ultrathin layered structures with a variety of applications. Amongst these are semiconductor lasers, ultrafast switching devices (e.g. the high electron mobility transistor, HEMT), waveguides, and high-efficiency solar cells. Examples of the last category are multi-quantum-well solar cells [1], and tandem solar cells, which consist of low and high-band-gap solar cells connected by a tunneljunction. The progress in III-V growth techniques also displayed highly interesting new physical phenomena such as the (integral) quantum Hall effect [2] and the fractional quantum Hall effect [3], which is believed to result from condensation of electrons into an incompressible liquid [4].

This thesis deals with work on III-V compound semiconductor materials and it is organized as follows: Chapter 2 describes the most important optical transitions occurring in semiconductors and techniques used to measure them. Especially, the effects that a magnetic field has on these transitions and the role of tunable lasers with extremely narrow linewidths are emphasized. A knowledge of shallow impurities is important in the preparation of high-quality semiconductor materials because it can help in tracing the sources of undesired impurity contamination and in optimizing growth conditions. As will be shown in Chapter 2, the identification of shallow acceptors is relatively easy. In contrast, a variety of experimental tricks is required to reveal the nature of shallow donors.

In Chapter 3, residual donors are identified from “two-electron” satellites in extremely high-purity GaAs. These satellites of the donor-bound-exciton (D^0, X) reflect the excited states of the donor, which can accurately be described by a hydrogen-like model. Resonant excitation of several (D^0, X) lines using a tunable ring dye laser at magnetic fields up to 7 T, has been used to study the correlation between the hydrogen states and the experimental TES spectrum.

When an n -type $\text{Al}_x\text{Ga}_{1-x}\text{As}$ layer is grown on a GaAs layer, the electrons are

spatially separated from their donor-cores and confined in a triangular potential well at the interface, thereby forming a degenerate two-dimensional electron gas (2DEG) which has quantized energy levels, so-called subbands. Photoluminescence (PL) on such a system is usually hindered because the photoexcited holes are rapidly diffusing away from the 2DEG region as a result of the repulsive intrinsic field. It is shown in Chapter 4 that the PL intensity from the 2DEG region increases profoundly when a magnetic field is applied. The reason for this is that the highest occupied subband then depopulates, causing a hybridization with the Fermi level. This, in turn, strongly enhances the matrix element for optical recombination. In Chapters 4 and 5 a wide variety of properties of the 2D system are reported. In Chapter 6 this magneto-optical characterization is applied to identify the presence of unintended 2DEG's.

A study of the optical and transport properties of the alloy GaInP_2 , which at this particular composition is lattice matched to GaAs, is presented in Chapter 7. This material is used in GaInP-GaAs tandem solar cells and as an active layer in (Al,Ga,In)P based lasers. Furthermore, the low surface recombination velocity of the GaInP/GaAs interface with respect to that of the AlGaAs/GaAs interface makes GaInP better suited as window layer on GaAs solar cells. In spite of its applications, various fundamental properties of the nearly equimolar GaInP_2 had not been understood so far, because they were hampered by the occurrence of regions of spontaneous long-range order of monolayer $(\text{GaP})_1(\text{InP})_1$ superlattices in the [111] direction. By combining data from photoluminescence, photoreflectance, Hall-van der Pauw and magneto-transport measurements, the majority of "anomalous" properties of the GaInP_2 alloy are now understood.

Despite various advantageous properties of GaInP_2 , the alloy $\text{Al}_x\text{Ga}_{1-x}\text{As}$ is far more often used in III-V technology. Reasons are the nearly perfect lattice matching to GaAs at all Al-fractions x , and the absence of hazardous phosphorous during growth. Improvement of the $\text{Al}_x\text{Ga}_{1-x}\text{As}$ material properties is necessary for various reasons. Optical characterization of high-purity $\text{Al}_x\text{Ga}_{1-x}\text{As}$ is the subject of Chapter 8. We report on $\text{Al}_x\text{Ga}_{1-x}\text{As}$ grown with the new aluminum precursor alane bis(dimethylethylamine). The most important conclusion here is a reduction in carbon incorporation by a factor 50, as compared with growth using the conventional trimethylaluminum. Furthermore, we report for the first time an exciton splitting in $\text{Al}_x\text{Ga}_{1-x}\text{As}$ with an Al fraction higher than 20%, and linewidths that are a factor two smaller than reported ever before for MOVPE grown samples.

Finally, relationships are reported between optical and electrical properties of series of high-purity GaAs and InP epilayers in Chapter 10. These data are particularly useful for obtaining the donor concentration in fully depleted samples, because no information on carrier concentration can be obtained via Hall measurements in very high-purity material, owing to full depletion of the epilayer.

References

1. K.W.J. Barnham, and G. Duggan, *J. Appl. Phys.* **67**, 3490 (1990).
2. K. von Klitzing, G. Dorda, and M. Pepper, *Phys. Rev. Lett.* **45**, 494 (1980).
3. D.C. Tsui, H.L. Störmer, and A.C. Gossard, *Phys. Rev. Lett.* **48**, 1559 (1982).
4. R.B. Laughlin, *Phys. Rev. Lett.* **50**, 1395 (1983).

Chapter 2

Optical transitions in semiconductors

This chapter introduces the reader to the extensive field of electronic states and optical transitions in semiconductors, and it treats the methods used to acquire information on these transitions. By no means, can this chapter be regarded as complete, and the interested reader is referred to review papers and books on the various topics. Introductory chapters on optical transitions in III-V semiconductors can be found in Willardson and Beer [1] and in the book by Bassani and Pastori Parravicini [2]. Impurity states in semiconductors are reviewed by Pantelides [3]. For a clear treatment on effective mass theory and excited states of impurities, the reader is referred to Henning [4]. An excellent book on recent achievements in exciton physics is “Excitons”, edited by Rashba and Sturge [5]. The book of Knox [6] on excitons is also recommended. Magnetic quantum effects are summarized by Roth and Argyres [7], and extensive treatments on the electronic properties of two-dimensional systems were given by Ando, Fowler and Stern [8] and in part 53 from the Springer series on Solid-State Sciences [9].

2.1 Donor and acceptor states in semiconductors

The properties that make semiconductors of such technological importance are conferred upon them by the presence of defects, normally in the form of chemical impurities. Most important is the class of shallow impurities: those which are ionized at room temperature: that around which most devices should operate. For virtually all shallow impurities the difference in the number of valence electrons from that of the host atoms is either +1 (donors) or -1 (acceptors). When ionized, the charged impurity core causes a hydrogen-like potential, given by $U(r) = \pm e^2/\epsilon_r r$, where ϵ_r is the dielectric constant, which is large (~ 10) for all III-V semiconductors. Because of the Bloch nature of electrons and holes, their effective masses m^* are reduced, which allows the energy levels to be described by effective mass theory (EMT) [10]. This results in a series of bound states that resemble those of hydrogen. For donors these are:

$$E_n = E_c - \frac{1}{n^2} \frac{m_e^*}{\epsilon_r^2} Ry \quad , \quad (2.1)$$

where n is the principal quantum number, m_e^* the effective electron mass in units of the free electron mass m_e , $Ry = 13.596$ eV the Rydberg energy, and E_c the bottom of the conduction band; the quantity $(m_e^*/\epsilon_r^2) Ry$ is often referred to as the effective Rydberg R^* .

These states extend over radii $n^2(\epsilon_r/m^*)a_B = n^2a_B^*$, where a_B and a_B^* are the real and the effective Bohr radii, respectively. The actual ionization energies of donors correspond to R^* within a few percent. The small deviations (0.01 – 0.2 meV for GaAs and InP) are caused by the short-range non-Coulombic part of the potential (the central-cell potential), which predominantly affects the $1s$ ground state; the shift of the $2s$ excited state is only $1/8^{\text{th}}$ of the $1s$ shift. The deviations of the ground state enable the identification of the nature of the donor, and are therefore called ‘chemical shifts’ or ‘central-cell corrections’. More details on this are given in sections 2.2.4, 2.3.2 and in Chapter 3.

For acceptors the energy levels are not well described by a simple hydrogen model because the valence band is split by spin-orbit interaction, and the central-cell potential is of greater influence because the heavier holes orbit the acceptor with considerably smaller radii. However, Baldereschi and Lipari [11,12] took the band structure details for holes into account and succeeded in giving a good qualitative description of the acceptor states using EMT. Again the central-cell potential predominantly affects the ground state, but a small part of its influence also extends to higher orbits with a non-vanishing wavefunction at the acceptor core.

2.2 Photoluminescence transitions

2.2.1 Excitons

The original concept of the exciton was developed by J.I. Frenkel in 1931 [13]: electron excitation waves which involve correlated motion of electrons and holes and do not carry electric current. This Frenkel exciton was calculated in the tight-binding approximation and described a single excited ionic level. In most semiconductors, the opposite extreme is the case: the electron and the hole separation is many inter-atomic spacings. Wannier first showed that EMT could be used in this case [14], resulting in a discrete set of hydrogenic bound states with energies $E_n = -(1/n^2)(\mu/\epsilon_r^2)Ry$ below the band edge E_g ; here μ is the exciton mass. Hence, excitons form the lowest excited state in a perfect crystal; this explains their importance in optical experiments, in which they are created by above band gap excitation. Excitons possess lifetimes of the order of a few ns, whereafter they recombine to yield free-exciton luminescence FX. When excitons are mentioned hereafter those with the properties described by Wannier are meant, also known as Wannier-Mott excitons.

The stability of excitons depends on the following parameters:

- the thermal energy (kT) should not exceed the exciton binding energy; for GaAs this is true for $T < 60\text{K}$.
- excitation density should be low to avoid screening of the exciton.
- strong electric fields tend to separate the polarized exciton.

2.2.2 Exciton-polaritons

In direct-band-gap semiconductors, there exists a strong coupling between the exciton dipole and photons of the same energy. In a PL experiment these photons are provided by a laser, and coupling only occurs with excitons that are aligned perpendicular to the beam (transverse excitons). Hopfield [15] showed that the coupling results in a mixed-mode excitation called an exciton-polariton (or polariton) with a two-branch dispersion curve given by:

$$\left(\frac{\hbar ck}{E}\right)^2 = \epsilon_r + \frac{2\epsilon_r E_{LT} E}{E_0^2(k) - E^2}, \quad (2.2)$$

where E_{LT} is the splitting between the uncoupled longitudinal and transverse excitons at $k = 0$, E the polariton energy, and $E_0(k)$ the energy of the transverse exciton plus the kinetic energy [16]. The polariton dispersion curve of GaAs is shown in Figure 10.4. The nature of the polariton dispersion relation has a profound effect on the luminescence mechanism [15,17], as will be further elaborated in Chapter 10.

2.2.3 Bound excitons

Apart from direct FX recombination, the exciton can bind to an impurity and form a bound exciton BX. Hopfield [18] showed that the exciton can always bind to a neutral impurity; for donors and acceptors these bound excitons are denoted as (D^0, X) and (A^0, X) , respectively. Binding to an ionized impurity depends on the effective mass ratio of electrons and holes $\sigma = m_e^*/m_h^*$; if $\sigma < 0.38$ binding to ionized donors (D^+, X) occurs and if $\sigma > 2.6$ binding to ionized acceptors (A^-, X) is the stable exciton complex [19]. All semiconductors in this thesis have $\sigma < 0.38$, and so (D^0, X) , (A^0, X) and (D^+, X) bound excitons are stable. The energy of a photon after recombination of a BX is:

$$\hbar\omega = E_g - E_{FX} - E_{BX}, \quad (2.3)$$

where $E_{FX} = (\mu/\epsilon_r^2)Ry$ is the free-exciton ionization energy and E_{BX} is the localization energy of the exciton on the impurity. An empirical rule of thumb, known as Haynes' rule [20], states that E_{BX} is approximately 10% of the impurity ionization energy.

A typical PL spectrum of a high-purity InP sample recorded at $T = 1.5$ K is shown in Figure 2.1. FX-polariton PL is observed below the energy of the band gap E_g ; the latter is indicated by an arrow. The various bound-exciton PL peaks are separated from the FX by their localization energies. The (A^0, X) luminescence exhibits a splitting into $J = 1/2, 3/2$ and $5/2$ angular momentum states that result from spin-orbit coupling of the two $J = 3/2$ holes with the $J = 1/2$ electron; at low T only the $(A^0, X)_{J=5/2}$ and $(A^0, X)_{J=3/2}$ states are observed due to thermalization. The splitting of (D^0, X) originates from rotation of the exciton around the neutral donor; it yields quantized rotational states [21,22]. For the sample shown in Figure 2.1 only around 1 per 10^9 atoms is an impurity. However, the contribution of BX luminescence to the spectrum is large because BX recombination is energetically favoured above FX recombination, and because the large exciton radius leads to a correspondingly large cross section for capture by an impurity. This makes PL

an extremely sensitive technique for the detection of impurities, allowing the detection of impurity concentrations as low as 10^{10} cm^{-3} [23]. The other PL lines in Figure 2.1 are treated in the following sections.

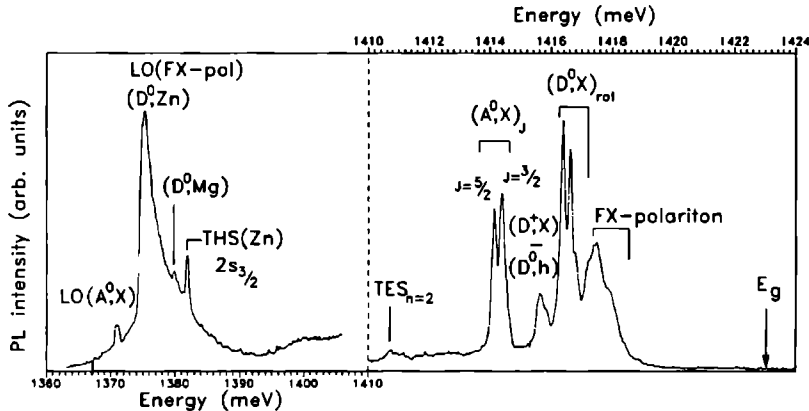


Figure 2.1 The 1.5-K PL spectrum of a high-purity InP epilayer; note the change in scale.

2.2.4 Two-electron satellites and resonant excitation

A schematic representation of the (D^0, X) complex is given in Figure 2.2(a). Although more complicated to calculate, the exciton binds to the donor as two hydrogen atoms bind to one another in the H_2 molecule [24]. After recombination, the ‘donor electron’ will be in the $n = 1$ ground state in most cases. The corresponding photon energy contributes to the well-known (D^0, X) peak; this process is shown in Figure 2.2(b). Another possibility for recombination is that an Auger-like interaction between the electrons and the hole brings the donor electron into one of its higher orbits given by equation 2.1 (e.g. $n = 2$), as shown schematically in Figure 2.2(c). The energy of the photon released in this process equals the (D^0, X) energy minus the difference between the $n = 2$ and $n = 1$ donor orbits. This process is called a “two-electron” satellite (TES) because two electrons are involved in the recombination process [25].

Because the real $n = 1$ energy differs from the hydrogenic one by the central-cell correction, the difference $\hbar\omega_{(D^0, X)} - \hbar\omega_{\text{TES}}$ enables the identification of the donor. The widths of both PL peaks restrict donor identification at zero field to extremely high-purity epilayers (see Chapter 3).

A small TES signal is observed in Figure 2.1. In order to increase the TES signal, the energy of a laser (in our experiments a ring dye laser on Styryl 9, and a Ti:sapphire ring laser) is exactly tuned to the energy of the (D^0, X) . This increases the probability that

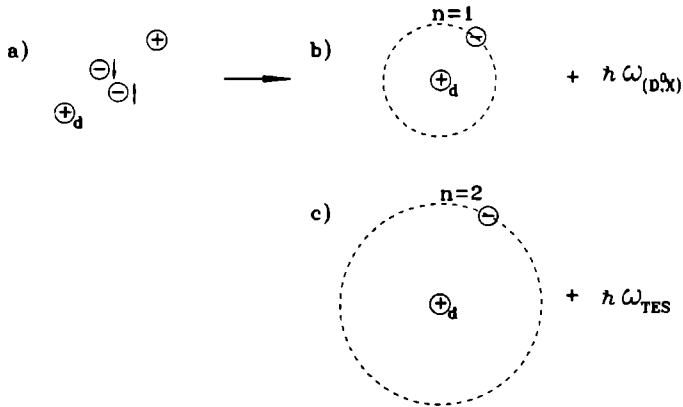


Figure 2.2 a) Schematic representation of the donor-bound-exciton, b) PL with the donor electron in the ground state, c) PL with the donor electron in an excited state, a two-electron satellite.

a (D^0, X) complex is formed, and therefore also the intensity of TES PL. This effect of resonant excitation is shown in Figure 3.1: a signal increase by at least a factor 10. The advantage of this PL technique is that donors can be identified in *p*-type, *n*-type and semi-insulating semiconductors. This is in contrast to, for instance, photothermal ionization spectroscopy [26], which is only suitable for *n*-type material.

2.2.5 Two-hole satellites

Analogous to the TES, a ‘two-hole’ satellite (THS) can appear: a transition in which the exciton bound to a neutral acceptor recombines and leaves the hole in an excited state of the acceptor. Using the Baldereschi-Lipari notation [11], the first such level above the ground state $1S_{3/2}$ the transition to which is parity-allowed is $2S_{3/2}$. The $1S_{3/2} - 2S_{3/2}$ energy separation contains virtually the entire central-cell correction, which enables, for example, the identification of the acceptor Zn in Figure 2.1.

2.2.6 (D^0, A^0) and (e, A^0)

Apart from binding an exciton, recombination directly involving the impurity can appear. If this occurs with free carriers, there are two possibilities: a free electron recombines with a hole bound to an acceptor (e, A^0), and a free hole recombines with an electron bound to a donor (D^0, h). For these two processes often the words ‘free-to-bound’ are used. A third possibility is that both carriers are trapped at shallow impurities denoted (D^0, A^0): recombination between donor-bound electrons and acceptor-bound holes.

The energies of the (e, A^0) and (D^0, h) transitions are the band-gap energy minus the ionization energy of the impurity involved. The PL energy of a (D^0, A^0) transition depends *inter alia* on the distance R between the donor and acceptor pair:

$$E_{(D^0, A^0)} = E_g - E_D - E_A + \frac{e^2}{\epsilon_r R} \quad (2.4)$$

The R -dependent term in the above equation arises because both impurities are charged in the final state; it results in an inhomogeneous broadening of the line shape. (D^0, A^0) recombination between distant pairs is energetically favoured. However, the recombination (tunneling) times for such pairs are very long and they saturate easily, making possible recombination between pairs with smaller separation (and shorter lifetimes). Therefore, the peak maximum of (D^0, A^0) pair luminescence depends on excitation density, which provides a method to distinguish (D^0, A^0) from other luminescence. Generally, free-to-bound and (D^0, A^0) luminescence can also be distinguished from BX PL by their broader line shapes and, in the case of acceptor-related transitions, their lower energy. Finally, another property of non-excitonic PL is that its intensity is less influenced by laser excitation density than that of excitonic PL. As an example, a GaAs spectrum in Figure 2.3 shows clearly separated (D^0, A^0) and (e, A^0) transitions involving the acceptors Zn and C; an extremely low excitation density of $6.25 \times 10^{-5} \text{Wcm}^{-2}$ was necessary to achieve the splitting. The InP spectrum in Figure 2.1 reveals, apart from the (D^0, A^0) transition involving the acceptor Zn, also that of Mg.

2.3 Effects of magnetic fields

2.3.1 Relation with astrophysics

As stated in section 2.1.1, shallow donors in GaAs and InP are accurately described by hydrogen-like states. Motivated by highly-magnetized objects in astrophysics, such as white dwarfs with $B \sim 10^2\text{-}10^5$ T and neutron stars with $B \sim 10^7\text{-}10^9$ T, the energy levels of the real hydrogen atom in magnetic field upto $B = 10^9$ T were calculated with high accuracy by various authors; see for example Rösner *et al.* [27] and references therein. A dimensionless unit of magnetic field is the ratio of magnetic energy and Coulomb energy: $\Gamma = \hbar\Omega_c/2Ry$, with $\Omega_c = eB/cm_e$ the cyclotron frequency. The magnetic-field energy exceeds the Coulomb energy in the high-field limit ($\Gamma > 1$; $B > 9.4 \times 10^5$ T). The hydrogenic wave functions are then strongly compressed and distorted, and their size is no longer characterized by the Bohr radius a_0 but rather by the radius of the cyclotron orbit $l = (\hbar/m_e\Omega_c)^{1/2}$. Consequently, the wave functions gradually change into Landau wave functions [7], which, upon applying a field in the z -direction, are given by:

$$\psi_{n\mathbf{k}}(\mathbf{r}) = (L_x L_y)^{-1/2} \phi_n(z - z_{\mathbf{k}}) e^{ik_x x} e^{ik_y y}. \quad (2.5)$$

Here, L_x and L_y are the corresponding normalization lengths, $\mathbf{k} = (k_x, k_y)$ is the two-dimensional wave vector, and the $\phi_n(z - z_{\mathbf{k}})$ are the normalized wave functions of a simple harmonic oscillator of angular frequency Ω_c centered at the point $z_{\mathbf{k}}$.

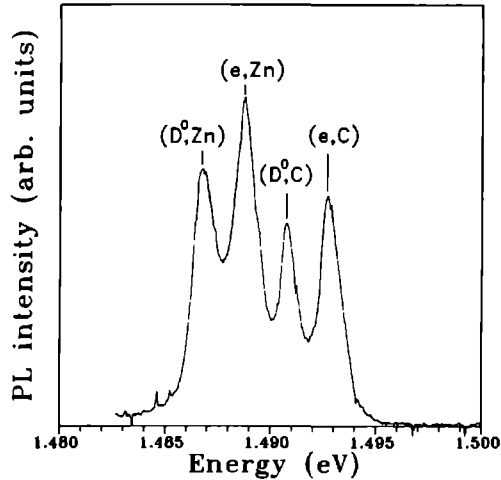


Figure 2.3 PL spectrum of the (D^0, A^0) and (c, A^0) region in GaAs, recorded at extremely low excitation density; transitions involving the acceptors Zn and C are clearly resolved.

For hydrogenic donors in semiconductors, Γ is rescaled to $\gamma = \hbar\omega_c/2R^* = (m^*/\epsilon_r)^{1/2}\hbar\Omega_c/2Ry$, which shows that the high-field limit is already reached at experimentally well-accessible magnetic fields (~ 6 T for GaAs). Therefore, the energy levels of the hydrogen atom in a magnetic field can be rescaled for the use in semiconductors¹. An illustration of various of these energy levels [27] is given in Figure 2.4. The vertical axis is scaled in effective Rydbergs, the top axis is given in the dimensionless field γ for the specific case of GaAs, and the bottom axis shows B . The dotted lines represent the $N = 0$ and 1 Landau levels of the conduction band. After an initial decrease, the donor ground state ($1s$) shifts at a slower rate than the $N = 0$ Landau level. Thereby, the donor ionization energy ($E_{N=0} - E_{1s}$) increases monotonically in magnetic field.

2.3.2 Donor identification

The application of a magnetic field is favorable for donor identification for a number of reasons. First, PL peaks are considerably narrowed because of the removal of orbital degeneracy. Second, the wave function shrinkage diminishes the effect of background Coulomb interaction of ionized impurities. And third, the increase of binding energy in magnetic field leads to a greater central-cell shift. A calculation of the latter effect was given by Fetterman *et al.* [28] using perturbation theory: in a magnetic field the separation

¹In Chapter 3 slightly different dimensionless units will be used: $\beta = \gamma/2$.

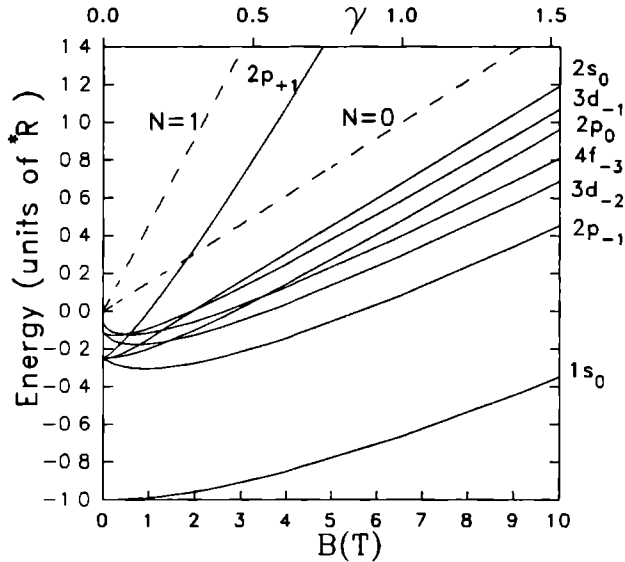


Figure 2.4 Energies of various hydrogen-like donor states in GaAs versus magnetic field B . The top axis shows the dimensionless field γ . The first two Landau levels are shown by dashed lines.

between two different donor species 1 and 2 increased as follows:

$$\Delta_{1,2}(B) = K_{1,2} |\chi_{1s}(O, B)|^2, \quad (2.6)$$

where $K_{1,2}$ is a field-independent, adjustable parameter, $\chi_{1s}(O, B)$ represents the EMT function of an electron in the $1s$ donor ground state at the origin O in B -field. Hence, the application of a magnetic field increases the sensitivity of the technique significantly and enables donor identification in less pure samples.

2.3.3 Landau levels in three dimensions

It is well established that in a magnetic field the continuum of conduction-band states transforms in a sequence of narrow bands [29] called Landau levels, which are separated by the cyclotron energy. These energy levels are given by:

$$E(N, k_z) = (N + 1/2)\hbar\omega_c + \frac{\hbar^2 k_z^2}{2m^*}, \quad (2.7)$$

where the first term on the right hand side corresponds to the magnetic quantization in the direction perpendicular to the B -field with N an integer, and the second term

corresponds to free motion parallel to the field. In the absence of spin splitting this magnetic quantization of levels changes the density of states (DOS) dramatically into [1]:

$$D^{3D}(E) = \frac{1}{4\pi^2} \left(\frac{2m^*}{\hbar^2} \right)^{3/2} \hbar\omega_c \sum_N [E - (N + 1/2)\hbar\omega_c]^{-1/2}, \quad (2.8)$$

resulting in a singularity at the bottom of each Landau level.

2.3.4 Landau levels in two dimensions

The spectrum given in equation 2.7 can be transformed into a completely discrete series if the motion parallel to the field also becomes quantized. This can be achieved, for example, in modulation-doped heterojunctions and quantum wells. The band structure of a GaAs/Al_xGa_{1-x}As modulation-doped heterojunction is shown schematically in Figure 2.5.

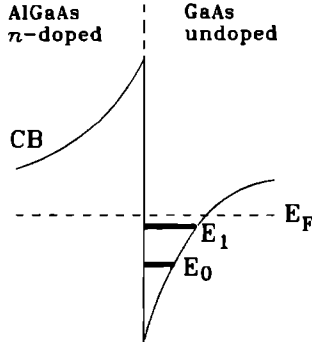


Figure 2.5 Conduction-band (CB) structure of a GaAs/AlGaAs modulation-doped heterojunction.

The band bending occurs because electrons provided by donors in the Al_xGa_{1-x}As move to the lower band gap material (GaAs) and are then attracted to the positively-charged donor cores left behind in the Al_xGa_{1-x}As. The resulting triangular-like potential well near the interface contains a degenerate two-dimensional electron gas: electrons are no longer free to move perpendicular to the interface but are quantized in discrete levels known as subbands E_i , where i is an integer. The energy spectrum in such a confined system is now completely quantized and given by:

$$E(N, i) = (N + 1/2)\hbar\omega_c + E_i, \quad (2.9)$$

The DOS now becomes [30]:

$$D^{2D}(E) = \frac{m^*}{\pi\hbar^2} \sum_i \Theta(E - E_i), \quad (2.10)$$

where $\Theta(E)$ is the Heavyside step function. Degenerate two-dimensional systems are the topic of Chapters 4-6.

2.3.5 Spin splittings

Another effect of magnetic field is that states of different spin, which are degenerate at zero magnetic field, split into multiplets of well-separated states. These spin splittings of electronic states in semiconductors are characterized by effective g -factors g_{eff} , where the deviation of g_{eff} from the free-electron value $g_e = 2$ can be correlated to the band structure [31]. In a degenerate system (such as a 2DEG), the g_{eff} can be enhanced to g^* by exchange interaction between electrons [32,33]. The enhancement is proportional to the difference in numbers of electrons with up and down spins:

$$g^* = g_{eff} + \frac{E_{ex}}{\mu_B B} \sum_N (n_{N\uparrow} - n_{N\downarrow}). \quad (2.11)$$

Here E_{ex} is the exchange parameter and $n_{N\uparrow}$ and $n_{N\downarrow}$ are the occupation factors of the spin levels. The difference becomes maximal when the Fermi level passes through the middle of a Landau level, which then has one completely filled and one empty spin component. The minimum value g_{eff} is reached if both spin components of a Landau level are occupied.

2.3.6 Experimental arrangement for PL

The experimental arrangement used to measure PL is shown schematically in Figure 2.6. Laser light from an Ar⁺ laser-pumped tunable ring laser (Styryl 9 dye laser, or Ti:sapphire laser) is directed via a beamsplitter (BS) and focused on a sample which is mounted in a strain-free way in the bore of a 7T superconducting split-pair magnet. The excitation beam is chopped at a frequency of 330 Hz.

The temperature in the separate sample space can be accurately controlled between 1.5 and 320 K. The PL from the sample is directed into a 0.65-m double monochromator with 1200 lines/mm gratings driven by a stepper motor, which is controlled by a 'Spectralink'. The output is detected by a photomultiplier (PM) with a GaAs photocathode or one with S1 response. The Peltier-cooled GaAs PM is used because of its high quantum efficiency at energies > 1.43 eV. The S1 PM, which is cooled to 190 K, is used for energies < 1.43 eV (e.g. InP samples). The signal is amplified by standard lock-in techniques and sent to a computer (PC).

2.4 Photoluminescence excitation spectroscopy

In the PL method mentioned above, electron-hole pairs are created which quickly relax to residual impurities or to (bound) excitons (on a typical timescale of 1 ps); radiative recombination (with timescale ranging from ns to μ s) from these meta-stable states is then detected with PL. However, PL does not provide information on the intermediate

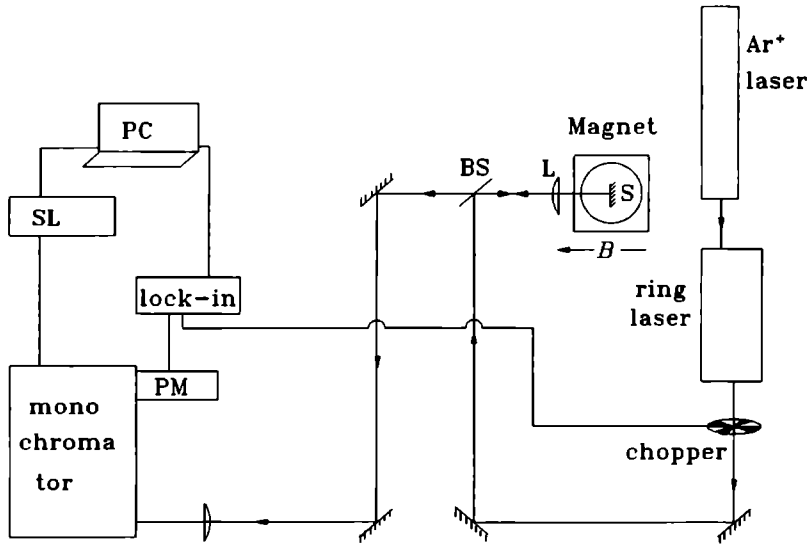


Figure 2.6 Experimental arrangement for PL measurements; see the text for explanation.

states through which the carriers pass in relaxing to the meta-stable states. In contrast, information on these states can be obtained with photoluminescence excitation (PLE) spectroscopy. In a PLE experiment only one radiative transition is detected because the monochromator energy is fixed and the exciting laser energy is scanned. To scan the laser, a stepper motor is installed on the birefringent filter and the etalons are removed. The latter is necessary to prevent mode hops, although this does cause slight spectral broadening of the laser.

If the laser is resonant with an excited state (or more generally, a related state), the intensity of the detected transition increases. Thus, for instance, excited impurity states, higher Landau levels, subbands and spin-split states, can be probed with PLE.

Furthermore, PLE can distinguish between bound-exciton PL on the one hand, and free-to-bound and (D^0, A^0) PL on the other [23]. In the case of bound-exciton PL, a PLE peak is observed when the laser is tuned to the energies of the exciton-polaritons because the resonantly created exciton-polaritons are preferentially trapped on impurities. For (D^0, A^0) and free-to-bound PL the PLE spectrum shows a dip at the exciton-polariton energies because the formation of these polaritons now creates a parallel recombination path in competition with the non-excitonic recombination.

In samples of low purity, broad (D^0, h) recombination strongly interferes with (D^0, X) PL, thereby obstructing a good measure of $\hbar\omega_{(D^0, X)} - \hbar\omega_{TES}$. In such cases a

PLE experiment with the monochromator fixed on a TES peak is advantageous for donor identification because only the related (D^0, X) lines are stimulated whereas the competitive (D^0, h) recombination is decreased [34].

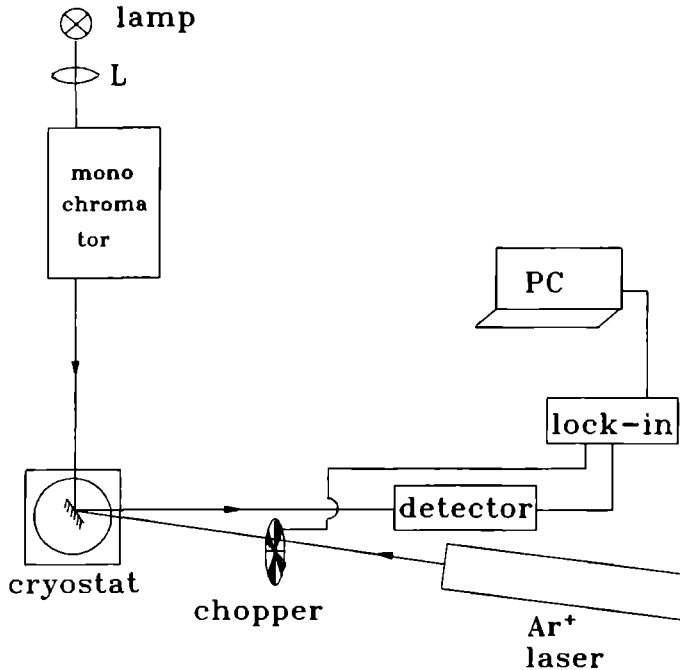


Figure 2.7 Experimental arrangement for PR measurements; see the text for explanation.

2.5 Photoreflectance

The techniques of electromodulation (EM) spectroscopy, mainly electroreflectance (ER) and photoreflectance (PR), have become popular as probes of bulk semiconductors and layered structures [35,36]. In both methods the dielectric function is modulated. With the PR technique field modulation occurs through changes in the photovoltage induced by the absorption of above-band-gap photons, and leads to derivative-like optical features.

A typical experimental arrangement for PR is shown in Figure 2.7. A Xe lamp and a single monochromator with a 1200 lines/mm grating produce monochromatic radiation which reflects at the crystal surface and is detected by a Si photodiode. An Ar⁺ laser is directed to coincide at the sample with the monochromatic lamp light. By chopping the

laser beam at ~ 330 Hz the reflectivity of the crystal is modulated and amplified with standard lock-in techniques.

Free electrons and holes are accelerated by changes in the electric field. Aspnes and Rowe [37] showed that for low electric fields the EM line shapes are then directly related to the third derivative with respect to photon energy of the zero-field dielectric function. At high fields, more complex line shapes are obtained because the Franz-Keldysh effect operates [38]. The EM line shapes of localized carriers are markedly different because these carriers cannot be accelerated if a field is applied in the direction of localization; the Stark effect on minibands or sublevels then results in a first-derivative line shape [39].

References

1. *Semiconductors and Semimetals* Vol. 8, edited by R.K. Willardson and A.C. Beer (New York, Academic Press, 1972).
2. Bassani and Pastori Parravicini, *Electronic States and Optical Transitions in Solids* (Pergamon Press, Oxford, 1975).
3. S.T. Pantelides, *Rev. Mod. Phys.* **50**, 797 (1978).
4. J.C.M. Henning, in *Proc. of the Intern. School of Physics "Enrico Fermi", Course XCVI*, edited by U.M. Grassano and N. Terzi (North Holland, Amsterdam, 1987), p.167.
5. E.I. Rashba and M.D. Sturge (editors), *Excitons*, North-Holland Publishing Company, Amsterdam, 1982.
6. R.S. Knox, *Excitons*, Academic Press, New York, 1963.
7. L.M. Roth and P.N. Argyres, in *Semiconductors and Semimetals* Vol. 1, edited by R.K. Willardson and A.C. Beer (New York, Academic Press, 1966), p.159.
8. T. Ando, A.B. Fowler, and F. Stern, *Rev. Mod. Phys.* **54**, 437 (1982).
9. *Two-Dimensional Systems, Heterostructures, and Superlattices*, Vol. 53 of Springer Series in Solid-State Sciences, edited by G. Bauer, F. Kuchar, and H. Heinrich (Springer, Berlin, 1984).
10. W. Kohn, *Solid State Phys.* **5**, 257 (1957).
11. A. Baldereschi, and N.O. Lipari, *Phys. Rev. B* **8**, 2697 (1973).
12. A. Baldereschi, and N.O. Lipari, *Phys. Rev. B* **9**, 1525 (1974).
13. J.I. Frenkel, *Phys. Rev.* **37**, 17 (1931); *ibid.*, 1276.
14. G.H. Wannier, *Phys. Rev.* **52**, 191 (1937).
15. J. Hopfield, *Phys. Rev.* **112**, 1555 (1958).
16. T. Steiner, M.L.W. Thewalt, E.S. Koteles, and J.P. Salerno, *Phys. Rev. B* **34**, 1006 (1986).
17. Y. Toyozawa, *Prog. Theor. Phys. Suppl.* **12**, 111 (1959).
18. J.J. Hopfield, in *Proc. 7th Int. Conf. Phys. Semicond.*, edited by Dunod, (Paris, 1964), p.725.
19. J. Lévy-Leblond, *Phys. Rev.* **178**, 1526 (1969).
20. J.R. Haynes, *Phys. Rev. Lett.* **4**, 361 (1960).
21. W. Rühle and W. Klingenstein, *Phys. Rev. B* **18**, 7011 (1978).
22. J. Rorison, D.C. Herbert, P.J. Dean, and M.S. Skolnick, *J. Phys. C: Solid State Phys.* **17**, 6435 (1984).
23. T. Steiner, Y. Zhang, S. Charbonneau, A. Villemaire, M.L.W. Thewalt, M. Maciaszek, and R.P. Bult, *Can. J. Phys.* **67**, 242 (1989).
24. M.A. Lampert, *Phys. Rev. Lett.* **1**, 450 (1958).
25. P.J. Dean, and M.S. Skolnick, *J. Appl. Phys.* **54**, 346 (1983).
26. G.E. Stillman, C.M. Wolfe, and J.O. Dimmock, in *Semiconductors and Semimetals* Vol. 12, edited by R.K. Willardson and A.C. Beer (New York, Academic, 1977), p.169.
27. W. Rösner, G. Wunner, H. Herold, and H. Ruder, *J. Phys. B: At. Mol. Phys.* **17**, 29

- (1984).
28. H.R. Fetterman, D.M. Larsen, G.E. Stillman, P.E. Tannenwald, and J. Waldman, *Phys. Rev. Lett.* **26**, 975 (1971).
 29. L.D. Landau, *Z. Physik* **64**, 629 (1930).
 30. M.J. Kelly, and R.J. Nicholas, *Rep. Prog. Phys.* **48**, 1699 (1985).
 31. L.M. Roth, S. Zwedling and B. Lax, *Phys. Rev* **114**, 90 (1959).
 32. T. Ando and Y. Uemura, *J. Phys. Soc. Japan* **37**, 1044 (1974).
 33. Th. Englert, D.C. Tsui, A.C. Gossard, and Ch. Uihlein, *Surf. Sci.* **113**, 295 (1982).
 34. T.D. Harris, M.S. Skolnick, J.M. Parsey Jr., and R. Bhat, *Appl. Phys. Lett.* **52**, 389 (1988).
 35. O.J. Glembock, B.V. Shanabrook, N. Bottka, W.T. Beard, and J. Comas, *Appl. Phys. Lett.* **46**, 970 (1985).
 36. H. Shen, S.H. Pan, F.H. Pollak, M. Dutta, and T.R. Aucoin, *Phys. Rev. B* **36**, 9384 (1987).
 37. D.E. Aspnes, and J.E. Rowe, *Phys. Rev. B* **5**, 4022 (1972).
 38. D.E. Aspnes, *Surf. Sci.* **37**, 418 (1973).
 39. R. Enderlein, in *Proceedings of the 20th International Conference on the Physics of Semiconductors*, edited by E.M. Anastassakis and J.D. Joannopoulos (World Scientific, Singapore, 1990), p.1089.

Chapter 3

An analysis of the two-electron satellite spectrum of GaAs in high magnetic fields

F.A.J.M. Driessen¹, H.G.M. Lochs¹, S.M. Olsthoorn and L.J. Giling

*Department of Experimental Solid State Physics, RIM,
Faculty of Science, University of Nijmegen,
Toernooiveld, 6525 ED Nijmegen, The Netherlands.*

Abstract

We report the observation of $2p_{0,-1}$, $2s_0$, $3d_{-1,-2}$, $3p_{-1}$ and $4f_{-3}$ structures in the “two-electron” satellite photoluminescence of excitons bound to the (hydrogenic) shallow donors Ge and Se/Sn in high-purity metalorganic vapour-phase epitaxy grown GaAs. The attribution is based upon selective excitation of the different principal donor-bound exciton (D^0, X) lines at magnetic fields of 7 T at $T=1.5$ K, combined with a careful analysis of the behaviour of the hydrogen atom in a magnetic field. The results are interpreted in terms of high-magnetic-field quantum numbers and in terms of shapes of hydrogen wave-functions in strong magnetic fields. One of the samples used in this work is so pure that for the first time donors have been identified from the relatively broad $n=2$ two-electron satellite involving the (D^0, X) ground state at zero field.

Published in:
Journal of Applied Physics **69**, 906-912 (1991)

¹This order has been chosen arbitrarily.

3.1 Introduction

Magnetophotoluminescence (MPL) spectroscopy is a powerful technique for identifying shallow donors in direct-gap semiconductors such as InP [1-3] and GaAs [4-11]. A knowledge of these impurities is important in the preparation of high-quality semiconductor materials, since it can help in tracing the sources of undesired impurity contamination and in optimizing growth conditions. As a result of the combination of a small electron effective mass m_0^* [12-15] and a large dielectric constant ϵ_r [12], the extent of the donor wave-function is large in these materials (effective Bohr radius $a_0^* \cong 100\text{\AA}$). The donor electron is therefore highly insensitive to the non-Coulombic part of the potential associated with the specific donor ion, the so-called central cell potential; a theoretical description of the donor may be made using states similar to the levels of a hydrogen atom [16]. The ionization energy of the hydrogen atom $Ry = 13.61$ eV is now replaced by the effective Rydberg $R^* = m_0^*/\epsilon_r^2 \cdot Ry$. Experimentally, the hydrogenic nature of these states has been confirmed with high accuracy [17], yielding a value of $R^* = 5.715$ meV for GaAs. The central cell potential mainly influences the $1s$ ground state [4], and the deviation from the hydrogenic $1s$ level is called the central cell correction ΔE_{cc} . The ionization energies $E_D = R^* + \Delta E_{cc}$ of all known donor species in GaAs vary by only ~ 0.2 meV. A measurement of the energy difference between the $1s$ (donor) state and a higher state will thus provide a tool for discriminating between different donor species.

In PL measurements this is done by measuring the energy difference between luminescence originating from the recombination of the donor-bound exciton (D^0, X) in which the donor's electron remains in the $1s$ ground state on the one hand, and luminescence in which this electron is left in a higher state on the other. The latter process is usually called a two-electron satellite (TES) [18]. Rotational states of the (D^0, X), *i.e.*, quantized states in which the exciton orbits the neutral donor [19,20], are also possible, and the luminescence from these states is located at energies in between the lowest energy (D^0, X) line and the free exciton recombination (FX). Thus several TES peaks involving different rotational (D^0, X) states appear. Donor identification remains a difficult task because of the combination of possible interference between the TES peaks of different chemical donors and the appreciable linewidth of the various peaks [4].

The introduction of a magnetic field [8,9] improves the accuracy of the technique and also makes it suitable for less pure material. The reason is that the magnetic field removes the orbital degeneracy of the hydrogenlike levels of the impurity, and splits their magnetic subcomponents. Furthermore, it reduces the spectral broadening due to random electric fields in the crystal as a result of the magnetic compression of the bound electron wave function [21] and, finally, it increases ΔE_{cc} [22] as a result of the increase in $|\psi^e|_{r=0}^2$. A further improvement is obtained by using selective excitation from a tunable dye laser to one of the narrow linewidth rotational states. In this way, the problem of interfering TES peaks is reduced [7,10,11,23].

In almost all MPL studies, donors are identified from the difference in photon energy between the luminescence associated with the electron in the final donor states $2p_{-1}$ and luminescence involving one of the $1s_0$ (D^0, X) rotational states, since the $2p_{-1}$ states are

the highest-intensity TES transitions. Another advantage of donor identification from the $2p_{-1}$ states is that at sufficiently high fields ($\geq 5T$) no interference is possible with another TES set reflecting the principal (D^0, X) lines.

Apart from the $2p_{-1}$ TES group, the exact structure of the TES spectrum is not understood. Usually, another sharp peak is observed, which is attributed to one of the $2p_0$ peaks [5,6,24,25]. In this paper it will be shown that this assignment is wrong and that it should be attributed to the $3d_{-1}$ TES reflecting the fourth rotational (D^0, X) state. Donor identifications from this peak [24] of course remain valid, since the $3d_{-1}$ peak also reflects the total ΔE_{cc} [26].

In this paper we have calculated the TES spectrum using precise energy values for the electron states in magnetic fields based on a combination of Rösner's calculations of the hydrogen atom [27], and Rorison's model of the (D^0, X) principal lines [20]. Resonant excitation of several (D^0, X) lines in very high-purity GaAs samples, using a tunable ring dye laser at magnetic fields up to 7 T, has been used to study the correlation between these calculated lines and the experimental TES spectrum.

3.2 Experimental Details

The experiments were carried out on two high-purity GaAs epilayers grown by metalorganic vapour-phase epitaxy (MOVPE). The layers were grown at 650°C on (1 0 0) semi-insulating substrates and were nominally undoped. At 77 K, sample 1-0132 had a net n -type carrier concentration $n_{77} = 1.1 \times 10^{14} \text{ cm}^{-3}$ and a Hall mobility $\mu_{77} = 1.37 \times 10^5 \text{ cm}^2\text{V}^{-1}\text{s}^{-1}$. Sample 1-0212 appeared to be fully depleted. Hence, no Hall measurements could be performed on this layer, despite its thickness of $21 \mu\text{m}$. From a comparison of PL linewidths and intensity ratios with those of undepleted samples, we derived values of $n_{77} \approx 1 \times 10^{13} \text{ cm}^{-3}$ and $\mu_{77} \approx 2.0 \times 10^5 \text{ cm}^2\text{V}^{-1}\text{s}^{-1}$ for sample 1-0212 [28]. The MPL measurements were performed with the entire sample mounted in a strain-free way, immersed in superfluid He at 1.5 K in the bore of a 7 T split pair superconducting magnet that had optical access both parallel to and perpendicular to the magnetic field. Optical excitation was provided by a ring dye laser using Styryl 9 dye, pumped by a 4 W all-lines Ar^+ laser. The linewidth of the laser was narrowed to 10^{-6} meV by inserting a thin etalon and a scanning 75 GHz etalon into the cavity, which also provided the tuning of the laser. A typical excitation density was 50 mW cm^{-2} . The luminescence was dispersed by a 0.6-m double monochromator with 1200 lines/mm gratings and detected by a cooled photomultiplier tube with a GaAs photocathode. The resolution was 0.04 meV at a slit opening of $40 \mu\text{m}$. All the measurements described here were performed in a Faraday configuration with $\mathbf{k} \parallel \mathbf{B} \parallel [1\ 0\ 0]$.

3.3 Theory

The main problems in identifying the various transitions in the TES spectrum are the differences in intensity between different TES groups and the different intensity patterns

within each group [29]. In order to gain insight into these patterns it is first necessary to understand the corresponding principal (D^0, X) transitions. Rühle and Klingenstein [19] described the principal (D^0, X) lines as p -like nonrigid rotational states of the exciton around the neutral donor, which was in agreement with the effective g factors that they measured for four of these lines for both GaAs and InP. A more detailed study by Rorison *et al* [20] in InP also incorporated the degeneracy and anisotropy of the valence bands, as well as diamagnetic effects. They showed that the (D^0, X) can be primarily described as a free exciton orbiting a neutral donor (*i.e.*, the electrons are strongly correlated to their respective centres) but they also included contributions in which the two electrons strongly interacted with each other. Within their model they could successfully predict the energies and the intensity patterns in the principal (D^0, X) group and the $2p_{-1,0}$ TES groups. The $2s$ TES group is predicted to have a very weak intensity. This model, originally derived for InP, will be used to treat GaAs in this paper. Apart from this, a precise knowledge of the energy levels of the hydrogen atom in a magnetic field is necessary if we are to explain the TES spectrum well. The application of a magnetic field in the z direction reduces the spherical symmetry of the electron wave functions to cylindrical symmetry along the z direction. The eigenstates $\psi_{m\pi}$ of the Hamiltonian can be classified by m , the z component of angular orbital momentum, and, the z parity π [27]. In the limit of $B \rightarrow 0$, $\psi_{m\pi}$ reduces to the well-known product of a radial wave-function $R_{nl}(r)$ and a spherical harmonic $Y_{lm}(\theta, \phi)$, and can thus be characterized by the set of quantum numbers n, l and m , where n is the principal quantum number. In the limit $B \rightarrow \infty$, $\psi_{m\pi}$ reduces to the product of exactly one Landau state Φ_{Nm} and a longitudinal function $g_{Nm\nu}$. In this case, N, m and ν form a good set of quantum numbers, where N indicates the Landau level and ν is the number of nodes on the z axis. The correspondence between these two sets of quantum numbers in the limits $B \rightarrow 0$ and $B \rightarrow \infty$ can be taken from Simola and Virtamo [30], who applied the noncrossing rule of quantum mechanics. A state can thus be labelled by its asymptotic quantum numbers $nl_m | Nm\nu$. Rosner *et al* [27] calculated the values of the energy levels of the hydrogen atom with high numerical accuracy for fields of arbitrary strength expressed in terms of $\beta = B/B_0$, where $B_0 = 2\alpha^2 m_0^* c^2 / \epsilon_r^2 \hbar$, with $\alpha \simeq 1/137$, the fine structure constant. For $\beta \leq 1$, $\psi_{m\pi}$ was expanded in terms of spherical harmonics $Y_{lm}(\theta, \phi)$ using a numerical procedure and, together with the Hamiltonian of the system, was inserted in the Schrodinger extremum principle of nonrelativistic quantum mechanics. The resulting set of coupled differential equations was then solved. For $\beta \geq 1$ the same procedure was followed except that $\psi_{m\pi}$ was expanded in terms of Φ_{Nm} .

In this paper, the donors are first identified from the $2p_{-1}$ substates that reflect the total ΔE_{cc} . Then, the TES spectrum is calculated by subtracting the $1s_0 - n l_m$ energy differences from the lowest energy (D^0, X) state for the donors involved. Satellites corresponding to rotational levels are obtained by adding the energy differences between the (D^0, X) ground state and several rotational levels to the calculated TES spectrum of the (D^0, X) ground state. After that, the calculated TES spectrum is compared with the measured spectrum to assign the different peaks.

3.4 Experimental Results and Discussion

Figure 3.1 shows the zero-field PL spectra of sample 1-0212. Spectrum 1A was obtained with excitation 6 meV above the band gap, well above the impurity states. The dominant features are the result of the recombination of neutral acceptor- and donor-bound excitons, denoted (A^0, X) and (D^0, X) respectively, and recombination of ionized donor-bound excitons (D^-, X) , which have the same photon energy as recombination of free holes at neutral donors (D^0, h) at zero field. Rotational states $(D^0, X)_r$, labeled α, β, γ for convenience, are observed in between the lowest-energy (D^0, X) and the free-exciton recombination FX.

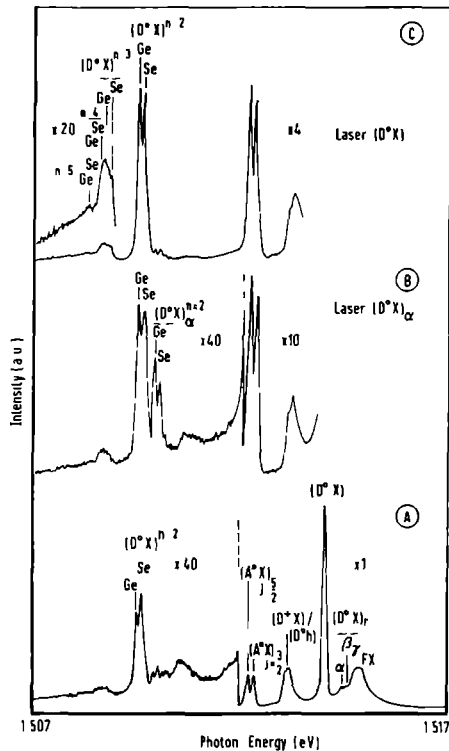


Figure 3.1 Zero-field photoluminescence spectra of the high-purity GaAs sample 1-0212 (A) shows the entire excitonic spectrum recorded with dye laser excitation 6 meV above the bandgap E_g (B) was recorded using resonant excitation of rotational level α (C) gives the spectrum with resonant excitation of the high intensity (D^0, X) peak. The relative gains used to record parts of the spectra are given in the figure. In order to achieve a clearly distinguishable peak labelling the notation for the second donor Se/Sn has been contracted to Se.

The two high-intensity TES peaks are transitions to the $n = 2$ terminal state of the impurity that correspond to the high intensity (D^0, X) line. The $n = 1$ to $n = 2$

energy separations that we measure are 4.42 and 4.53 meV. The latter value agrees closely with the value for Ge observed by Watkins *et al.* [10] and Almassy *et al.* [4] and is in excellent agreement with the data of Ozeki *et al.* [31]. Furthermore, it is also known from photothermal ionization data [32] that Ge is one of the dominant residual donors in MOVPE-grown GaAs. The former value, 4.42 meV, is in agreement with the value measured for S by several groups [4,10,23] who identified donors from satellites involving narrow-linewidth rotational states. The central cell corrections of Se and Sn, which have almost identical ΔE_{cc} [33,34], are, however, only 0.03 meV smaller than that of S. At 0 T, therefore, the width of this peak does not permit an unambiguous donor identification. At a field of 7 T the difference in ΔE_{cc} between the second donor and Ge is 0.20 meV. From (a) an extrapolation of the data of Ozeki *et al.* [31] for Si, Se, S and Ge to a field of 7 T, (b) the precisely determined values of ΔE_{cc} for Se and Ge obtained via neutron transmutation doping [35], and (c) the MPL data of Watkins *et al.* [10] at 7 T for Ge, S and Si, it is obtained that the distances of S and Se with respect to Ge are 0.16 and 0.21 meV, respectively. Hence, the second donor in sample 1-0212 is identified either as Se or as Sn. The notation for this second donor has been contracted to Sc in the figures in order to achieve a clearly distinguishable peak labelling. Additional, weaker Ge and Sc/Sn $n = 2$ peaks are seen at the high-energy side of the two main TES peaks. They arise from rotational levels $(D^0, X)_{\alpha, \beta, \gamma}$, as indicated in Fig. 3.1A. In Fig. 3.1B the two peaks involving $(D^0, X)_{\alpha}$ are strongly increased as a result of resonant excitation of the $(D^0, X)_{\alpha}$ level. The same $n = 1$ to $n = 2$ separations are measured. As shown in Fig. 3.1C, these two peaks are still observed, with low intensity, if the laser is tuned to the (D^0, X) ground state as a result of multistep excitation processes. In this spectrum, the broader peak at lower energy is observed most clearly. This peak corresponds to overlapping $n = 3$ and $n = 4$ TES transitions located, respectively, $(8/9 - 3/4) \cdot R^* = 0.794$ meV and $(15/16 - 3/4) \cdot R^* = 1.072$ meV lower in energy than the $n = 2$ transitions of Ge and Sc/Sn. In the figure the calculated Ge and Sc/Sn $n = 3$ levels are drawn, assuming that they arise from the (D^0, X) ground state. Furthermore, a feature is observed corresponding to the Ge $n = 5$ TES; the Sc/Sn $n = 5$ TES is overlapped by the Ge $n = 4$ peak. TES transitions with $n > 2$ have not previously been reported in either GaAs or InP.

Up to now, donor identification using the lowest $n = 2$ TES has not been possible at zero field. Almassy *et al.* [4] identified donors from a TES involving a narrow-linewidth rotational state, using an extremely precise spectrometer. Watkins *et al.* [10] used resonant excitation of the same narrow linewidth rotational state, and were thus able to identify donors with a less precise spectrometer. The best samples used in their work had a background impurity concentration $n_{77} = 8 \times 10^{13} \text{ cm}^{-3}$.

The fact that, in our study, donors can for the first time be identified from the broader TES involving the (D^0, X) ground state proves that the samples have very high quality. This is in agreement with the value of the donor concentration that we deduced for sample 1-0212 from the exciton spectrum [28].

Figure 3.2 shows the excitonic parts of the luminescence for both samples at $B = 7.0$ T, recorded with the laser tuned 0.2 meV below the bandgap. The principal (D^0, X) lines

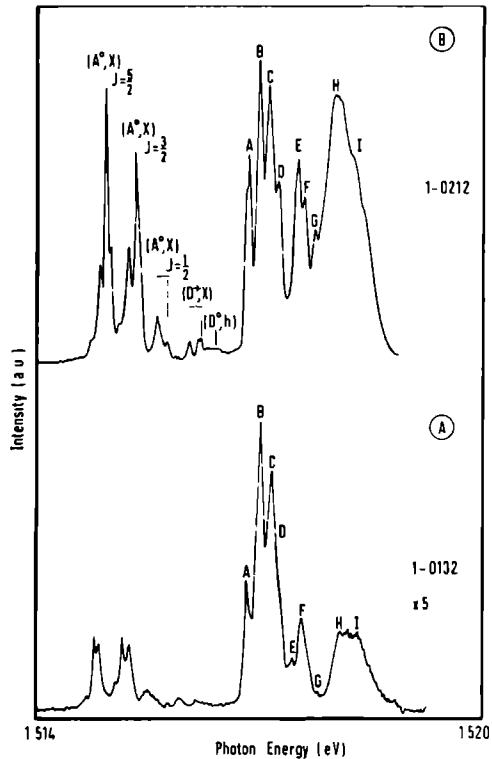


Figure 3.2 Magnetophotoluminescence spectra of the principal bound exciton and free-exciton transitions of the two GaAs samples studied in this work, recorded at 7 T. The laser was tuned 0.2 meV below the band gap at 7 T. The (D^0, X) and FX lines are labelled A to I.

have split and are sharper than in the 0 T case. For convenience, the peak positions of sample 1-0212 at 7 T are labelled A to I. In the less pure sample 1-0132, these peaks are broader and the intensities of the higher rotational levels are smaller. Hence, peak D is only observed as a shoulder on C, peaks E and F partly overlap, and peak G can hardly be distinguished.

The residual donors in sample 1-0132 are also found to be Ge and Se/Sn. The ratio of concentration between the different donor species can be determined directly from the relative TES peak heights in a nonresonant excitation measurement [23]. For samples 1-0132 and 1-0212 these ratios $[Ge]/[Se \text{ or } Sn]$ are 3 (see below) and 0.9 (Fig. 3.1A) respectively.

The TES spectrum can hence be interpreted more clearly in sample 1-0132, since for every TES transition, two peaks of unequal height are present, whereas in sample 1-0212 these peaks have equal intensities, which complicates the interpretation of the data unnecc-

essarily; therefore sample 1-0132 is emphasized in the following, where the TES spectrum is measured as a function of excitation energy. Resonant excitation measurements were performed on all peaks of both samples. The measurements on sample 1-0212 served as a reference.

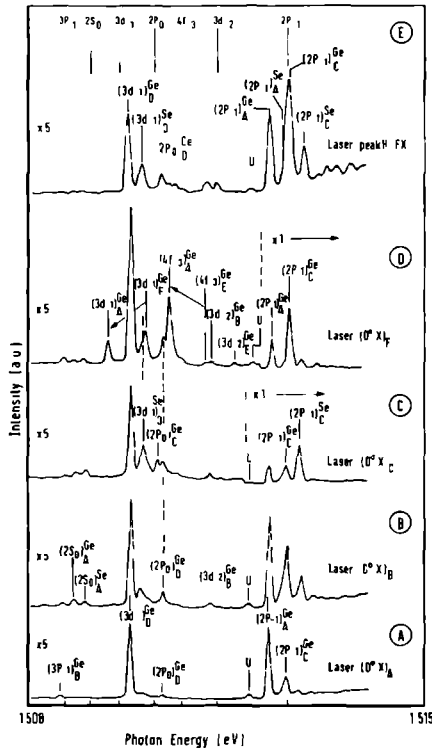


Figure 3.3 Two-electron satellite spectra of the GaAs sample 1-0132 obtained by resonant excitation of different principal (D^0, X) lines, as indicated on the right. Relative gains are given in the figure. Theoretical energy levels of the various substates with respect to (D^0, X)_A are indicated by the vertical lines at the top and bottom of the figure; no central cell correction is incorporated. In Fig. 3.3D, induced peaks are indicated by arrows. In order to achieve a clearly distinguishable peak labelling the notation for the second donor Se/Sn has been contracted to Se.

The corresponding MPL spectra of sample 1-0132 are plotted in Fig. 3.3, in which peak intensities can be compared directly. The lines above Fig. 3.3E indicate the calculated positions of the hydrogenic energy levels of the various magnetic substates with respect to the $1s$ peak (D^0, X)_A; no central cell correction has been applied to these values. The values were obtained by interpolation of Rosner's [27] energy levels, using the appropriate value $B_0 = 13\,175$ T for shallow donor electrons in GaAs. In Table I these energy differences

TABLE I: Energy differences at a field of 7 T between the $1s_0$ ground state and the various magnetic substates, which are represented by their low- and high-field limit quantum numbers respectively. The order of the states is that of increasing energy differences.

nl_m	$N m \nu$	$E(1s_0) - E(nl_m)$ meV
$2p_{-1}$	0 -1 0	4.315
$3d_{-2}$	0 -2 0	5.52
$4f_{-3}$	0 -3 0	6.14
$2p_0$	0 0 1	6.64
$3d_{-1}$	0 -1 1	7.25
$2s_0$	0 0 2	7.80
$3p_{-1}$	0 -1 2	8.20
$3p_0$	0 0 3	8.61
$4d_{-1}$	0 -1 3	8.73
$4f'_{-1}$	0 -1 4	8.99
$3s_0$	0 0 6	9.24
$4p_{-1}$	0 -1 6	9.28

between the $1s_0$ and the nl_m level are given for fields of 7 T. The TES peaks are labelled $(nl_m)_r^{\text{Se,Ge}}$, where nl_m refers to the quantum numbers in the low-field limit of the state, r indicates the corresponding principal (D^0, X), state and Se [or Sn] or Ge denotes the donor involved.

The $2p_{-1}$ satellites are discussed first. High-intensity $2p_{-1}$ peaks correspond to the principal states $(D^0, X)_A$ and $(D^0, X)_C$, where the subscripts refer to the labels in Figure 3.2. For both Ge and Se/Sn, they are indicated in Fig. 3.3E, recorded using resonant excitation of FX. The $(2p_{-1})_C^{\text{Ge}}$ state partly overlaps with the $(2p_{-1})_A^{\text{Se/Sn}}$ state. It appears that a nonresonant spectrum and a spectrum with the laser tuned to FX show the same intensity ratios for Ge and Se/Sn peaks. Accordingly, the concentration ratio $[\text{Ge}]/[\text{Se or Sn}] \approx 3$. Since the non-resonant spectrum does not add any extra information, it is not shown in Fig. 3.3. Excitation at different $(D^0, X)_r$ can cause an intensity shift between Ge and Se/Sn, as pointed out by Skromme *et al.* [23]. This is seen, *e.g.*, in Fig. 3.3C, where $(2p_{-1})_C^{\text{Se/Sn}} > (2p_{-1})_C^{\text{Ge}}$. Rorison *et al.* [20], who discussed primarily the four lowest rotational states in their theory, showed that for these four states, transitions to $2p_{-1}$ states are electric dipole allowed. The two highest energy states, however, appeared less intense in their experiments, which was in agreement with their calculations. These two low-intensity states, and the higher ones not discussed by Rorison *et al.*, appear more pronouncedly in our spectra if the laser excites FX, since all excitons are in thermal equilibrium with the free excitons [19] (see the peaks at the high energy side of $(2p_{-1})_C^{\text{Se/Sn}}$ in Fig. 3.3E).

A remarkable feature in the spectra is labelled u . It is present in all spectra with an

approximately constant intensity with respect to the main Se/Sn and Ge $2p_{-1}$ peaks. The fact that it is still observed if the lowest (D^0, X) state is excited (see Fig. 3.3A) indicates that a new donor has probably been found, with a relatively large central cell correction $\Delta E_{cc} = 0.64$ meV at 7 T. From photoconductivity experiments using back-doping [31] and neutron transmutation doping [35] the donor with the largest ΔE_{cc} is known to be Ge, having a $\Delta E_{cc} = 0.28$ meV at 7 T [10]. Bose [6] also found evidence for an unknown donor. This donor, however, had a ΔE_{cc} that was 0.05 meV smaller than that of Ge. Hence, it cannot be identical to the donor found here. In sample 1-0212 feature u is absent in all spectra. This supports the attribution of this feature to a new donor.

Apart from the sharp $2p_{-1}$ peaks, another sharp and intense feature at 1.5098 eV is observed in all 7-T TES spectra. It is usually ascribed to “one of the $2p_0$ peaks” [5,6,7,23,25]. However, a comparison of its location with the theoretical $2p_0$ level clearly shows that it can neither be attributed to a Se/Sn nor to a Ge $2p_0$ TES involving any rotational level. Furthermore, it cannot be attributed to a $2s$ state either.

A careful analysis of the energy levels shows that the only possibility is that this peak is the $3d_{-1}$ TES of Ge corresponding to $(D^0, X)_D$. In sample 1-0212, the principal peak $(D^0, X)_D$ appears more clearly. If this state is excited, the linewidth of the $3d_{-1}$ peak reduces by a factor 0.8 compared with excitation at other rotational states. Such a reduction in linewidth is also seen for the $2p_{-1}$ lines when the corresponding $(D^0, X)_r$ state is excited. This supports the above attribution to $(3d_{-1})_D^{Ge}$. The corresponding state $(3d_{-1})_D^{Se/Sn}$ is present with a lower intensity. Since for every donor only one $3d_{-1}$ TES arises if FX is excited, namely that which arises from the $(D^0, X)_D$ state, the determination of the relative donor concentration from this substate is more accurate: $[Ge]/[Se \text{ or } Sn] = 2.85 \pm 0.05$.

If state $(D^0, X)_F$ is excited (Fig. 3.3D), it is not only the $(3d_{-1})_D^{Ge}$ TES which is observed, but also the $(3d_{-1})_F^{Ge}$ TES which corresponds to the excited principal state. Most remarkably, $(3d_{-1})_A^{Ge}$ is also observed in this case. The latter peak is not observed if the laser excites either $(D^0, X)_{A,B,C}$ or a higher rotational state. Measurements at lower field indeed confirm the appearance of this induced peak when $(D^0, X)_F$ is excited.

A similar process, induced by $(D^0, X)_F$, is also observed for $4f_{-3}|0 -3 0$ satellites. The $(4f_{-3})_A^{Ge}$ is observed in this substate. In Fig. 3.3D these induced peaks are indicated by arrows. A low intensity $(3d_{-2})_B^{Ge}$ state is observed in all spectra except for spectrum 3A, which confirms the attribution. Furthermore, since state $(D^0, X)_F$ is only 0.08 meV higher in energy than $(D^0, X)_E$, the finite energy width of the states allows the observation of $(3d_{-2})_E^{Ge}$ when $(D^0, X)_F$ is excited. According to Rorison *et al.* [20], allowed $2p_0|0 0 1$ transitions are predicted for the two highest rotational states that they discussed. One of these states, $(2p_0)_D^{Ge}$, is observed in all spectra. The other one, $(2p_0)_C^{Ge}$, is only detected if the laser excites $(D^0, X)_C$ (Fig. 3.3C). Furthermore, the electric dipole forbidden $2s_0|0 0 2$ satellites which are predicted to be very weak, especially at high fields, are indeed only very weak in our spectra. They basically involve the ground state $(D^0, X)_A$. Finally, at an energy just below the $2s_0$ states, a $3p_{-1}|0 -1 2$ state corresponding to $(D^0, X)_B$ is observed with a low intensity.

The usual explanation for the strength of the $2p_{-1}$ satellites is given by a model which assumes that they are electric dipole allowed transitions within a spherical approximation.

This means that the selection rule $\Delta m = \pm 1$ for a Faraday configuration holds. Rorison *et al.* showed that the electrons in the (D^0, X) complex are strongly correlated with their respective centers. In the (D^0, X) complex the “donor electron” thus moves close to the donor core in the $1s_0$ orbit. The high-intensity $2p_{-1}$ TES peaks have high-magnetic-field quantum numbers $Nm\nu = 0 -1 0$. These states are thus not only compressed in the direction perpendicular to the applied magnetic field, but also in the direction parallel to the field (since $\nu = 0$) and they are therefore tightly bound states [27]. It is thus seen that the highest intensity TES peaks correspond to terminal donor states where the electron is still close to the donor center.

The high-magnetic-field quantum numbers of $3d_{-1}$ are $Nm\nu = 0 -1 1$. The observed high intensity transition from $(D^0, X)_D$ to this odd parity state $3d_{-1}$ [parity $\pi = (-1)^\nu$], which also has $\Delta m = -1$, indicates that this particular rotational state has even parity, since Dean *et al.* [36] showed that transitions which change parity are the dominant ones. The $(3d_{-1})_F$ TES, observed if state $(D^0, X)_F$ is excited, shows that $(D^0, X)_F$ is also an even parity state. Remarkably, $(3d_{-1})_A$ also appears if $(D^0, X)_F$ is excited. Since it does not appear when the ground state $(D^0, X)_A$ is excited directly, the $(D^0, X)_F$ complex must play a crucial role. The most probable explanation for the process is that the $(D^0, X)_F$ complex emits an acoustic phonon with an energy of 0.68 meV, and relaxes to the ground state $(D^0, X)_A$. An estimate of the wavelength of the acoustic phonon $\lambda_{ac\ ph} = c_s h / E_{phonon}$, where $c_s = 3.57 \times 10^5 \text{ cm s}^{-1}$ is the mean sound velocity in GaAs [37] and $E_{phonon} = 0.68 \text{ meV}$, shows that $\lambda_{ac\ ph} \cong 200 \text{ \AA}$. Since this wavelength approximately equals the size of a (D^0, X) complex, the phonon-exciton coupling will be very strong (quasi-resonant) and therefore a favourable mechanism for the induced process in which parity selection rules are broken. A second possibility for the process is that the interaction between the $(D^0, X)_F$ and the $(D^0, X)_A$ exciton states, which are both formed if the laser excites $(D^0, X)_F$, causes the induced peak.

The orbits $3d_{-2}$ and $4f_{-3}$, with their respective high-field quantum numbers $0 -2 0$ and $0 -3 0$, are also tightly bound states and, as can be seen from Table I, they are the states with the lowest energy distance to $1s_0$ after $2p_{-1}$. Since $\Delta m \neq \pm 1$ they are electric dipole forbidden. Strain, disorder and the additional Coulomb potential arising from all other charged impurity ions in the lattice can, however, relax this selection rule [21]. This is the reason that a small $(3d_{-2})_B$ peak is still observed. In less pure samples the strength of this peak increases correspondingly. Using this kind of argument, states with $|\Delta m| > 2$ are expected to be even less intense than the $3d_{-2}$ state. Hence the strong $(4f_{-3})_A$ peak that is induced by $(D^0, X)_F$ has to be explained in a similar manner to the observation of $(3d_{-1})_A$, using one of the two postulated coupling mechanisms; this coupling now induces a change of $\Delta m = -3$. Since no induced $3d_{-2}|0 -2 0$ TES of comparable strength is observed, the coupling mechanism cannot induce a change $\Delta m = -2$. We believe that the resonant acoustic phonon-exciton coupling is the most probable mechanism since in both induced cases the wavelength of the phonon involved in the process is comparable to the typical size of a (D^0, X) complex, and no induced peaks are observed from higher or lower rotational states to the $(D^0, X)_A$ ground state, in which the phonon wavelength does not match the size of the bound exciton.

3.5 Conclusions

In this paper, we have shown that the two electron satellite spectrum of the donor-bound exciton (D^0, X) in magnetic fields can be explained using the quantum numbers in the high-field limit $N m \nu$. Apart from the tightly bound states ($\nu = 0$) $2p_{-1}|0 -1 0$ that show an intensity pattern as explained by Rorison *et al.* [20], less intense transitions to the subsequent tightly bound states $3d_{-2}|0 -2 0$ and $4f_{-3}|0 -3 0$ are also observed. Furthermore, transitions to the state $3d_{-1}|0 -1 1$ are seen: a high-intensity peak originates from rotational level (D^0, X)_D. Up to now, this state has been attributed to one of the $2p_0$ states. If the laser excites (D^0, X)_F, two additional $3d_{-1}|0 -1 1$ states appear. One of these states reflects the excited state; the other one, however, involves the ground state (D^0, X)_A. A $3d_{-1}$ TES of this ground state appears neither if this state is excited directly nor if any other rotational state is excited. A similar induced process is observed for $4f_{-3}|0 -3 0$. The process can be explained by an acoustic phonon-exciton interaction, which is very strong due to the similarities of the phonon wavelength to the exciton size.

One of the transitions to the allowed states of $2p_0|0 0 1$ is observed in all spectra, but the other is only observed if the corresponding principal state is excited. The intensity of the $2s_0|0 0 2$ states is much smaller, which is in agreement with Rorison's data.

In one of the samples (1-0132), a new donor has probably been found, with a relatively large $\Delta E_{cc} = 0.64$ meV at 7 T. Evidence for this new donor is based upon the fact that the feature *u* is absent in sample 1-0212 and other samples investigated previously. Furthermore, this feature is still observed if the ground state (D^0, X)_A is excited. Finally, its intensity ratio with respect to Ge and Se/Sn remains comparable.

Finally, in the very high-purity sample 1-0212, donors have for the first time been identified at 0 T from the broad $n = 2$ TES reflecting the lowest (D^0, X), and transitions with $n = 3, 4$ and 5 are reported at zero field.

Acknowledgements

The authors are grateful to A.W. Gal of Billiton Precursors B.V. for providing the samples, and to J. Singleton for helpful discussions and for a critical reading of the manuscript.

References

1. P.J. Dean, M.S. Skolnick and L.L. Taylor, *J. Appl. Phys.* **55**, 957 (1984).
2. M.S. Skolnick, P.J. Dean, L.L. Taylor, D.A. Anderson, S.P. Najda, C. Armistead and R.A. Stradling, *Appl. Phys. Lett.* **44**, 881 (1984).
3. M.S. Skolnick, P.J. Dean, S.H. Groves and E. Kuphal, *Appl. Phys. Lett.* **45**, 962 (1984).
4. R.J. Almassy, D.C. Reynolds, C.W. Litton, K.K. Bajaj and G.L. McCoy, *Solid State Commun.* **38**, 1053 (1981).
5. S.S. Bose, B. Lee, M.H. Kim and G.E. Stillman, *Appl. Phys. Lett.*, **51**, 937 (1987).

6. S.S. Bose, M.H. Kim and G.E. Stillman, *Appl. Phys. Lett.* **53**, 980 (1988).
7. T.D. Harris, M.S. Skolnick, J.M. Parsey, Jr., and R. Bhat, *Appl. Phys. Lett.* **52**, 389 (1988).
8. D.C. Reynolds, K.K. Bajaj, C.W. Litton and E.B. Smith, *Phys. Rev. B* **28**, 3300 (1983).
9. D.C. Reynolds, P.C. Colter, C.W. Litton and E.B. Smith, *J. Appl. Phys.* **55**, 1610 (1984).
10. S.P. Watkins, G. Haacke and H. Burkhard, *Appl. Phys. Lett.* **52**, 401 (1988).
11. S.P. Watkins, G. Haacke, H. Burkhard, M.L.W. Thewalt and S. Charbonneau, *J. Appl. Phys.* **64**, 3205 (1988).
12. Recent cyclotron-resonance measurements on bulk GaAs by Hopkins *et al.* [13], Zawadzki and Pfeffer [14], and Sigg *et al.* [15], revealed an accurate low-energy cyclotron effective mass of $m_0^* = 0.0660 \cdot m_0$. Hence, from $R^* = \frac{m_0^*}{\epsilon_r} \cdot Ry$ with $R^* = 5.715$ meV (see text) and $Ry = 13.61$ eV, we obtain a value $\epsilon_r = 12.51$ for the relative dielectric constant.
13. M.A. Hopkins, R.J. Nicholas, P. Pfeffer, W. Zawadzki, D. Gauthier, J.C. Portal and M.A. DiForte-Poisson, *Semicond. Sci. Technol.* **2**, 568 (1987).
14. W. Zawadzki and P. Pfeffer, in *High Magnetic Fields in Semiconductor Physics*, Vol. 71 of *Springer Series in Solid-State Sciences*, edited by G. Landwehr (Springer, Berlin, 1987), p. 523.
15. H. Sigg, J.A.A.J. Perenboom, P. Pfeffer and W. Zawadzki, *Solid State Commun.* **61**, 685 (1987).
16. C. Aldrich and R.L. Greene, *Phys. Stat Sol.(b)* **93**, 343 (1979).
17. G.E. Stillman, David M. Larsen, C.M. Wolfe, *Solid State Commun.* **7**, 2245 (1971).
18. P.J. Dean and M.S. Skolnick, *J. Appl. Phys.* **54**, 346 (1983).
19. W. Rühle and W. Klingenstein, *Phys. Rev. B* **18**, 7011 (1978).
20. J. Rorison, D.C. Herbert, P.J. Dean and M.S. Skolnick, *J. Phys. C* **17**, 6435 (1984).
21. D.M. Larsen, *Phys. Rev. B* **8**, 535 (1973).
22. H.R. Fetterman, D.M. Larsen, G.E. Stillman, P.E. Tannenwald and J. Waldman, *Phys. Rev. Lett.* **26**, 975 (1971).
23. B.J. Skromme, R. Bhat, H.M. Cox and E. Colas, *IEEE Journ. of Quantum Electronics* **25**, 1035 (1989).
24. G. Haacke, S.P. Watkins and H. Burkhard, *Appl. Phys. Lett.* **54**, 2029 (1989).
25. S.K. Shastry, S. Zemon, D.G. Kenneson and G. Lambert, *Appl. Phys. Lett.*, **52**, 150 (1988).
26. $|\psi_{nlm}^e|_{r=0}^2 = 0$ if $l \neq 0$ since the radial part of the wave-function behaves as $R(r) = Ar^l$ for $r \rightarrow 0$.
27. W. Rösner, G. Wunner, H. Herold and H. Ruder, *J. Phys. B: At. Mol. Phys.* **17**, 29 (1984).
28. see Chapter 10.
29. P.J. Dean and M.S. Skolnick, *J. Appl. Phys.* **54**, 346 (1983).
30. J. Simola and J. Virtamo, *J. Phys. B: At. Mol. Phys.* **11**, 3309 (1978).
31. M. Ozeki, K. Kitahara, K. Nakai, A. Shibatomi, K. Dazai, S. Okawa and O. Ryuzan,

- Jap. J. Appl. Phys. **16**, 1617 (1977).
32. T.S. Low, B.J. Skromme and G.E. Stillman, in *Proceedings of the International Symposium on GaAs and Related Compounds*, Inst. Phys. Conf. Ser. **65** (Institute of Physics, London, 1983), 515 (1982).
 33. P.D. Dapkus, H.M. Manasevit, K.L. Hess, T.S. Low and G.E. Stillman, *J. Crystal Growth* **55**, 10 (1981).
 34. T.S. Low, G.E. Stillman, A.Y. Cho, H. Morkoc and A.R. Calawa, *Appl. Phys. Lett.* **40**, 611 (1982).
 35. T.S. Low, M.H. Kim, B. Lee, B.J. Skromme, T.R. Lepkowski and G.E. Stillman, *J. of Electronic Materials* **14**, 477 (1985).
 36. P.J. Dean, D.C. Herbert, and A.M. Lahee, *J. Phys. C* **13**, 5071 (1980).
 37. W.Pötz and P. Kocevar, *Phys. Rev. B* **28**, 7040 (1983).

Chapter 4

Influence of magnetic fields on an extremely narrow exciton line in a high-carrier-density heterojunction

F.A.J.M. Driessen^a, S.M. Olsthoorn^a, T.T.J.M. Berendschot^a, H.F. Pen^a, L.J. Giling^a,
G.A.C. Jones^b, D.A. Ritchie^b, and J.E.F. Frost^b

^a*Department of Experimental Solid State Physics, Research Institute for Materials, University of Nijmegen, Toernooiveld, NL 6525 ED Nijmegen, The Netherlands*

^b*Cavendish Laboratory, University of Cambridge, Madingley Road, Cambridge CB3 0HE, United Kingdom*

Abstract

High-resolution magnetophotoluminescence measurements are reported on a GaAs-Al_xGa_{1-x}As heterojunction that has two occupied subbands at zero magnetic field. A very efficient, extremely narrow-band luminescence involving the two-dimensional electron gas is observed above a certain critical field strength in spite of the large built-in electric field acting on the photoexcited holes. The photoluminescence peak shows pronounced magneto-oscillations in peak energy, as well as in luminescence intensity and peak width. The luminescence is attributed to the exciton of the second subband, which hybridizes with the Landau level of the first subband in which the Fermi level resides. This many-body interaction is most efficient at odd filling factors, *i.e.*, if the Fermi level lies in the extended states. The oscillations in photon energy and full width at half maximum originate from $n_c = 1$ Landau-level crossings with the lowest $n_c = 2$ Landau level. The optical data show that the exciton of the second subband is consecutively populated and depopulated. Tilted-field measurements enable the determination of the intrasubband diamagnetic shift in a parallel field $\delta E_{12}/\delta B$.

Published in:
Physical Review B **45**, 11823-11828 (1992)

4.1 Introduction

Magneto-optical studies of two-dimensional electron gases (2DEG's) in semiconductor heterostructures have revealed a variety of information on, for example, Landau quantization [1], electron-electron interactions [2], and both the integer and fractional quantum Hall effect [3-5]. In order to observe photoluminescence (PL) from the 2DEG a large concentration of holes is required. This has been realized either by hole confinement in a modulation-doped quantum well (MDQW) [1,6] or by growing an additional δ -layer of acceptors at a well-defined distance from the heterointerface in the GaAs buffer layer [2,7,8]. In other work, structures with a thin GaAs buffer layer were chosen in order to prevent bulk luminescence from dominating the spectrum [9,10].

Recently, Chen *et al.* [11] reported very pronounced magneto-oscillations in the PL intensity of an excitonlike interband transition in an (In,Ga)As MDQW in which the Fermi level was just below the $n_c = 2$ subband. This behaviour, which had $1/B$ periodicity, originated from a many-body interaction between the $n_c = 2$ conduction subband and the Landau level of the $n_c = 1$ conduction subband in which the Fermi level resided. The interaction was found to be largest when the Fermi level lay within the extended states, *i.e.* at odd-integer Landau-level filling factors. This is known as the optical Shubnikov-de Haas (OSdH) effect. Using three-band model calculations without including magnetic field, Mueller [12] showed that a reduction of the separation between an unoccupied second subband and the Fermi level caused an excitonic enhancement owing to hybridization between the $n_c = 1$ Fermi-edge resonance [13] and the excitonic resonance of the $n_c = 2$ subband. This led to a strong enhancement of the optical matrix element for this mixed state, even in the absence of a real $n_c = 2$ population because virtual $n_c = 2$ excitons are formed as a result of intrasubband scattering. Moreover, it is also the case under conditions of PL experiments because of the presence of photoexcited nonequilibrium electrons and holes.

In this paper we present magnetophotoluminescence spectra of a high-carrier-density GaAs-Al_xGa_{1-x}As heterojunction with two populated subbands for which the holes were subjected to a very strong built-in electric field. This is in contrast to the previously mentioned magneto-optical publications on 2D systems, in which holes were either localized or trapped in thin buffer layers, quantum-well structures or at additional acceptor sites. An extremely narrow PL line was observed when the strength of the magnetic field first caused depopulation of the second subband. This emission tended to dominate the spectrum at increasing fields. As with the emission reported in Ref.[11], this luminescence involves second-subband electrons and photoexcited holes with a small exciton binding energy, and is caused by the many-body interaction of the Fermi-edge electrons with the lowest Landau level of the second subband. Apart from the oscillations in PL intensity with SdH periodicity in a MDQW with one occupied subband which were previously reported by Chen *et al.*[11], we have been able also to resolve oscillations in both energy and width of the luminescence as a result of the extreme sharpness of the PL line (≈ 30 times narrower than that in Ref.[11]). The small width of the emission also enables us clearly to distinguish between various exciton peaks originating from the buffer layer and those

from the 2D luminescence. Furthermore, we report the determination of the intrasubband diamagnetic shift, which was obtained from tilted-field measurements.

4.2 Experimental Details

The experiments were carried out on a high-carrier-density GaAs-Al_xGa_{1-x}As heterojunction grown by molecular-beam epitaxy (MBE). The structure was grown on a semi-insulating GaAs substrate and consisted of a 20-period GaAs-AlAs superlattice buffer, a 1- μm -thick undoped GaAs buffer layer, an 80 nm Al_{0.33}Ga_{0.67}As layer, and finally, a 10-nm GaAs capping-layer. The Al_{0.33}Ga_{0.67}As was undoped except for one monolayer 10 nm from the heterointerface, which was doped with $5 \times 10^{16} \text{m}^{-2}$ Si atoms on Ga sites. Monolayer doping of the barrier of a GaAs-Al_xGa_{1-x}As heterojunction results in higher carrier densities n and increased mobilities μ of the 2DEG [14]. Values of these quantities for the aforementioned heterojunction measured in the dark were $n_{\text{dark}} = 6.4 \times 10^{15} \text{m}^{-3}$ and $\mu_{\text{dark}} = 39 \text{m}^2 \text{V}^{-1} \text{s}^{-1}$ for our sample [15]; after saturation of the persistent photoconductivity [16] by illumination with a red LED the values were $n_{\text{light}} = 11.3 \times 10^{15} \text{m}^{-3}$ and $\mu_{\text{light}} = 39 \text{m}^2 \text{V}^{-1} \text{s}^{-1}$ [15]. Other sample parameters can be found in the work of Kusters *et al.* [15,17].

PL measurements were performed with the sample mounted in a strain-free way in the bore of a 7T split-pair superconducting magnet. Optical excitation was provided by a tunable cw ring dye laser using Styryl 9 as dye at typical excitation densities of 10^3Wm^{-2} . The luminescence was dispersed by a 0.6-m double monochromator with 1200-lines/mm gratings and was detected by a cooled photomultiplier tube with a GaAs photocathode. The measurements were mostly performed in a Faraday configuration with $\mathbf{k} \parallel \mathbf{B} \parallel [1\ 0\ 0]$. The persistent photoconductivity [16,18] was saturated during the measurements because the laser energy was slightly higher than that of the GaAs band gap. From this it may also be inferred that both ionization of deep donor states (DX centres) in the Al_xGa_{1-x}As and generation of electron-hole pairs in the GaAs occurred. A reduction of the carrier density due to neutralization of DX centers in the Al_xGa_{1-x}As under continuous photoexcitation (as reported by Kukushkin *et al.* [20]) did not influence our measurements because in our case the excitation energy was too low to neutralize the DX centers.

4.3 Results and Discussion

Figure 4.1 shows the excitonic part of the PL spectrum of the sample at various magnetic-field strengths recorded at $T=1.5$ K. The zero-field spectrum is dominated by the PL of the GaAs buffer layer; it shows free excitons FX, as well as excitons bound to residual acceptors (A^0, X) and donors (D^0, X). The dominance of the PL signal of the GaAs buffer layer over any possible luminescence involving confined electrons at the GaAs-Al_xGa_{1-x}As interface is, of course, due to the large built-in electric field near the heterointerface. Hence, photoexcited holes will quickly move away from the interface to the GaAs buffer layer where recombination with photoexcited electrons can occur.

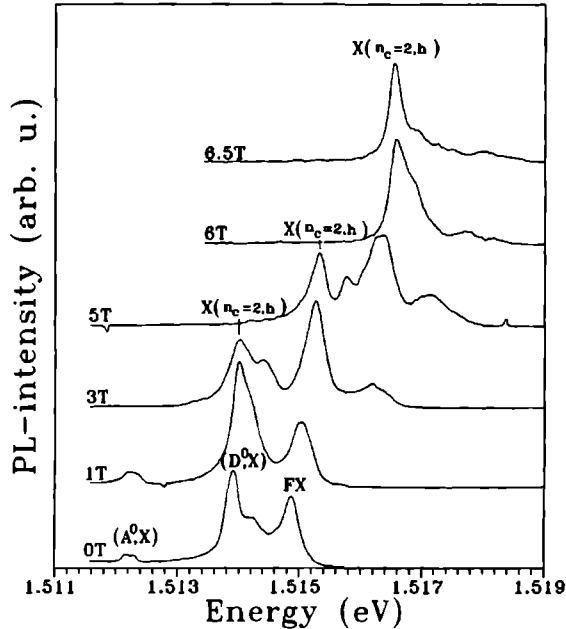


Figure 4.1 Excitonic parts of the PL spectra at various magnetic-field strengths.

This situation changes if a magnetic field is applied. An intense and narrow PL line, which is absent in the spectrum of bulk GaAs and labelled $X(n_c = 2, h)$, is observed if the magnetic field has passed a certain critical field value of about 2.5 T. As can be seen in Figure 4.2, the energy of this PL peak shows oscillations which are periodic in $1/B_{\perp}$, where B_{\perp} the component of the field perpendicular to the interface. That the periodicity of these oscillations depends only on the perpendicular component is shown by the upper trace in Figure 4.2 in which the magnetic field was at an angle of 45° with respect to the 2DEG. Changes in photon energy in the tilted field will be discussed later in this paper. Therefore, despite the large built-in electric field acting on the holes, luminescence of the 2DEG is observed in a magnetic field. As the field strength increases, the intensity of this line becomes so strong that it eventually dominates the entire spectrum as is shown in Figure 4.1.

Apart from the well-resolved oscillations in photon energy, magneto-oscillations are also observed both in peak intensity and in peak width (see Figure 4.3). Maxima in the peak intensity occur at odd filling factors. A similar periodically enhanced PL signal at odd filling factors was observed by Chen *et al.*[11] in a MDQW with one occupied subband. This PL signal resulted from nonequilibrium $n_c = 2 \rightarrow n_v = 1$ excitonlike

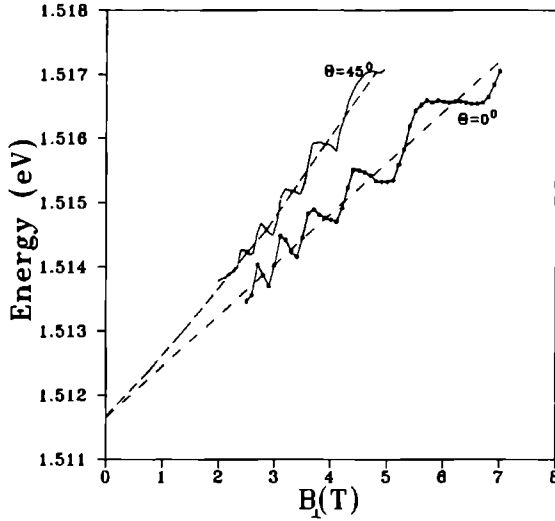


Figure 4.2 Energy position of peak $X(n_c = 2, h)$ versus the perpendicular component of magnetic field. The upper line shows the behaviour of the peak if the field is tilted 45° with respect to the 2DEG.

emission, which hybridized with the energetically proximate 2DEG. The strength of this many-body (Coulomb) interaction was maximal if E_F lay in the extended states of the particular Landau level (LL) of the lowest subband.

In our sample the electron concentration of the second subband is $n_2 = 1.0 \times 10^{15} \text{m}^{-2}$ at zero field, and the zero-field Fermi level is located, therefore, approximately 3.5 meV above $n_c = 2$ [15]. In a magnetic field the position of E_F oscillates, owing to the highly singular density of states and the field proportionality of the Landau-level degeneracy [19,21]. Using the relationship between magnetic field and Fermi level in Ref.[21], we estimate that E_F shifts below the lowest spin split LL of the second subband at a field of about 2.5 T. Consequently, above this field strength hybridization can be observed between the exciton of the lowest LL of the second subband and the particular LL of the $n_c = 1$ subband in which E_F resides. Because the luminescence is first observed (or at least gains enormously in strength) above the field strength at which the second subband initially depopulates and, furthermore, because maxima in PL intensity are observed at odd ν , we expect the origin of the PL signal to be similar to that described by Chen *et al.*[11]. Apart from the fact that our sample has two populated subbands, the most important physical difference from the system of Chen *et al.*[11] is that in our system the photoexcited holes are not located close to the interface in a hole subband, and as a result the magneto-optical characterization of a single heterojunction with thick buffer

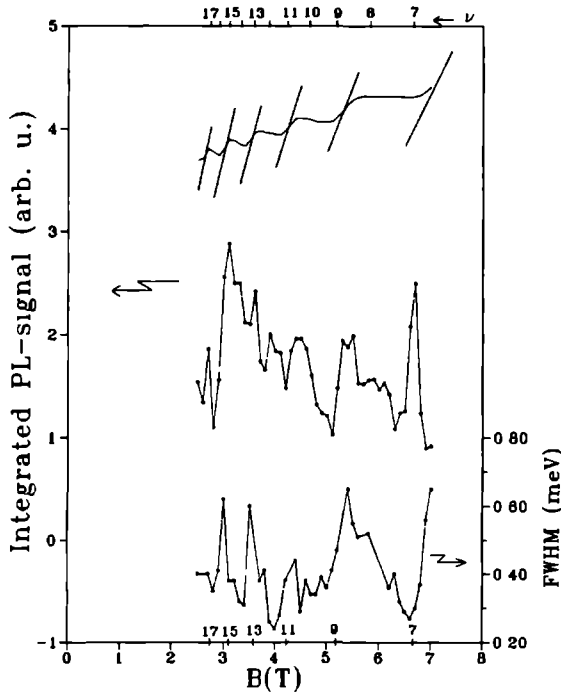


Figure 4.3 Integrated PL intensity (left axis) and full width at half maximum (right axis) of peak E_f as a function of magnetic field. For clarity, the photon-energy data of Figure 4.2 are also shown in this figure. The top axis shows the filling factor ν , at the bottom axis odd ν values are repeated.

layers is possible. The exciton binding energy between the $n_c = 2$ subband electrons and the holes is expected to be considerably smaller than that in the work of Chen *et al.* [11] due to the lack of hole confinement.

Assuming that the luminescence involves the exciton of the lowest LL of the second subband, hereafter denoted $X(n_c = 2, h)$, then the Landau fan diagram of the sample can be calculated as follows. It is shown below that the exciton binding energy is negligible and, therefore, that the dashed line in Figure 4.4 reflects the photon energy of the $n_c = 2$ subband were it not influenced by the LL's of the $n_c = 1$ subband. A second subband effective electron mass of $m_2^* = 0.069 m_0$ (where m_0 is the free electron mass) was calculated from the slope of the $n_c = 2$ LL. Linear extrapolation of this lowest $n_c = 2$ LL yields a zero-field energy of 1.51165 eV for $X(n_c = 2, h)$.

The zero-field energies of the Fermi level E_f and the subband $n_c = 1$ follow from

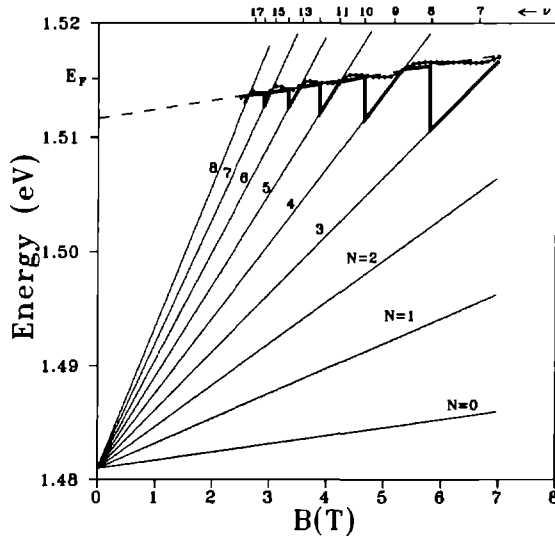


Figure 4.4 Measured position of $X(n_c = 2, h)$, the Landau-level fan diagram and the calculated position of E_F versus the magnetic field in the field region of interest (bold line). The dashed line is the lowest Landau level of the $n_c = 2$ subband. The top axis shows the filling factor ν .

the relationships $E(n_c = 2) - E(n_c = 1) = 30.3$ meV and $E_F - E(n_c = 2) = 3.5$ meV, as determined by magnetotransport measurements[15].

Cyclotron-resonance (CR) measurements revealed an effective electron mass $m_1^* = 0.074 m_0$ for this sample. This value cannot directly be used because it is known that effective masses as measured by magneto-optics are generally higher than those obtained by CR owing to the sensitivity of magneto-optics to electron-electron interactions [3]. In contrast, the energy separation between a full and an empty LL as measured by CR is not affected by electron-electron interactions[22]. Plaut *et al.*[3] measured effective masses as a function of electron concentration n (up to $n = 7 \times 10^{15} \text{m}^{-2}$) by magneto-optics. At high carrier concentrations the effective mass increased owing to effects of nonparabolicity. The energy dependence of the effective mass is described by the relationship [23,24] $m^* = m_0 / (1 + 2\kappa_2 \epsilon / E_g)$, where the relative Fermi level $\epsilon = E_F - E_g$ is proportional to n , and the coefficient $\kappa_2 \approx -1.4$ [25] is a measure of the low-energy nonparabolicity. Because the second term in the denominator is much less than unity, the equation can be written as $m^* \approx m_0 (1 - 2\kappa_2 \epsilon / E_g)$. We used this relationship to extrapolate the magneto-optical effective mass $0.079 m_0$ for our sample with $n = 11.3 \times 10^{15} \text{m}^{-2}$. This value for the effective electron mass was used to construct the Landau fan diagram of the $n_c = 1$

subband.

The calculated energy of E_F at $T = 0$ assuming δ -function-shaped Landau levels is now shown by the bold line in Figure 4.3 in the field range of interest. It is seen that field intervals in which the Fermi level follows a Landau level of $n_c = 1$ (*i.e.*, regions with a depopulated second subband) are consecutively followed by field intervals in which E_F populates the lowest LL of $n_c = 2$.

The plot shows that at filling factors $\nu = 7$ and 9 the second subband is not populated. Hence, effective coupling occurs between the extended states of the uppermost occupied $n_c = 1$ LL and $X(n_c = 2, h)$, thus resulting in the sharp intensity maxima at $\nu = 7$ and 9 shown in Figure 4.3. At slightly higher values of the magnetic field, maxima in the width of the PL line are observed, namely at $B = 5.4$ T and $B \geq 7.0$ T for $\nu = 9$ and $\nu = 7$, respectively. These field values correspond exactly to the crossing between the $N=4$ and $N=3$ Landau levels of $n_c = 1$ with the $X(n_c = 2, h)$. At the crossing points of these levels both the energy and width of the $X(n_c = 2, h)$ are most influenced by the $n_c = 1$ LL's, the latter having a much larger width than the narrow exciton emission. The photon energy of $X(n_c = 2, h)$ is influenced least at field values in between two successive crossings. The field values of minimum influence were used to construct the dashed line in Figure 4.4. This leads to a perfectly linear dependence of the photon energy upon magnetic field with no detectable quadratic behaviour. From this it can be concluded (as was claimed above) that the exciton binding energy is very small.

It is seen in Figure 4.4 that below $B \approx 4$ T the second subband is again populated at odd filling factors (*cf.* $\nu=13, 15$ and 17). This follows both from the crossing levels in the fan diagram as well as from the lower field values at which maxima in line width occur compared to the field values of maximal intensity. The origin of these maxima in PL intensity, which are less pronounced at $\nu = 13, 15$ and 17, are partly caused by oscillations in the population of the $n_c = 2$ subband with magnetic field, as was pointed out by Skolnick, Simmonds and Fisher [26] for an MDQW. An enhancement of the PL intensity is expected if this state is populated as a result of the greater spatial extension of the $n_c = 2$ subband wave function compared to that of $n_c = 1$. These intensity oscillations due to population of the second subband are also expected for even filling factors [5]. In fact, we observe less pronounced maxima in the intensity at even filling factors too ($\nu = 8, 10, 12, 14$); however, since the maxima at odd ν are considerably more intense, we conclude that in spite of the slight population of $n_c = 2$ at $\nu=13, 15$ and 17, coupling with the delocalized electrons still occurs.

It was already seen in Figure 4.2 that the oscillatory behaviour in photon energy of $X(n_c = 2, h)$ depended only on the magnetic-field component which was perpendicular to the 2DEG. It is also seen in Figure 4.2 that the photon energy of the second subband exciton is higher in the tilted-field measurement. This additional shift in parallel magnetic field is obtained from the difference between the two dotted lines because $B_{\perp} = B_{\parallel}$ here. If we assume a quadratic relationship between B_{\perp} and $E_{21}(B_{\parallel})$, where E_{21} is the difference between the two subbands [19], namely,

$$E_{21}(B_{\parallel}) = E_{21} + \alpha B_{\parallel}^2,$$

then from our data α is found to be $(8.0 \pm 0.5) \times 10^{-5} \text{eVT}^{-2}$. This value corresponds within experimental error with the value $\alpha = (8.6 \pm 0.4) \times 10^{-5} \text{eVT}^{-2}$ which we calculated using the experimental data of Kusters [15], who performed parallel-field magnetoresistance measurements on the same sample [29]. This correspondence for the intrasubband diamagnetic shift of $E_{21}(B_{\parallel})$ is a further strong indication that the luminescence involves the second subband and that exciton binding energies are small.

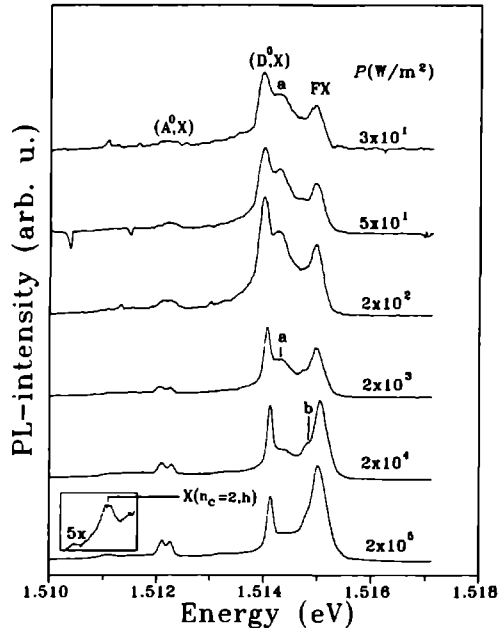


Figure 4.5 Zero-field spectrum as a function of laser power density; the enlarged part of the spectrum at the bottom shows the exciton luminescence of the populated $n_c = 2$ subband.

We have already mentioned above that the extrapolation of the the photon energy of $X(n_c = 2, h)$ to zero field reveals a value 1.51165 eV. At high power densities P , a peak of low intensity is observed at the slightly lower energy of 1.5112 eV in the zero-field PL spectrum (Figure 4.5). It is possible that this peak is the $X(n_c = 2)$ peak shifted to lower energy owing to changes in the confining potential. The electric field in the GaAs buffer layer is vanishingly small at higher P as a result of the neutralization of the depletion charge, and this results both in a greater spatial extension of the $n_c = 2$ subband and lower E_{21} . This “flattening” of the bands in the GaAs layer also causes an enhanced hole density near the 2DEG, which results in an increased wave-function overlap with

the $n_c = 2$ electrons. The reduction of depletion charge is also reflected by the relative enhancement of the (A^0, X) peak from the GaAs buffer layer compared to other buffer-layer PL emission. The ionized acceptors in the depletion region at low P are neutralized at higher excitation densities of the laser light, so that a bound state between a neutral acceptor and an exciton becomes possible. Further 3D peaks correspond to donor-bound excitons (D^0, X) in the buffer layer, which show saturation effects at high P owing to the limited amount of donors present in the buffer layer. In contrast, no such saturation occurs for the FX emission.

Two other emissions, which are labelled a and b in Figure 4.5, show interesting behaviour as a function of excitation density. With increasing P , peak a shifts to slightly higher energy and shows a less pronounced increase in intensity than either (A^0, X) , (D^0, X) , or FX. A possible explanation for the origin of this peak is that it directly reflects the observation of PL from electrons at the Fermi level. Mueller [12] showed that PL from Fermi electrons could be observed if the Fermi level was located just below the second subband. In our sample at zero field the Fermi level is located below the third subband, so a many-body interaction is possible between the Fermi electrons and the virtual exciton of the third subband. At the highest excitation densities used the third subband is likely to be populated, thereby leading to a suppression of the E_F peak and the appearance of the $n_c = 3$ exciton. In comparison with the $n_c = 1$ and $n_c = 2$ subbands, the spatially extended $n_c = 3$ subband has a larger wave-function overlap with the photoexcited holes. Provided that the oscillator strength that results from this overlap is large enough, peak b at 1.5147 eV in Figure 4.5 can be tentatively assigned to the transition between $n_c = 3$ subband electrons and photoexcited holes.

An alternative origin for peak b is via the formation of molecular excitons (or biexcitons: a bound state between a pair of free excitons) in the GaAs buffer. This tentative attribution is based on the appearance of peak b at high excitation density and the photon energy of 1.5147 eV which correspond to an additional binding energy of 0.4 meV between the two excitons. This difference is close to the calculated 0.35 meV for molecular excitons in GaAs [30].

4.4 Conclusions

We have investigated the magneto-optical behaviour of a single heterojunction with two populated subbands. Extremely narrow exciton luminescence involving $n_c = 2$ electrons and photoexcited holes is reported above field values at which the Fermi level shifts for the first time below the lowest Landau level of the $n_c = 2$ subband. Magneto-oscillations in intensity of the exciton peak are explained by a combination of population effects and, more importantly, a many-body interaction between the $n_c = 2$ exciton and the extended states of the $n_c = 1$ Landau level in which E_F resides. Oscillations in photon energy and width of the exciton peak result from crossing of $n_c = 1$ Landau levels with the exciton of the lowest Landau level of the $n_c = 2$ subband. Finally, the intrasubband diamagnetic shift has been determined from tilted-field measurements.

Acknowledgements

The authors wish to thank R.M. Kusters and P.C.M. Christianen for stimulating discussions, and G.J. Bauhuis for technical assistance. D.M. Frigo is gratefully acknowledged for reading the text.

References

1. M.S. Skolnick, K.J. Nash, S.J. Bass, P.E. Simmonds and M.J. Kane, *Solid State Commun.* **67**, 637 (1988).
2. A.S. Plaut, K. v. Klitzing, I.V. Kukushkin and K. Ploog, in *Proceedings of the 20th International Conference on the Physics of Semiconductors*, edited by E.M. Anastassakis and J.D. Joannopoulos (World Scientific, Singapore, 1990), p.1529.
3. A.S. Plaut, I.V. Kukushkin, K. v. Klitzing and K. Ploog, *Phys. Rev. B* **42**, 5744 (1990).
4. H. Buhmann, W. Joss, K. v. Klitzing, I.V. Kukushkin, A.S. Plaut, G. Martinez, K. Ploog and V.B. Timofeev, *Phys. Rev. Lett.* **66**, 926 (1991).
5. A.J. Turberfield, S.R. Haynes, P.A. Wright, R.A. Ford, R.G. Clark, J.F. Ryan, J.J. Harris and C.T. Foxon, *Phys. Rev. Lett.* **65**, 637 (1990).
6. D. Heiman, B.B. Goldberg, A. Pinczuk, C.W. Tu, A.C. Gossard and J.H. English, *Phys. Rev. Lett.* **61**, 605 (1988).
7. I.V. Kukushkin, A.S. Plaut, K. v. Klitzing and K. Ploog, *Surface Science* **229**, 447 (1990).
8. I.V. Kukushkin, K. v. Klitzing, K. Ploog and V.B. Timofeev, *Phys. Rev. B* **40**, 7788 (1989).
9. I.V. Kukushkin, K. v. Klitzing and K. Ploog, *Pis'ma Zh. Eksp. Teor. Fiz.* **47**, 511 (1988) [*JETP Lett.* **47**, 598 (1988)].
10. I.V. Kukushkin, K. v. Klitzing and K. Ploog, *Phys. Rev. B* **37**, 8509 (1988).
11. W. Chen, M. Fritze, A.V. Nurmikko, D. Ackley, C. Colvard and H. Lee, *Phys. Rev. Lett* **64**, 2434 (1990); M. Fritze, W. Chen, A.V. Nurmikko and D. Ackley, in *Proceedings of the 20th International Conference on the Physics of Semiconductors*, edited by E.M. Anastassakis and J.D. Joannopoulos (World Scientific, Singapore, 1990), p.825; W. Chen, M. Fritze, A.V. Nurmikko, M. Hong and L.L. Chang, *Phys. Rev. B* **43**, 14738 (1991).
12. J.F. Mueller, *Phys. Rev. B* **42**, 11189 (1990).
13. G.D. Mahan, *Phys. Rev.* **153**, 882 (1967).
14. J.E. Cunningham, W.T. Tsang, G. Timp, E.F. Schubert, A.M. Chang, and K. Owusu-Sekyere, *Phys. Rev. B* **37**, 4317 (1988).
15. R.M. Kusters, F.A. Wittekamp, J. Singleton, J.A.A.J. Perenboom, G.A.C. Jones, D.A. Ritchie, J.E.F. Frost, and J.-P. André, *Phys. Rev. B* **46**, 10207 (1992).
16. J.J. Harris, D.E. Lacklison, C.T. Foxon, F.M. Selden, A.M. Suckling, R.J. Nicholas and K.W.J. Barnham, *Semicond. Sci. Technol.* **2**, 783 (1987).

17. R.M. Kusters, J. Singleton, G. Gobsch, G. Paasch, D. Schulze, F.A. Wittekamp, G.A.C. Jones, J.E.F. Frost, D.C. Peacock and D.A. Ritchie, *Superlattices and Microstructures* **9**, 55 (1991).
18. R. Fletcher, E. Zaremba, M. D'Iorio, C.T. Foxon and J.J. Harris, *Phys. Rev. B* **41**, 10649 (1990).
19. T. Ando, A.B. Fowler and F. Stern, *Rev. Mod. Phys.* **54**, 437 (1982).
20. I.V. Kukushkin, K. von Klitzing, K. Ploog, V.E. Kirpichev and B.N. Shepel, *Phys. Rev. B* **40**, 4179 (1989).
21. The behaviour of E_F in a two-dimensional electron gas with two occupied subbands has been reported by J.C. Portal, R.J. Nicholas, M.A. Brummel, A.Y. Cho, K.Y. Cheng and T.P. Pearsall, *Solid State Commun.* **43**, 907 (1982).
22. W. Kohn, *Phys. Rev.* **123**, 1242 (1961).
23. M.E. Hopkins, R.J. Nicholas, M.A. Brummel, J.J. Harris and C.T. Foxon, *Superlattices and Microstructures* **2**, 319 (1986).
24. E.D. Palik, G.S. Picus, S. Teitler and R.F. Wallis, *Phys. Rev.* **122**, 475 (1961).
25. M.E. Hopkins, R.J. Nicholas, M.A. Brummel, J.J. Harris and C.T. Foxon, *Phys. Rev. B* **36**, 4789 (1987).
26. M.S. Skolnick, P.E. Simmonds and T.A. Fisher, *Phys. Rev. Lett.* **66**, 963 (1991).
27. H. Reisinger and F. Koch, *Surf. Sci.* **170**, 397 (1986).
28. F. Nasir, J. Singleton and R.J. Nicholas, *Semicond. Sci. Technol.* **3**, 654 (1988).
29. These parallel-field magnetoresistance measurements revealed the depopulation of the second subband [27,28]. In the work of Kusters *et al.* [15] the relation

$$\alpha B_{\parallel,dep}^2 = 2(E_F - E(n_c = 2))_{B_{\parallel}=0}$$

was used. With $B_{\parallel,dep} = 9.0 \pm 0.1$ T and $E_F - E(n_c = 2) = 3.5 \pm 0.5$ meV this yields $\alpha = (8.6 \pm 0.4) \times 10^{-5} \text{eVT}^{-2}$.

30. G.W. 't Hooft, W.A.J.A. van der Poel, L.W. Molenkamp and C.T. Foxon, *Phys. Rev. B* **35**, 8281 (1987).

Chapter 5

Fermi-edge-induced magnetophotoluminescence in high-carrier-density single heterojunctions

F.A.J.M. Driessen^a, S.M. Olsthoorn^a, T.T.J.M. Berendschot^b, L.J. Giling^a, D.M. Frigo^c,
G.A.C. Jones^d, D.A. Ritchie^d, and J.E.F. Frost^d,

^a*Department of Experimental Solid State Physics, Research Institute for Materials, University of Nijmegen, Toernooiveld, NL 6525 ED Nijmegen, The Netherlands*

^b*High Field Magnet Laboratory, University of Nijmegen, Toernooiveld, NL 6525 ED Nijmegen, The Netherlands*

^c*Billiton Research B.V., P.O. Box 40, NL 6800 AA Arnhem, The Netherlands*

^d*Cavendish Laboratory, University of Cambridge, Madingley Road, Cambridge CB3 0HE, United Kingdom*

Abstract

Fermi-edge-induced excitonic magnetophotoluminescence (MPL) of second ($n_c = 2$)-subband electrons and photoexcited holes $X(n_c = 2, h)$ is reported in high-carrier-density GaAs/ $\text{Al}_x\text{Ga}_{1-x}\text{As}$ single heterojunctions for two-dimensional carrier densities in the range $(6.6 - 16.2) \times 10^{15} \text{m}^{-2}$. The MPL shows magneto-oscillatory behaviour of intensity, photon energy and peak width. Furthermore, $n_c = 2$ subband recombination with light holes $X(n_c = 2, l)$ is reported. A splitting of the $X(n_c = 2, h)$ is reported at low carrier density, which results from the separate interaction of the two spin-split states of the $n_c = 1$ Landau level in which the Fermi level resides on the second subband. The dependence of the spectra on both excitation density and temperature indicates strongly that photoluminescence (PL) from the $n_c = 3$ subband occurs. PL originating from the two-dimensional electron gas (2DEG) and that from the GaAs buffer layer could be distinguished by excitation below and above the GaAs band gap. In the highest-carrier-density sample evidence is found for the formation of a band of localized states between the spin components of a Landau level. Recombination occurs between the exponentially decaying tails of the photoexcited holes, which relax to the flat band region of the GaAs. Additional information on the 2DEG was obtained via resonant-excitation experiments. Phonon replicas of both the second subband exciton and the *unpopulated* third subband are observed. The latter very sharp replica appears if a non-equilibrium electron concentration is created in the resonantly excited third subband. Resonant excitation also reveals the recombination of electrons in the $n_c = 2$ subband with holes located at neutral acceptors. Strong indications were found for PL of the $n_c = 1$ lowest Landau level upon resonantly exciting the $X(n_c = 2, h)$ transition in the lowest-carrier-density sample.

Published in:
Physical Review B 47, 1282-1291 (1993).

5.1 Introduction

The presence of exciton states at the Fermi edge of degenerate semiconductors, as a result of electron-hole multiple scattering, was demonstrated by calculations of Mahan [1]. These many-body excitons are observed as a logarithmic singularity in low temperature absorption spectra: the Fermi-edge singularity (FES). The FES is usually not seen in luminescence spectra because conservation of momentum requires that mainly holes near $\mathbf{k}=0$ are involved in emission. Skolnick *et al.* [2] circumvented momentum conservation by real-space localization of the holes as a result of alloy fluctuations in a modulation doped $\text{In}_{0.47}\text{Ga}_{0.53}\text{As-InP}$ quantum well structure. Hence, luminescence from all electrons up to E_F could be observed, thereby obtaining the density of states between the Landau levels in the two-dimensional electron gas (2DEG) [3].

Various other properties of 2DEG's have been studied magneto-optically, such as electron-electron interactions [4], the integral and fractional quantum Hall effects [5-7] and Auger recombination within Landau levels [8]. In these studies use was made of modulation-doped quantum wells (MDQW's) because of the presence of hole subbands n_v [3,9] and GaAs- $\text{Al}_x\text{Ga}_{1-x}\text{As}$ single heterojunctions, for which photoluminescence (PL) from the GaAs buffer layer was prevented from dominating the spectrum. This was achieved either by choosing very thin buffer layers [10] or by placing an additional δ -layer of acceptors in the GaAs buffer [5, 11, 12].

Partly motivated by recent spectroscopic observations of the fractional and integral quantum Hall effect [6,7,13,14], renewed theoretical interest has arisen in the subject of a confined Fermi sea [15-19]. The latter references examined the influence of the Fermi sea on a single subband in a magnetic field.

The presence of a second subband has been shown experimentally to be of great influence. Chen *et al.* [20] showed that the hybridization between the Fermi-edge resonance and the second subband appeared to result in strong magneto-oscillations with Shubnikov-de Haas (SdH) periodicity in the intensity of an excitonlike PL transition. In their MDQW the Fermi level was located just below the $n_c = 2$ subband. Without including the effect of a magnetic field Mueller, Ruckenstein and Schmitt-Rink [21,22] examined theoretically the influence of an excitonic resonance originating from a higher conduction subband on the optical spectra of an n -type degenerate semiconductor.

In a recent paper [23], we reported the observation of the second-subband exciton $X(n_c = 2, h)$ in a high-carrier-density single heterojunction. This exciton could be observed because of hybridization between the Fermi-edge resonance and the second subband. The $X(n_c = 2, h)$ was observed if the magnetic field strength was large enough to depopulate the second subband. In contrast to the previously mentioned magneto-optical publications on 2D-systems, the holes in the heterojunction were not localized or trapped in thin buffer layers, quantum well structures, or at additional acceptor sites. The intensity of the $X(n_c = 2, h)$ luminescence showed oscillatory behaviour with SdH periodicity. The extremely small linewidth of the PL signal also permitted the observation of magneto-oscillations in both photon energy and peak width. These oscillations were caused by crossing Landau levels of the $n_c = 1$ subband with the lowest Landau level of

the $n_c = 2$ subband. Furthermore, tilted-field measurements enabled the determination of the intrasubband diamagnetic shift in a parallel field.

In this paper we further investigate Fermi-edge-induced magnetophotoluminescence (MPL) in three high-carrier-density heterojunctions with total sheet carrier densities n_T ranging between 6.6 and $16.2 \times 10^{15} \text{m}^{-2}$. New Fermi-edge-induced emissions and other information of the 2D system are reported. We discuss temperature-dependent behaviour and excitation-density-dependent behaviour for excitation both below and above the GaAs band gap.

Finally, we present PL measurements in which the laser was resonantly tuned to several 2D emissions. Strongly enhanced 2D-PL processes, which are related to the resonantly excited states and not observable in the nonresonant spectra, yield additional information on the 2D system.

5.2 Experimental Details

The experiments were carried out on three monolayer-doped GaAs- $\text{Al}_x\text{Ga}_{1-x}\text{As}$ heterojunctions with high carrier density grown by molecular-beam epitaxy at the Cavendish Laboratory, Cambridge.

TABLE I: Properties of the samples: spacer thickness z , total sheet carrier density (n_T) and mobility (μ) measured in the dark and after saturation of the persistent photoconductivity effect by illumination with a red LED (after [24]). Separate sheet carrier densities of the two subbands $n_{1,2}^{\text{light}}$ at zero field are specified.

Sample	1	2	3
Growth run	A233	A232	A227
$z(\text{nm})$	20	10	5
$n_T^{\text{dark}}(10^{15} \text{m}^{-2})$	3.8	6.4	8.9
$n_T^{\text{light}}(10^{15} \text{m}^{-2})$	6.6	11.3	16.2
$n_1^{\text{light}}(10^{15} \text{m}^{-2})$	6.3	10.3	14.5
$n_2^{\text{light}}(10^{15} \text{m}^{-2})$	0.3	1.0	1.7
$\mu^{\text{dark}}(\text{m}^2 \text{V}^{-1} \text{s}^{-1})$	55	39	9.8
$\mu^{\text{light}}(\text{m}^2 \text{V}^{-1} \text{s}^{-1})$	56	39	8.5

The sample structure has been described in our previous paper [23]. The distance z between the Si doping layer in the $\text{Al}_x\text{Ga}_{1-x}\text{As}$ and the GaAs/ $\text{Al}_x\text{Ga}_{1-x}\text{As}$ hetero-interface differed between the samples. These spacer thicknesses z for the heterojunctions, as well as the corresponding carrier densities and mobilities both measured in the dark and after saturation of the persistent photoconductivity [25] by illumination with a red light-emitting diode (LED) are shown in Table I. Other sample parameters can be found in the work of Kusters *et al.* [24,26]. The experimental conditions for the MPL measurements have also been described previously [23].

5.3 Results and Discussion

5.3.1 Lowest carrier density

$X(n_c = 2, h)$ and $X(n_c = 2, l)$

The excitonic part of the spectrum of sample 1 at various magnetic-field strengths recorded at $T = 1.5$ K is given in Figure 5.1. For this sample with the lowest carrier density a few peaks showed magneto-oscillatory behaviour of photon energy as is shown in Figure 5.2.

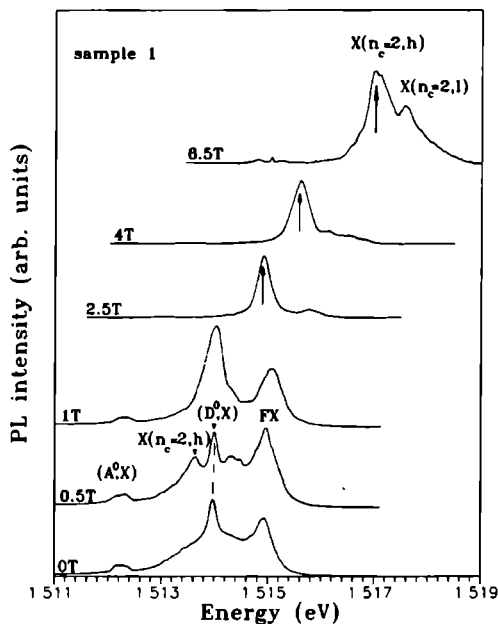


Figure 5.1 PL spectra of sample 1 at various magnetic fields B .

Because the most intense line has qualitatively the same magneto-optical properties as the $X(n_c = 2, h)$ in sample 2, reported on in our previous paper [23], it has also been assigned to second-subband luminescence, which can be observed owing to the involvement of the Fermi sea. Because the second subband of sample 1 has a lower electron concentration than that of sample 2, a lower magnetic field is required to depopulate the second subband, so the $X(n_c = 2, h)$ can be resolved at fields as low as 0.8 T. The PL line of sample 1 is narrower than that of sample 2 because of the thicker $\text{Al}_x\text{Ga}_{1-x}\text{As}$ spacer layer that separates the 2DEG from the ionized impurities in the sheet-doping layer. The same procedure we used previously [23] for sample 2 was applied to construct the Landau

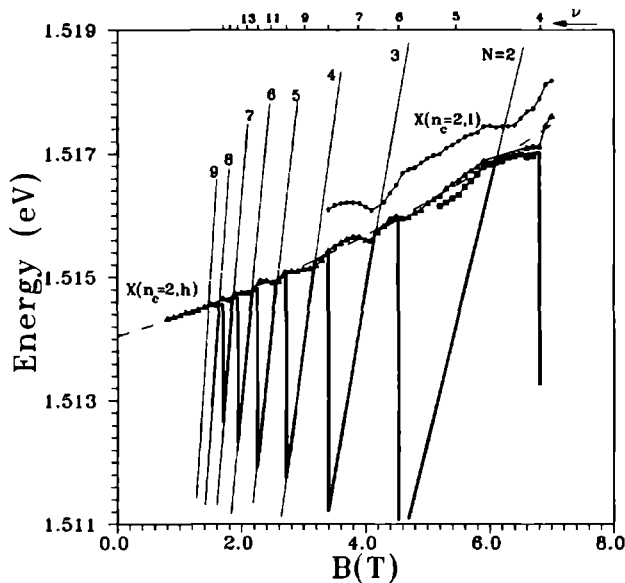


Figure 5.2 Photon energies of various Fermi-edge-induced 2D peaks in sample 1, parts of Landau-level fan diagram of the $n_c = 1$ subband, and the calculated energy of the Fermi level in the field range of interest (bold line) assuming δ -function shaped Landau levels. Filling factors ν are shown at the top axis.

fan diagram of the $n_c = 1$ subband and the behaviour of the Fermi energy. First, the energy of the second subband was extrapolated to zero field, and the energies of the lowest subband and that of the Fermi level were calculated using $E_2 - E_1 = 22.3$ meV and $E_F - E_2 = 1.1$ meV, which values were taken from magneto-transport measurements on this sample for $B = 0$ T [24]. Second, the Landau fan diagram was constructed taking an effective mass of $0.070 m_0$, where m_0 is the mass of a free electron. This value was calculated directly from the relationship between sheet carrier density and the effective mass valid for magneto-optics [4]. The calculated energy of the Fermi level at $T=0$, assuming δ -function shaped Landau levels, is shown by the bold line in Figure 5.2 in the pertinent range of field strengths. The dotted line shows the photon energy of the second subband if it were unaffected by the Fermi electrons. It should be noted that this photon energy shows a detectable quadratic dependence upon B , which implies a small exciton binding energy. This is in contrast to results obtained for sample 2 [23], and can be attributed both to the smaller value for the intrinsic electric field, which acts on the photoexcited holes, and the larger extent of the $n_c = 2$ subband, which results in a greater overlap with these holes.

Above $B = 4$ T another remarkable peak is observed at higher energy (see the upper line in Figure 5.2). The photon energy of this peak is also affected by crossing $n_c = 1$ Landau levels, which indicates that 2D electrons are involved in the recombination process. Furthermore, the peak disappears above $\cong 20$ K. These observations show that the peak is induced by the Fermi sea. Because of the strong interaction between the $n_c = 2$ subband and the Fermi electrons, the most likely candidate for the emission is an exciton consisting of $n_c = 2$ electrons and light holes, hereafter denoted $X(n_c = 2, l)$. Fermi-edge-induced emission of the $n_c = 3$ subband is highly unlikely because the relaxation time between the $n_c = 3$ and $n_c = 2$ subbands (which both have nonequilibrium concentrations of electrons in them) should then exceed the typical timescale for Fermi-edge-induced luminescence. This intrasubband relaxation time can be estimated to be around 100 ps [27,28]. The even smaller recombination times of the induced processes would then imply lifetime broadening of the peaks of at least 10 meV, which was not observed in our experiments. Furthermore, larger excitonic effects are expected for Fermi-edge-induced PL from the $n_c = 3$ subband, owing to the greater extent of the $n_c = 3$ wavefunction; these effects were not observed in our experiments either.

Effects of spin splitting of $n_c = 1$ Landau levels on $X(n_c = 2, h)$

Apart from these two dominating PL processes involving the $n_c = 2$ subband, the $X(n_c = 2, h)$ shows a splitting at high fields (around $\nu = 5$). This splitting can be observed in this sample because the $X(n_c = 2, h)$ emission is the narrowest. The detailed spectra in this field region are shown in Figure 5.3.

The energy difference between both components of the $X(n_c = 2, h)$ peak increases until filling factor 5 has been reached; at higher fields it decreases again. It is well established that the effective g factor, which determines the separation between two spin-split states, is enhanced at odd filling factors. This g -factor enhancement is caused by exchange interaction among electrons, and is proportional to the population difference between two spin components of a Landau level [29,30]. Maximal enhancement is therefore obtained at odd filling factors, at which one spin level is fully occupied and the other is unoccupied. The measured increase in energy difference at filling factor $\nu = 5$, therefore, shows that spin splitting of the Landau level in which E_F resides influences the $X(n_c = 2, h)$. The quantity $g^* = \Delta E / \mu_B B$, where ΔE is the energy splitting between the two peaks and μ_B is the Bohr magneton, is plotted versus the field strength in the inset of Figure 5.3. It must be stressed that this is not necessarily the real value of the enhanced g factor at $\nu = 5$: it is the effect which these two spin-split states have on the photon energy of the $X(n_c = 2, h)$. The inset, therefore, serves only to visualize the maximum at $\nu = 5$ ($B=5.4$ T).

Deviation from linear behaviour of Landau levels

In Figure 5.2 it was seen that the energy of the $X(n_c = 2, h)$ is affected by the crossing of the $n_c = 1$ Landau levels. A less pronounced, though remarkable deviation of ~ 0.2 meV in photon energy was observed at $B = 4.6$ T: exactly the field at which E_F shifts dramatically ($\nu = 6$). Skolnick *et al.* [3] observed deviations from the linear behaviour of Landau

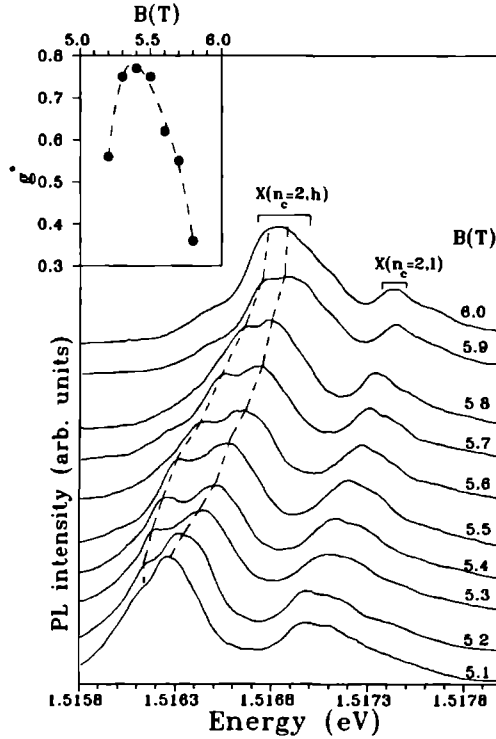


Figure 5.3 Detailed spectra of sample 1 for $5.1 < B < 6.0$ T. The inset shows the quantity $g^* = \Delta E / (\mu_B B)$, with ΔE the energy difference between the two $X(n_c = 2, h)$ peaks, μ_B the Bohr magneton and B the magnetic field.

levels as soon as they began to depopulate (*i.e.* at even ν) in a MDQW with one occupied subband. The deviations were of order 5 meV and were mainly attributed to the dependence of excitonic effects on Landau-level filling. Because the exciton binding energies are considerably greater in a MDQW than in a single heterojunction, we expect that the same effect causes the small deviations from linearity upon depopulating the lowest Landau level of the $n_c = 2$ subband.

5.3.2 Intermediate carrier density

Low-field data: Crossing behaviour of (A^0, X) and $X(n_c = 2, h)$

Earlier data on sample 2 (Ref.23) reported the situation in which the Fermi level E_F lay either below or in the lowest Landau level of the $n_c = 2$ subband. Below $B \approx 2.5$ T

this is no longer the case and the intensity of the second-subband exciton $X(n_c = 2, h)$ is greatly reduced because then the transition probability for $X(n_c = 2, h)$ emission is no longer enhanced. Very low intensity $X(n_c = 2, h)$ luminescence can, however, still be seen in the spectra at low magnetic fields because a non-vanishing wave function overlap with the photoexcited holes exists as a result of the relatively large mean extent $\langle z \rangle_2$ of the $n_c = 2$ subband electrons from the interface. This $\langle z \rangle_2$ is especially large if the depletion charge is neutralized as a result of electron-hole pair generation [31], as is the case under our experimental conditions. Figure 5.4 shows portions of the spectra

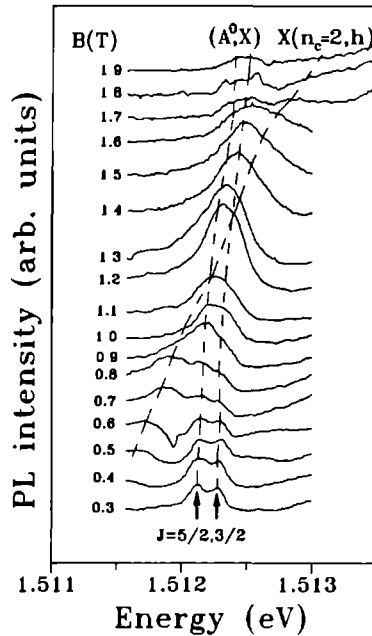


Figure 5.4 The low-field crossing behaviour of the second subband exciton $X(n_c = 2, h)$ and “bulk” acceptor-bound excitons (A^0, X) in sample 2.

for fields between $B=0.3$ and 1.9 T. Below $B=0.8$ T the $X(n_c = 2, h)$ has clearly lower energy than the two $(A^0, X)_{J=5/2, 3/2}$ states. The $X(n_c = 2, h)$ follows the lowest Landau level of the second subband and the photon energy of (A^0, X) shows a less pronounced dependence upon B , which is a characteristic behaviour of a bound exciton. The spectra show that the two (A^0, X) states are indistinguishable from the second subband exciton $X(n_c = 2, h)$ between $B=0.8$ and 1.3 T. Above $B=1.3$ T the $X(n_c = 2, h)$ has a higher energy than (A^0, X) and, as shown in Figure 5.4 of Ref.23, at higher field strengths $X(n_c = 2, h)$ shows its characteristic magneto-oscillatory properties. This crossing of

$X(n_c = 2, h)$ and (A^0, X) indicates that the interaction between the “bulk excitons” and the “2D-excitons” is negligible, otherwise the noncrossing rule of quantum mechanics would have applied [32], resulting in mixed character of the two transitions.

Excitation-density dependence of the emissions

The efficiency of the Fermi-edge-induced $X(n_c = 2, h)$ transition in magnetic field was found experimentally to be very large, both by Chen *et al.* [33] in MDQW’s and in our work on single heterojunctions [23]. Here we present the behaviour of the PL spectrum of sample 2 as a function of excitation density P for laser excitation at $B = 5.4$ T ($\nu = 7$) at energies both below and above the band gap. Figure 5.5(a) shows the spectra for above-band gap excitation with $E_l = 1.537$ eV, whereas Figure 5.5(b) shows the P -dependence for $E_l = 1.52$ eV, which is below the band gap at $B = 5.4$ T. The $X(n_c = 2, h)$ peak is seen to be considerably broader when $E_l > E_{\text{gap}}$. This is presumably caused by exciton scattering by “hot” electrons. This scattering mechanism is known to have a profound effect on exciton kinetics [34]. Furthermore, luminescence from the GaAs buffer layer (A^0, X) and especially FX is seen in Figure 5.5(a) to increase faster than that from the $X(n_c = 2, h)$ upon increasing P . The intensity rise of (A^0, X) and FX is considerably less pronounced for the below-band-gap excitation in Figure 5.5(b). If $E_l > E_{\text{gap}}$, excitons in the GaAs buffer layer are formed from free electrons and holes; whereas for $E_l < E_{\text{gap}}$, no free carriers are present. Obviously, the exciton formation probability for below-band-gap excitation cannot compete with the probability of exciton formation via free carriers in this heterojunction. The relative suppression of 3D excitons observed in Figure 5.5(b) is accompanied by the appearance of a shoulder at higher energy which appears at high P . This shoulder is absent in Figure 5.5(a), which indicates that its origin lies in the 2D system and not in the GaAs buffer layer. In view of its properties, discussed below, the shoulder has been labelled $(n_c = 3, h)$. The peak labelled $X(n_c = 2, l)$ in Figure 5.5(b) has slightly higher energy than that of the FX, which is more clearly observed in Figure 5.5(a). The FX energy is shown in Figure 5.5(b). As with the previously described light exciton of the $n_c = 2$ subband in sample 1, upon changing B the energy of this $X(n_c = 2, l)$ peak also appears to be affected by crossing $n_c = 1$ Landau levels. This can be seen in Figure 5.5(c), where the energy of $X(n_c = 2, l)$ is shown together with that of $X(n_c = 2, h)$ and parts of the Landau-level fan diagram. Therefore, the Fermi-edge-induced light exciton of the $n_c = 2$ subband has also been observed in sample 2 by studying the excitation density and excitation energy dependence of the spectra.

Temperature dependence of the spectra

Figure 5.6 shows the temperature dependence of sample 2 at $B=7.0$ T. At this field the $n_c = 2$ subband is not populated by equilibrium electrons, as can be seen in Figure 4.4 of our previous paper [23]. Two subpeaks appear on the high-energy side of $X(n_c = 2, h)$ upon increasing temperature; their origin is uncertain. A possibility is that thermal population of holes in higher J_z states may result in additional PL peaks. Another possibility for the origin of one subpeak concerns a separate many-body interaction on

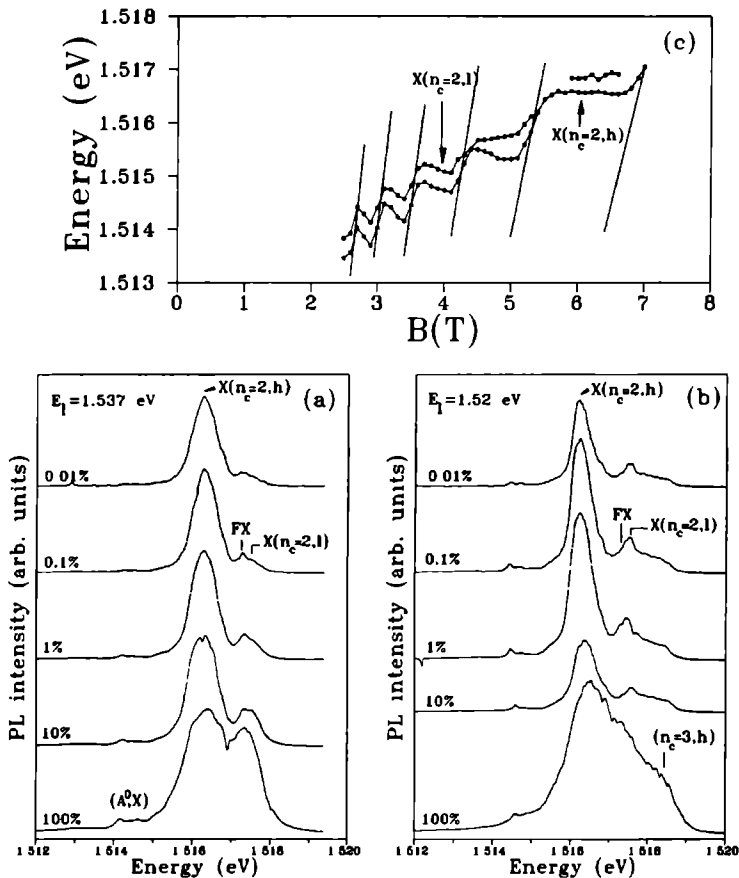


Figure 5.5 The PL spectrum of sample 2 versus excitation density at $B=5.4$ T ($\nu = 7$) for (a) above and (b) below band gap laser excitation. The energy of IX decay is also shown in (b). Energies of the $X(n_c = 2, l)$ and the $X(n_c = 2, h)$ shown in (c) with parts of the Landau fan diagram.

the second subband of two spin-split states of the particular $n_c = 1$ Landau level in which E_F resides, as was also found above for sample 1 through the observation of g -factor enhancement. This can occur here because the experiment was performed at $B = 7$ T, just above the $\nu = 7$ field. Therefore, thermal depopulation of the slightly populated energetically lowest spin component of Landau level $N=3$ of the $n_c = 1$ subband may lead to the same effect described above: separate influence of both spin components on the $X(n_c = 2, h)$, resulting in the observation of a splitting of $X(n_c = 2, h)$. The entire

disappearance at ~ 20 K of the broadened complex of peaks is not surprising because the interaction between the Fermi electrons and the second subband is highly sensitive to temperature [3,21].

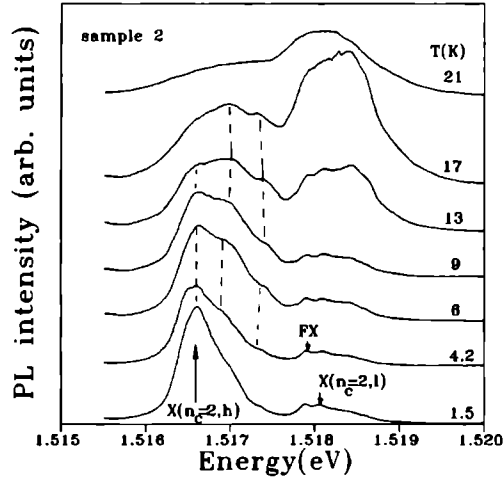


Figure 5.6 The temperature dependence of the PL spectrum of sample 2 at $B=7$ T.

Free-exciton PL of the buffer layer was observed around 1.518 eV and disappeared at about 50 K. At higher temperatures a peak appeared which at low T was observed around 1.5184 eV. The luminescence of this peak could still be clearly observed at temperatures up to 320 K, which is the upper limit in our sample cell at $B \neq 0$. The energy of this peak followed that of the GaAs band gap as a function of temperature. At $T = 320$ K the PL intensity depended quadratically on the excitation density: $I \propto P^2$. This behaviour is not expected for buffer layer excitons because of screening of ionized impurities. In quantum wells it is well known that electrons and holes exhibit a strong exciton binding owing to their large wave-function overlap [35,36], and exciton PL can still be observed at higher temperatures compared to bulk exciton PL [37]. In our system the $n_c = 3$ subband has similar properties. First, this subband has a large spatial extension into the flat-band region, which ensures a considerable overlap with photoexcited holes; second, ionized impurities are spatially separated in the $\text{Al}_x\text{Ga}_{1-x}\text{As}$. Therefore we believe that the highest-energy peak corresponds to $(n_c = 3, h)$ recombination, which possibly has an exciton binding energy. Temperature-dependent measurements on samples 1 and 3 showed qualitatively the same behaviour. At low temperature an $X(n_c = 2, h)$ peak was observed, and at high temperature a new peak at higher energy appeared. The energy difference between these two peaks increased upon increasing sheet carrier density: they were 0.9, 1.7 and 3.5 meV for samples 1, 2 and 3, respectively. This supports the

assignment to $(n_c = 3, h)$ because all subband separations increase if the intrinsic electric field increases [38]. Further experimental data supporting the $(n_c = 3, h)$ assignment are reported below in the resonant excitation experiments.

5.3.3 Highest carrier density

For sample 3 (that with the highest carrier density) luminescence was observed with the characteristic 2D magneto-oscillatory properties above ~ 4 Tesla. This field is stronger than the critical values of the other two samples because this is required to depopulate the second subband (*cf.* our previous paper [23]). Figure 5.7 shows the very rapid rise

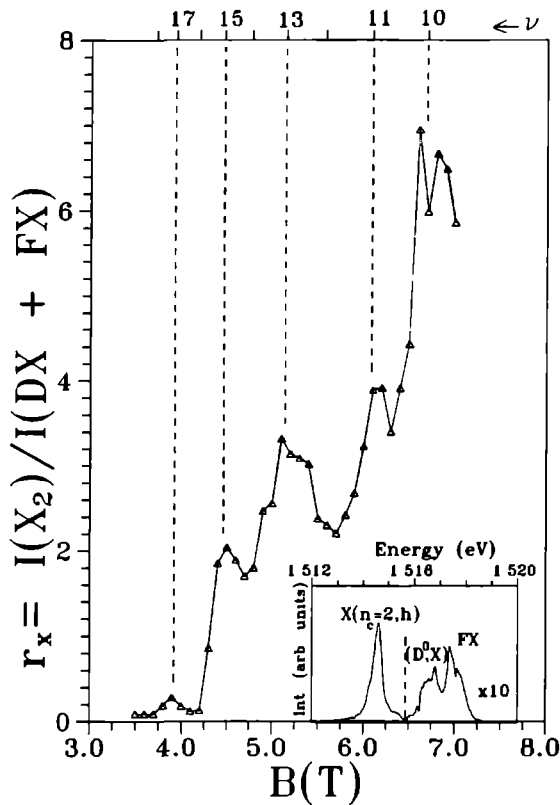


Figure 5.7 The ratio of total integrated $X(n_c = 2, h)$ PL to that of the bulk lines (D^0, X) and FX , versus magnetic field for sample 3. The inset shows the 6-8-T spectrum, the relative gain for the (D^0, X) - FX PL is 10.

in the 2D-luminescence efficiency for this sample: below ~ 4 T the PL is unobservable, whereas at $B = 6.8$ T its integrated intensity is about seven times larger than the sum of integrated (D^0, X) and FX buffer layer PL. As an illustration, the 6.8-T spectrum of this sample is shown in the inset of Figure 5.7. Maxima in the PL intensity are observed at the odd filling factors 11, 13, 15 and 17. Furthermore, a pronounced maximum is observed at $\nu = 10$. In our previous paper [23] we also observed maxima at even ν , which were less pronounced than those at odd integers. We argued that, in spite of population fluctuations in the second subband, the Fermi sea was also of influence in observing even ν intensity maxima. The present observation of a maximum at $\nu = 10$ and the absence of maxima at higher even integer filling factors shows that merely the appearance of population fluctuations, which occur at all ν , is not sufficient to account for the observed even ν maxima in our single heterojunctions. Moreover, the observation of a maximum at $\nu = 10$ points to the formation of a band of localized states between the spin components of the respective Landau level of the $n_c = 1$ subband. This occurs if the spin splitting $g^* \mu_B B$ is large compared with both the thermal broadening kT and the broadening of the Landau levels Γ . The effective g -factors g^* of both subbands are known to be fairly large from magneto-transport measurements: typical values are 3 for the $n_c = 1$ subband and 8 for the $n_c = 2$ subband [26]. Using $g^* = 3$ we find at $B = 6.7$ T that $g^* \mu_B B = 1.1$ meV, $kT = 0.12$ meV and $\Gamma(n_c = 1) \cong 0.4$ meV for this sample. Hence, the above spin-splitting criterion is fulfilled and Fermi-induced PL at even filling factors is possible in the high-field regime. The previously observed presence of less pronounced even ν maxima (shoulders in sample 2 [23]) can also be ascribed in the same way.

Magneto-oscillatory behaviour of the $X(n_c = 2, h)$ photon energy and its width were also observed for sample 3. Owing to the thin spacer layer in this sample, an overall larger width was measured that oscillated between 0.4 and 0.8 meV. For constructing the Landau fan diagram the magneto-optical effective mass of the $n_c = 1$ subband electrons at $n = 16.2 \times 10^{15} \text{m}^{-2}$ was obtained by linear extrapolation of the relationship between m^* and n (reported by Plaut *et al.* [4]), as was previously performed for sample 2 [23]. Because of this large value of n , the extrapolation gives rise to an uncertainty in the effective mass, namely $0.084 < m^*/m < 0.087$. Using $m^* = 0.085m$ a remarkably good match was obtained between the fan diagram and the field intervals at which the photon energy increases relatively quickly.

5.3.4 PL mechanism

A new phenomenon was observed by comparing the three similar heterojunctions with variable sheet carrier densities. To wit, Table II summarizes the zero-field energies of the $n_c = 2$ subband, the calculated zero-field energy separation between Fermi level and the $n_c = 2$ subband E_{f2} and that between the $n_c = 2$ and $n_c = 1$ subbands E_{21} , and finally the calculated zero-field energy of the Fermi level E_f , for all three samples investigated in this paper. It is seen that within experimental error this zero-field Fermi energy is found to be 1.515 eV in all samples. To a good approximation this Fermi energy equals the Fermi energy in the n -type GaAs buffer layer, which lies $\sim 0.6 \times E_D$ below the band

gap [39], where E_D , the donor ionization energy in GaAs, is 5.715 meV. The fact that the inferred Fermi energy in Table II equals 1.515 eV implies that the photoexcited holes, which participate in the various Fermi-induced 2D-excitons, are situated in the flat band region of the GaAs: recombination takes place between their exponentially decaying tails and the 2D electrons. In our PL experiments, therefore, the energies of the subbands decrease if the sheet carrier density increases.

TABLE II: Energy of the $n_c = 2$ subband at zero field E_2 , zero-field energy separation between Fermi level and the $n_c = 2$ subband E_{f2} , and that between the $n_c = 2$ and $n_c = 1$ subbands E_{21} , and the calculated energy of the Fermi level E_f at zero field.

Sample	E_2 (eV)	E_{f2} (meV)	E_{21} (meV)	E_f (eV)
1	1.5137	1.1	22.3	1.5148
2	1.5116	3.6	30.3	1.5152
3	1.5087	6.1	40.0	1.5148

5.3.5 Resonant Excitation

So far we have studied the various Fermi-edge-induced emissions of the 2D system by using excitation just above the band gap of GaAs. In the following we used exact tuning of the laser energy to certain PL peaks. This resonant excitation on a PL peak enhances the probability of formation of the particular luminescent process [40-42]. The intensities of all peaks that are related to the resonantly excited peak then increase considerably. We used resonant excitation (RE) of 2D luminescence to obtain additional information on the 2D system, which remained hidden in nonresonant measurements; most data were obtained on the sample with the highest carrier density. A compilation of PL spectra, which were obtained by use of resonant excitation (RE) experiments on sample 3 at a field of $B=7$ T, is given in Figure 5.8. Figure 5.8(a) was obtained with the laser tuned well above the exciton emissions; it shows $X(n_c = 2, h)$ and residual (D^0, X) and FX PL of the GaAs buffer layer. In Figure 5.8(b) resonant tuning of the laser to the $X(n_c = 2, h)$ luminescence resulted in a shoulder (e_2, A^0) at the high-energy side of the (D^0, A^0) buffer PL, where A^0 refers to the carbon acceptor. This (e_2, A^0) peak is separated 19 meV from $X(n_c = 2, h)$, which is in excellent agreement with a result of Kukushkin, von Klitzing, and Ploog [43], who attributed this PL to recombination of a confined $n_c = 2$ electron with a hole located at an acceptor. This neutral acceptor is located in the vicinity of the 2DEG where a nonvanishing wave-function overlap exists between the acceptor and the exponentially decaying $n_c = 2$ wave-function. The small separation between acceptor and electron leads to a final-state Coulomb energy, which is why the separation between (e_2, A^0) and the $X(n_c = 2, h)$ is considerably smaller than the carbon acceptor ionization energy of 26.4 meV [44].

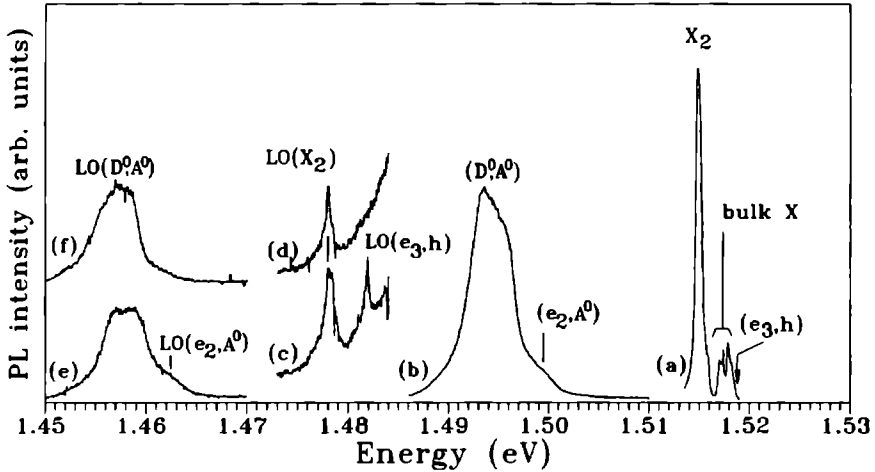


Figure 5.8 PL spectra obtained via resonant excitation experiments on sample 3 at $B=7$ T. The laser was tuned: well above the exciton energies for spectra (a) and (f); to the $X(n_c = 2, h)$ peak (abbreviated to X_2 in the Figure) for (b), (d) and (e); and to the $n_c = 3$ shoulder (denoted (e_3, h)) for (c).

Peak (e_2, A^0) was accompanied by its phonon replica, which is shown in Figure 5.8(e). Both (e_2, A^0) and this phonon replica were absent if the laser were not tuned to $X(n_c = 2, h)$, as can be seen in Figure 5.8(f), obtained with the laser energy tuned above that of the exciton emissions. A further indication that $n_c = 2$ electrons are involved here is that the (e_2, A^0) transition shifted within experimental error equivalently to the lowest $n_c = 2$ Landau level if the RE experiment was repeated on the $X(n_c = 2, h)$ at lower fields.

Apart from resonant excitation of the second subband exciton, we also investigated the PL that we ascribed to the $n_c = 3$ subband in sample 3. To this end the temperature dependence of the PL spectrum was required; that at $B = 7$ T is shown in Figure 5.9. This figure and some spectra for temperatures between 1.5 and 4.2 K allowed an accurate determination of the energy of the unoccupied third subband $E(n_c = 3, h)$ of 1.51879 ± 0.00004 eV at $T=1.5$ K. In the 1.5-K spectrum a small change in slope could also be observed at this energy, as can be seen in Figure 5.9. Resonant excitation was also performed at the energy of this third subband. Although there was no equilibrium electron population in the $n_c = 3$ subband at 1.5 K, a quasipopulation was created by the RE because of the enhanced probability of exciting a valence electron to the $n_c = 3$ subband. An extremely sharp phonon replica of this quasipopulated $(n_c = 3, h)$ subband was then observed at 1.48192 eV, as can be seen in Figure 5.8(c), for which the laser was resonant with the $n_c = 3$ shoulder. The phonon energy of 36.86 ± 0.04 meV appeared to deviate

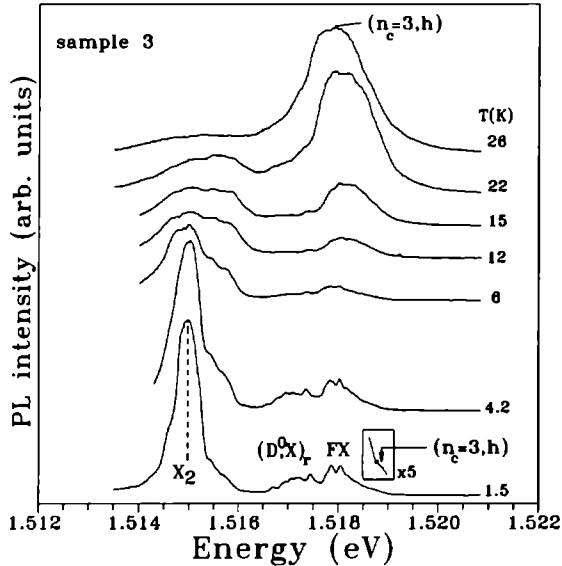


Figure 5.9 Temperature dependence of the 7 T PL spectrum of sample 3. The $X(n_c = 2, h)$ has been abbreviated to X_2 , GaAs buffer layer PL involving rotational states of the donor-bound exciton $(D^0, X)_{\text{rot}}$ and FX can be clearly distinguished.

slightly from the phonon energy of 36.75 ± 0.04 meV reported for bulk GaAs [45]. Strosio, Kim and Hall [46] demonstrated with a strain-dependent nearest-neighbour linear-chain model that the frequencies of LO-like phonon modes were shifted by a few percent in a superlattice structure. We expect that, in the case of a single heterojunction and, moreover, one in which the mean distance of $n_c = 3$ electrons to the interface is fairly large (of order 50 nm), this shift will be considerably smaller. Therefore, the measured increase in phonon energy may be tentatively ascribed to the presence of the heterointerface. These additional experimental observations confirm our hypothesis that third-subband electrons are involved in the PL emission.

Apart from the information obtained by the RE experiments on sample 3, we obtained additional results that could only be obtained for the sample with the lowest carrier density. Figure 5.10 shows PL spectra from sample 1 that were obtained by exact tuning of the laser to the energy of $X(n_c = 2, h)$. The uppermost spectrum was recorded at $B=7$ T with the laser tuned well above the $X(n_c = 2, h)$ emission and showed only (D^0, A^0) PL of the GaAs buffer layer. Resonant excitation of $X(n_c = 2, h)$ at 7 T led to the observation of additional peaks, *inter alia* the broad (e_2, A^0) peak, separated 19.4 meV from $X(n_c = 2, h)$, which can again be attributed to recombination of electrons in the

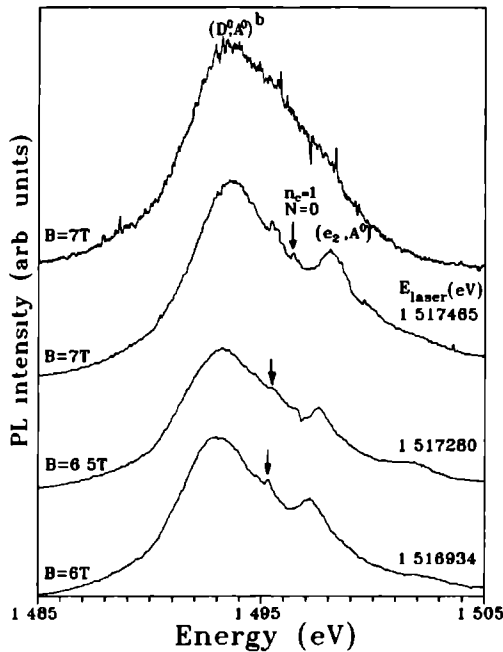


Figure 5.10 Resonant excitation spectra of sample 1 at 6-7 T. Uppermost is the non-resonant spectrum at $B=7$ T with the laser tuned well-above the excitonic emissions

$n_c = 2$ subband with holes located at acceptors. Upon repeating the RE experiment at lower fields, this PL line shifted within experimental error equivalently to the lowest Landau level of the $n_c = 2$ subband

An additional peak with an energy between those of (D^0, A^0) and (e_2, A^0) appeared if the $X(n_c = 2, h)$ was resonantly excited. This peak cannot be attributed to (e, A^0) recombination in the GaAs buffer layer because the latter PL shifts linearly in magnetic field towards 14991 eV at $B = 7$ T [47]. Furthermore, the attribution to excited acceptor states as a result of selective (D^0, A^0) pair luminescence (SPL) can also be refuted for two reasons. First, SPL peaks would disappear if the laser were tuned above energies of bound excitons, such as is the case here; second, SPL peaks should be present in the spectra of all samples, especially in that of sample 3 for which the energy of the $X(n_c = 2, h)$ (to which the laser was tuned) lay well below all GaAs buffer layer bound excitons. Calculation of the energy of the $N=0$ Landau level of the $n_c = 1$ subband yielded 14972 eV (from $14914 + 7\mu_B/0.070$), very close to that of the observed peak 14964 eV. Therefore, we believe that this peak involves recombination of $N=0$ $n_c = 1$ electrons with photoexcited holes. The shift of this peak in the lower-field RE spectra yields $m^* = 0.070m$, which cor-

responds to the effective mass of the $n_c = 1$ subband in this sample. Because no increase in the fully occupied $n_c = 1$ electron concentration is possible, an enhanced ($n_c = 1, \hbar$) recombination can be observed here because of the enhanced density of photoexcited holes in the 2DEG region upon resonant excitation of $X(n_c = 2, \hbar)$. This enhanced hole density results from the increased probability to excite a valence electron to the $n_c = 2$ subband in the RE experiment. To our knowledge, this is the first time that PL from the $n_c = 1$ subband has been observed in a high-carrier-density single heterojunction without hole confinement. This $n_c = 1$ PL could not be observed in the two samples with higher carrier densities, presumably because of their greater intrinsic electric field, which acts on the photoexcited hole density.

5.4 Conclusions

We have presented PL measurements on three single heterojunctions which have two occupied subbands at zero magnetic field. Despite the lack of hole confinement, we observed $n_c = 2$ subband excitons $X(n_c = 2, \hbar)$ in all samples owing to the hybridization between this subband and the Landau level of the $n_c = 1$ subband in which the Fermi level resides. This many-body interaction, which is maximal at odd filling factors, led to the observation of oscillations with Shubnikov-de Haas periodicity in the intensity of $X(n_c = 2, \hbar)$. Furthermore, we reported magneto-oscillations in both peak energy and peak width which are caused by the crossing of $n_c = 1$ Landau levels. Apart from the Fermi-edge-induced peaks $X(n_c = 2, \hbar)$, which appeared in all samples, a second Fermi-edge-induced peak involving the 2DEG was most clearly observed in the sample with lowest carrier density, most likely originating from the recombination of $n_c = 2$ subband electrons with photoexcited light holes $X(n_c = 2, l)$. A second-subband exciton splitting, which was maximal at $\nu = 5$, was also observed in this sample. This observation points to separate interaction of the two spin states of Landau level $N = 2$ of the $n_c = 1$ subband with the second-subband exciton.

Excitation below and above the GaAs band gap was found useful to distinguish PL from the 2DEG and that from the GaAs buffer layer. From this behaviour and temperature-dependent measurements, strong indications were found for luminescence of the $n_c = 3$ subband. Evidence for the formation of a band of localized states between the spin components of a Landau level comes from a maximum intensity at even filling factor in the sample with the highest carrier density.

The zero-field energy of the Fermi level has been found to be 1.515 eV for all samples. This pinning to the energy of the Fermi level in the GaAs buffer layer shows that the photoexcited holes, which participate in the recombination process, are essentially located in the flat-band region of the GaAs. Therefore, the PL energies of the subbands decrease if the electron concentration of the 2DEG increases.

Resonant excitation (RE) was shown to be a useful method for providing additional information on the 2D system. First, RE on the $X(n_c = 2, \hbar)$ resulted in the appearance of various peaks that were related to the $X(n_c = 2, \hbar)$. Apart from the direct phonon replica of the $X(n_c = 2, \hbar)$, recombination was observed of $n_c = 2$ electrons with holes

located at acceptors and the corresponding phonon replica therefrom. Second, resonant excitation of the third subband was used to create a nonequilibrium electron concentration in this subband. This led to the observation of an extremely sharp phonon replica of the $n_c = 3$ subband. The sample with the lowest carrier density showed unprecedented luminescence of the lowest Landau level of the $n_c = 1$ subband upon resonant excitation of the second-subband exciton.

Acknowledgements

The authors wish to thank H.F. Pen for assistance. This work was supported by the Nederlandse Maatschappij voor Energie en Milieu (NOVEM). The project was also sponsored by the SCIENCE programme of the European Community.

References

1. G.D. Mahan, *Phys. Rev.* **153**, 882 (1967).
2. M.S. Skolnick, J.M. Rorison, D.J. Mowbray, P.R. Tapster, S.J. Bass and A.D. Pitt, *Phys. Rev. Lett.* **58**, 2130 (1987).
3. M.S. Skolnick, K.J. Nash, S.J. Bass, P.E. Simmonds and M.J. Kane, *Solid State Commun.* **67**, 637 (1988).
4. A.S. Plaut, K. v. Klitzing, I.V. Kukushkin and K. Ploog, in *Proceedings of the 20th International Conference on the Physics of Semiconductors*, edited by E.M. Anastassakis and J.D. Joannopoulos (World Scientific, Singapore, 1990), p.1529.
5. A.S. Plaut, I.V. Kukushkin, K. v. Klitzing and K. Ploog, *Phys. Rev. B* **42**, 5744 (1990).
6. H. Buhmann, W. Joss, K. v. Klitzing, I.V. Kukushkin, A.S. Plaut, G. Martinez, K. Ploog and V.B. Timofeev, *Phys. Rev. Lett.* **66**, 926 (1991).
7. A.J. Turberfield, S.R. Haynes, P.A. Wright, R.A. Ford, R.G. Clark, J.F. Ryan, J.J. Harris and C.T. Foxon, *Phys. Rev. Lett.* **65**, 637 (1990); A.J. Turberfield, S.R. Haynes, P.A. Wright, R.A. Ford, R.G. Clark, J.F. Ryan, J.J. Harris and C.T. Foxon, in *Proceedings of the 20th International Conference on the Physics of Semiconductors*, edited by E.M. Anastassakis and J.D. Joannopoulos (World Scientific, Singapore, 1990), p.805.
8. M. Potemski, R. Stepniewski, J.C. Maan, G. Martinez, P. Wyder, and B. Etienne, *Phys. Rev. Lett.* **66**, 2239 (1991).
9. D. Heiman, B.B. Goldberg, A. Pinczuk, C.W. Tu, A.C. Gossard and J.H. English, *Phys. Rev. Lett.* **61**, 605 (1988).
10. I.V. Kukushkin, K. von Klitzing and K. Ploog, *Pis'ma Zh. Eksp. Teor. Fiz.* **47**, 511 (1988) [*JETP Lett.* **47**, 598 (1988)].
11. I.V. Kukushkin, A.S. Plaut, K. von Klitzing and K. Ploog, *Surf. Sci.* **229**, 447 (1990).
12. I.V. Kukushkin, K. v. Klitzing, K. Ploog and V.B. Timofeev, *Phys. Rev. B* **40**, 7788 (1989).
13. H. Buhmann, W. Joss, K. v. Klitzing, I.V. Kukushkin, G. Martinez, A.S. Plaut, K. Ploog and V.B. Timofeev, in *Proceedings of the 20th International Conference on*

- the Physics of Semiconductors*, edited by E.M. Anastassakis and J.D. Joannopoulos (World Scientific, Singapore, 1990), p.1585.
14. B.B. Goldberg, D. Heiman, M. Dahl, A. Pinczuk, L. Pfeiffer and K. West, *Phys. Rev. B* **44**, 4006 (1991).
 15. G.E.W. Bauer, *Solid State Commun.* **78**, 163 (1991).
 16. V.M. Apal'kov and É.I. Rashba, *Pis'ma Zh. Eksp. Teor. Fiz.* **53**, 420 (1991) [*JETP Lett.* **53**, 442 (1991)]
 17. V.M. Apal'kov and É.I. Rashba, *Pis'ma Zh. Eksp. Teor.* **53**, 46 (1991) [*JETP Lett.* **53**, 49 (1991)]
 18. I.E. Perakis and Yia-Chung Chang, *Phys. Rev. B* **43**, 12566 (1991).
 19. T. Uenoyama and L.J. Sham, *Phys. Rev. Lett.* **65**, 1048 (1990).
 20. W. Chen, M. Fritze, A.V. Nurmikko, D. Ackley, C. Colvard and H. Lee, *Phys. Rev. Lett* **64**, 2434 (1990); M. Fritze, W. Chen, A.V. Nurmikko and D. Ackley, in *Proceedings of the 20th International Conference on the Physics of Semiconductors*, edited by E.M. Anastassakis and J.D. Joannopoulos (World Scientific, Singapore, 1990), p.825.
 21. J.F. Mueller, *Phys. Rev. B* **42**, 11189 (1990).
 22. J.F. Mueller, A. Ruckenstein and S. Schmitt-Rink, *Mod. Phys. Lett.* **5**, 135 (1991).
 23. F.A.J.M. Driessen, S.M. Olsthoorn, T.T.J.M. Berendschot, H.F. Pen, L.J. Giling, G.A.C. Jones, D.A. Ritchie and J.E.F. Frost, *Phys. Rev. B* **45**, 11823 (1992).
 24. R.M. Kusters, F.A. Wittekamp, J. Singleton, J.A.A.J Perenboom, G.A.C. Jones, D.A. Ritchie, J.E.F. Frost, and J.-P. André, *Phys. Rev. B* **46**, 10207 (1992).
 25. J.J. Harris, D.E. Lacklison, C.T. Foxon, F.M. Selten, A.M. Suckling, R.J. Nicholas and K.W.J. Barnham, *Semicond. Sci. Technol.* **2**, 783 (1987).
 26. R.M. Kusters, J. Singleton, G. Gobsch, G. Paasch, D. Schulze, F.A. Wittekamp, G.A.C. Jones, J.E.F. Frost, D.C. Peacock and D.A. Ritchie, *Superlattices and Microstructures* **9**, 55 (1991).
 27. W.H. Knox, D.S. Chemla, and G. Livescu, *Solid State Electr.* **31**, 425 (1988).
 28. B.K. Ridley, *Rep. Prog. Phys.* **54**, 169 (1991).
 29. T. Ando, *J. Phys. Soc. Japan* **43**, 1616 (1977).
 30. Th. Englert, D.C. Tsui, A.C. Gossard and Ch. Uihlein, *Surface Sci.* **113**, 295 (1982).
 31. R. Fletcher, E. Zaremba, M. D'Iorio, C.T. Foxon and J.J. Harris, *Phys. Rev. B* **41**, 10649 (1990).
 32. D.M. Larsen in *Polarons in Ionic Crystals and Polar Semiconductors*, edited by J.T. DeVreese (North-Holland, Amsterdam, 1972).
 33. W. Chen, M. Fritze, A.V. Nurmikko, M. Hong and L.L. Chang, *Phys. Rev. B* **43**, 14738 (1991).
 34. J. Aaviksoo, I. Reimand, V.V. Rossin and V.V. Travnikov, *Phys. Rev. B* **45**, 1473 (1992).
 35. M. Shinada, and S. Sugano, *J. Phys. Soc. Japan* **21**, 1936 (1966).
 36. A.M. Kazaryan, and E.M. Kazaryan, *Fiz. Tekh. Poluprov.* **11**, 1383 (1977) [*Sov. Phys. Semicond.* **11**, 813 (1977)].
 37. F.-Y. Juang, Yasunobu Nashimoto, and Pallab K. Bhattacharya, *J. Appl. Phys.* **58**, 1986 (1985).

38. The illustrative example of the simple triangular potential well was treated by W. Zawadzki in *Two-Dimensional Systems, Heterostructures and Superlattices*, Solid-State Sciences **53**, edited by G. Bauer, F. Kuchar, and H. Heinrich (Springer, Berlin, 1984), 2.
39. B.I. Shklovskii and A.L. Efros, *Electronic Properties of Doped Semiconductors*, (Springer, Berlin, 1984).
40. P.J. Dean and M.S. Skolnick, *J. Appl. Phys.* **54**, 346 (1983).
41. This method is used (*inter alia*) for identifying residual donor species. The intensities of so-called “two-electron” satellite peaks are increased if the (D^0, X) peak is resonantly excited (Refs.40 and 42).
42. F.A.J.M. Driessen, H.G.M. Lochs, S.M. Olsthoorn and L.J. Giling, *J. Appl. Phys.* **69**, 906 (1991).
43. I.V. Kukushkin, K. von Klitzing and K. Ploog, *Phys. Rev B* **37**, 8509 (1988).
44. B.J. Skromme, S.S. Bose and G.E. Stillman, *J. Electron. Mater.* **15**, 345 (1986).
45. J.S. Blakemore, *J. Appl. Phys.* **53**, R123 (1982).
46. M.A. Stroscio, K.W. Kim and J.C. Hall, *Superlatt. Microstruct.* **7**, 115 (1990).
47. S. Zemon, P. Norris, E.S. Koteles and G. Lambert, *J. Appl. Phys.* **59**, 2828 (1986).

Chapter 6

Detection of two-dimensional electron gases in undoped heterojunctions with magnetophotoluminescence

F.A.J.M. Driessen, S.M. Olsthoorn and L.J. Giling.

Department of Experimental Solid State Physics, Research Institute for Materials, University of Nijmegen, Toernooiveld, NL 6525 ED Nijmegen, The Netherlands

Abstract

We report the observation of a magneto-exciton in undoped GaAs/Al_xGa_{1-x}As heterojunctions by photoluminescence. The exciton originates from photoexcited holes and two-dimensional electrons, which are confined in the shallow potential at the heterointerface. The observation of this exciton is particularly useful for identification of unintended two-dimensional electron gases in cases where detection by temperature-dependent Hall measurements is difficult.

Accepted for publication in:
Applied Physics Letters

In recent years there has been great interest in the study of two-dimensional electron gases (2DEG) using contactless optical techniques, such as photoluminescence (PL)[1-13] and photoreflectance (PR) spectroscopy [14-17]. Because the zero-field PL spectrum of a GaAs/Al_xGa_{1-x}As single heterojunction is dominated by intense bulk-GaAs recombination [1], research has focused on structures with confined holes in the vicinity of the 2DEG, such as quantum wells [2,3], modulation-doped quantum wells [4-7], and modulation-doped single heterojunctions with hole confinement [8-10]. Recently, we showed that strong PL from the 2DEG could also be observed in high-carrier-density single heterojunctions without hole confinement upon application of a magnetic field [12,13]. In this paper we show that such measurements can be used to detect the presence of a 2DEG in undoped GaAs/Al_xGa_{1-x}As single heterojunctions.

Experiments were carried out on several undoped GaAs/Al_xGa_{1-x}As heterojunctions in which the Al_xGa_{1-x}As was deposited directly on semi-insulating GaAs substrates by metalorganic vapour-phase epitaxy. Because results were similar with different samples, we show data only from a sample with a 5.1 μm thick, high-purity Al_{0.22}Ga_{0.78}As epilayer for which Hall measurements at 77 K showed an *n*-type carrier concentration of 5.5 × 10¹⁴ cm⁻³. Experimental conditions for the high-resolution magnetophotoluminescence (MPL) measurements (Faraday configuration) have been described previously [18]; the laser energy was chosen well below the Al_{0.22}Ga_{0.78}As band gap, making it transparent.

Fig. 6.1 shows the PL spectrum around the energy of the GaAs excitons at various magnetic field strengths, all recorded at *T*=1.5 K. The low-field spectra are similar to those of the GaAs substrate and show free excitons FX as well as excitons bound to residual acceptors (A⁰,X) and donors (D⁰,X). Upon applying a magnetic field, a narrow PL line (labeled *X*_{2D}) is observed which is absent in the MPL spectrum of GaAs without the Al_xGa_{1-x}As epilayer; a reference spectrum at *B* = 7 T of the uncapped GaAs is shown in the upper graph of Fig. 6.1. From Fig. 6.1 it is clear that the intensity of *X*_{2D} increases markedly with the magnetic field. However, a precise determination of this relationship is hindered by interference with the bulk-GaAs luminescence. At low fields a quadratic relationship between photon energy *E* and the magnetic field *B* is observed, which is typical exciton behaviour [19]: $E(B) = E_0 + \alpha B^2$, where *E*₀ is the zero-field energy and

$$\alpha = \frac{e^2 a_B^2}{4m^* c^2} \quad (6.1)$$

(*a*_B and *m*^{*} are respectively the effective Bohr radius of the exciton and its effective mass). We measure α = 0.1 meVT⁻², which implies that the exciton radius is approximately 280 Å. This is twice as large as that of the bulk FX and shows that the built-in electric field near the heterointerface tends to separate the exciton. At zero field, *X*_{2D} extrapolates to *E*₀ = 1.515 eV and it cannot be distinguished from the GaAs free exciton. (For a sample with the slightly higher carrier concentration of 1.8 × 10¹⁵ cm⁻³ this zero-field value was 1.514 eV.)

The band structure of the GaAs/Al_xGa_{1-x}As heterojunction is shown schematically in Fig. 6.2. Owing to the low donor concentration in the Al_xGa_{1-x}As, the potential well at the interface is very shallow and only one subband (*n*_c = 1) will be occupied.

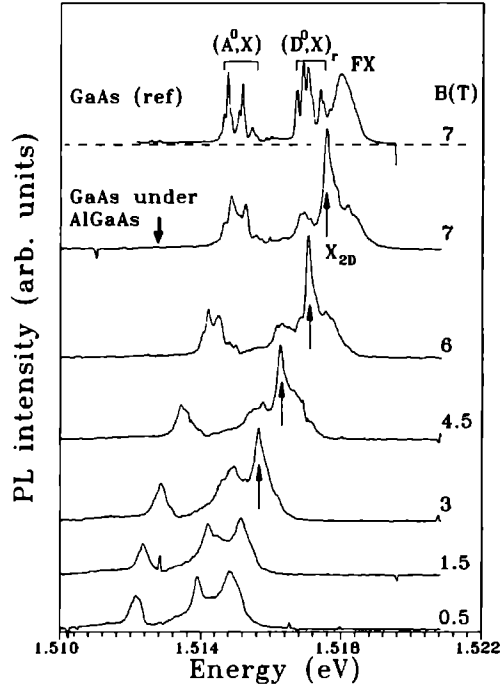


Figure 6.1 Exciton region of PL spectra of the GaAs/Al_xGa_{1-x}As heterojunction at various magnetic fields B . The upper graph shows the 7-T spectrum of a GaAs reference sample without Al_xGa_{1-x}As top layer.

Therefore, the magneto-exciton that is observed in this undoped heterojunction will most likely involve the lowest Landau level ($N = 0$) of the $n_c = 1$ subband. The density of states in this $N = 0$ Landau level increases linearly with magnetic field [20], which explains the intensity increase of X_{2D} observed in Fig. 6.1. By analogy with our work on high-carrier-density heterojunctions [12,13], this increase might also be stimulated by wave-function mixing of the Fermi-edge resonance and the $n_c = 1$ subband. This provides a mechanism for enhancement of the matrix element for optical recombination.

In conclusion, we have shown that, even in high-purity GaAs/Al_xGa_{1-x}As heterojunctions, the presence of a 2DEG at the heterointerface can be easily detected with magnetophotoluminescence through the observation of an exciton whose intensity increases upon increasing B . The method is applicable to other III/V heterostructures and is not restricted to the GaAs/Al_xGa_{1-x}As combination. This magneto-optical method could be of particular use where it is suspected that temperature-dependent Hall measurements

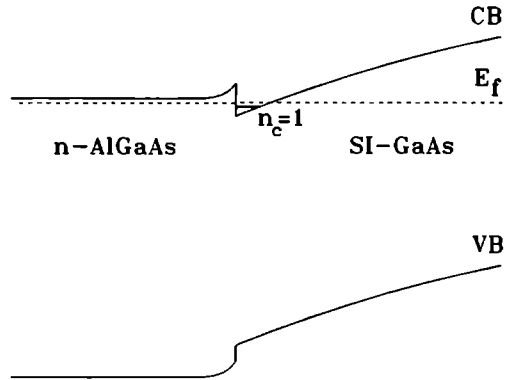


Figure 6.2 Schematic representation of the band structure of n -type $\text{Al}_x\text{Ga}_{1-x}\text{As}$ grown on a semi-insulating GaAs substrate.

are affected by a 2DEG.

The authors are grateful to Billiton Precursors B.V. for providing samples and to D.M. Frigo for his critical reading of the manuscript.

References

1. C.A. Yang, S.A. Lyon, and C.W. Tu, *Superlattices and Microstruct.* **3**, 269 (1987).
2. F. Meseguer, J.C. Maan, and K. Ploog, *Phys. Rev. B* **35**, 2505 (1987).
3. M.C. Smith, A. Petrou, C.H. Perry, and J.M. Worlock, *Surf. Sci.* **174**, 136 (1986).
4. M.S. Skolnick, K.J. Nash, S.J. Bass, P.E. Simmonds and M.J. Kane, *Solid State Commun.* **67**, 637 (1988).
5. D. Heiman, B.B. Goldberg, A. Pinczuk, C.W. Tu, A.C. Gossard and J.H. English, *Phys. Rev. Lett.* **61**, 605 (1988).
6. W. Chen, M. Fritze, A.V. Nurmikko, D. Ackley, C. Colvard and H. Lee, *Phys. Rev. Lett* **64**, 2434 (1990); W. Chen, M. Fritze, A.V. Nurmikko, M. Hong and L.L. Chang, *Phys. Rev. B* **43**, 14738 (1991).
7. M. Potemski, J.C. Maan, A. Fasolino, K. Ploog, and G. Weimann, *Phys. Rev. Lett.* **63**, 2409 (1989).
8. I.V. Kukushkin, K. von Klitzing and K. Ploog, *Pis'ma Zh. Eksp. Teor. Fiz.* **47**, 511 (1988) [*JETP Lett.* **47**, 598 (1988)].
9. I.V. Kukushkin, K. v. Klitzing, K. Ploog and V.B. Timofeev, *Phys. Rev. B* **40**, 7788 (1989).
10. A.S. Plaut, I.V. Kukushkin, K. v. Klitzing and K. Ploog, *Phys. Rev. B* **42**, 5744 (1990).

11. A.J. Turberfield, S.R. Haynes, P.A. Wright, R.A. Ford, R.G. Clark, J.F. Ryan, J.J. Harris, and C.T. Foxon, *Phys. Rev. Lett.* **65**, 637 (1990).
12. F.A.J.M. Driessen, S.M. Olsthoorn, T.T.J.M. Berendschot, H.F. Pen, L.J. Giling, G.A.C. Jones, D.A. Ritchie and J.E.F. Frost, *Phys. Rev. B* **45**, 11823 (1992).
13. F.A.J.M. Driessen, S.M. Olsthoorn, T.T.J.M. Berendschot, L.J. Giling, D.M. Frigo, G.A.C. Jones, D.A. Ritchie and J.E.F. Frost, *Phys. Rev. B* **47**, 1282 (1993).
14. X. Yin, F.H. Pollak, L. Pawlowicz, T. O'Neill, and. M. Hafizi, *Appl. Phys. Lett.* **56**, 1278 (1990).
15. A.A. Berbussi, F.H. Pollak, P. Basmaji, I.F.L. Dias, in *Proceedings of the 20th International Conference on the Physics of Semiconductors*, edited by E.M. Anastassakis and J.D. Joannopoulos (World Scientific, Singapore, 1990), p.1065.
16. M. Sydor, A. Badakhshan, J.R. Engholm, and D.A. Dale, *Appl. Phys. Lett.* **58**, 948 (1991).
17. N. Bottka, D.K. Gaskill, P.D. Wright, R.W. Kaliski, and D.A. Williams, *J. Cryst. Growth* **107**, 893 (1991).
18. F.A.J.M. Driessen, H.G.M. Lochs, S.M. Olsthoorn and L.J. Giling, *J. Appl. Phys.* **69**, 906 (1991).
19. R. Dingle, *Phys. Rev. B* **8**, 4627.
20. H. Aoki, *Rep. Prog. Phys.* **50**, 655 (1987).

Chapter 7

Effects of confined donor states on optical and transport properties of ordered GaInP₂ alloys

F.A.J.M. Driessen, S.M. Olsthoorn, G.J. Bauhuis, L.J. Giling.

Department of Experimental Solid State Physics, Research Institute for Materials, University of Nijmegen, Toernooiveld, NL 6525 ED Nijmegen, The Netherlands

Abstract

We report properties of long-range ordered GaInP₂ alloys as a function of temperature by a combination of photoreflectance (PR), photoluminescence (PL) and Hall-van der Pauw measurements. Below $T \approx 200$ K optical and transport properties are strongly influenced by a donor state which, owing to confinement in the ordered domains, has a large binding energy of 36 meV. Evidence for strong localization was obtained for $T < 30$ K: the PR spectra showed a pronounced first-derivative line shape at the same energy where PL emission occurs, the conductivity was dominated by hopping (ϵ_3) conduction, and the temperature dependence of the PL intensity was consistent with localized states. Between 30 and 70 K the dominating conduction mechanism was identified as ϵ_2 conduction via negatively charged donors: the D^- band. At 70 K, Hall data showed a changeover from ϵ_2 to band conduction. It is proposed that the origin of the inverted-S shape of PL energy as a function of temperature is connected with thermal population of the D^- band. In the entire T interval between 30 and 200 K, the PR spectra showed a complex line shape owing to the absence of carriers in the disordered regions. Above $T = 200$ K pronounced effects of cluster scattering are observed in the Hall mobility. Supported by data from PR and PL, this shows that carriers are then present in both ordered and disordered regions of the epilayer.

Submitted to Physical Review B

7.1 Introduction

The ternary semiconductor $\text{Ga}_x\text{In}_{1-x}\text{P}$ forms an attractive alternative to $\text{Al}_x\text{Ga}_{1-x}\text{As}$ in optoelectronic devices, such as $\text{Ga}_x\text{In}_{1-x}\text{P}/\text{GaAs}$ tandem junction solar cells, which exhibit amongst the highest energy conversion efficiencies reported so far [1], and $(\text{Al,Ga,In})\text{P}$ laser diodes in which $\text{Ga}_x\text{In}_{1-x}\text{P}$ is used as the active layer [2-5]. Reasons for using $\text{Ga}_x\text{In}_{1-x}\text{P}$ are, first, that a direct-band-gap value as high as 2.2 eV can be obtained with $\text{Ga}_x\text{In}_{1-x}\text{P}$, whereas for $\text{Al}_x\text{Ga}_{1-x}\text{As}$ this value is 1.9 eV at the direct-to-indirect crossover. Second, the surface recombination velocity of the $\text{Ga}_x\text{In}_{1-x}\text{P}/\text{GaAs}$ interface is 1.5 cm/s [6], some two orders of magnitude lower than for a typical $\text{Al}_x\text{Ga}_{1-x}\text{As}/\text{GaAs}$ interface. Third, the carrier-trapping DX centre is not occupied in $\text{Ga}_{0.52}\text{In}_{0.48}\text{P}$ (hereafter abbreviated as GaInP_2), which is the composition at which lattice matching with GaAs is achieved. For $\text{Al}_x\text{Ga}_{1-x}\text{As}$ the DX center is already occupied above $x = 0.22$, where it leads to a decrease of the free carrier concentration [7].

In spite of its successful application, various fundamental material properties of GaInP_2 are not well understood. The reason for this is that optical and transport properties of the equimolar GaInP_2 are complicated by the occurrence of regions of spontaneous long-range order of the CuPt type, namely as monolayer $(\text{GaP})_1(\text{InP})_1$ superlattices in the [111] direction. As a consequence of this ordering the symmetry of the crystal is lowered in these regions, which leads to a splitting of the valence band and a decrease of the band gap [8]. For an infinitely large, ordered GaInP_2 crystal a reduction of 260 meV was calculated [9] whereas values around 100 meV [10-12] and recently even 190 meV [13] have been found experimentally. The degree of ordering -size, shape, homogeneity and density of the ordered domains- depends on growth kinetics, which in turn is determined by growth conditions such as temperature of growth, V/III ratio and substrate orientation. Growth of GaInP_2 epilayers without ordering has also been achieved [14,15]. The optical properties of ordered GaInP_2 show several anomalies: the so-called inverted-S shaped behaviour of PL energy as a function of temperature [16,17]; the strong shift of the dominant PL peak towards higher energy upon increasing the excitation density P ; and the long carrier lifetimes, which also depend strongly on P [18]. DeLong *et al.* [18] concluded from the last two properties that spatially indirect recombination took place in the alloy.

In this paper we present variable-temperature photoreflectance (PR), photoluminescence (PL) and Hall-van der Pauw measurements on long-range ordered GaInP_2 . We show that optical and transport properties are greatly influenced by localization on relatively deep donor states that are confined in the ordered domains.

7.2 Experimental Details

7.2.1 Experimental Techniques

Variable temperature ($4.2 < T < 450$ K) Hall-van der Pauw measurements were performed using a clover-leaf sample shape. The Hall factor (the ratio of Hall mobility

and drift mobility) was taken as unity. Details on the PL experiment were described in Ref.[19] except that an Ar⁺ laser at 514 nm was used for excitation. The PR technique has been described previously in the literature [20]. Here, an Ar⁺ laser (again 514 nm) was used for modulating the built-in surface field of the sample that was mounted in a variable-temperature optical flow cryostat. During PR, typical values of excitation density of the modulating source were 0.1-100 mW over a 0.5 cm² spotsize. The background of additionally modulated PL signal, which was constant during each PR measurement, was subtracted from the signal.

7.2.2 Samples and their degree of ordering

The experiments were carried out on GaInP₂ epilayers grown by metalorganic vapour-phase epitaxy at a pressure of 20 mbar. The 2.1- μ m thick epilayers were grown lattice matched on a (100) 2^o off towards (110) semi-insulating GaAs substrate at $T = 700^{\circ}$ C and V/III ratios of 400 (sample 1) and 870 (sample 2). The epilayers were nominally undoped and showed *n*-type conductivity. At room temperature the values for carrier concentration and mobility were 4.2×10^{15} cm⁻³ and 2500 cm²/Vs for sample 1, and 3.4×10^{15} cm⁻³ and 2250 cm²/Vs for sample 2. The aforementioned growth conditions are known to produce samples with long-range regions of monolayer superlattice ordering; the degree of ordering being larger for sample 2 [10,15,21,22].

The existence of the ordered structure in these samples was confirmed by transmission electron microscopy (TEM) which showed extra diffraction spots for the ($\bar{1}$ 1 1) and (1 $\bar{1}$ 1) directions corresponding to long-range ordering of the CuPt-type. The TEM diffraction patterns also showed diffused streaks in the (0 0 1) directions, which provides evidence for the quasi two-dimensionality of the ordered domains: thin in the direction of growth and extended in the directions perpendicular thereto. Furthermore, qualitative measures of the degree of ordering of GaInP₂ epilayers are the values for both the anomalously strong shift of PL energy as a function of excitation density P (the so-called "moving emission" [10,11,18,23]) and for the carrier lifetime, which is extremely long ($\sim \mu$ s-ms) [18] compared with random alloys (\sim ns). The moving components of the 4K-PL spectra of samples 1 and 2 increased 4.7 meV and 6.1 meV per order of magnitude increase in excitation density; values which, under the given growth conditions, are in good agreement with other published data [10]. A qualitative measure of the long carrier lifetimes τ can be obtained by determining the decrease of PL intensity upon increasing the PL chopping frequency ν_{chop} [18]. The decrease starts as soon as this modulation frequency ν_{chop} is of the order of the inverse lifetime τ^{-1} because then a phase difference occurs between the PL and the reference signal. For samples 1 and 2 roll-off frequencies of approximately 12.1 kHz and 8.8 kHz were measured at an excitation density of 2.6×10^{-2} Wcm⁻²; this implies lifetimes (1/e time constant) of 80 and 110 μ s, respectively. A time-resolved PL experiment on sample 1 confirmed the long lifetimes: $\tau = 200 \mu$ s at $T = 4.2$ K (the higher τ is a result of a slightly lower excitation density). These results are also in good agreement with those reported in literature for samples grown under the same conditions. Hence, although strongly dependent on growth conditions, GaInP₂ epilayers

with a specific degree of ordering can be grown reproducibly. Almost all measurements we performed gave comparable results on both samples, so we report the results of only sample 1.

7.3 Results and Discussion

7.3.1 Photoreflectance

PR spectra recorded at various temperatures are shown in Fig.7.1. In those recorded at 240 and 293 K, a third-derivative line shape (TDLS) is observed. For semiconductors with a homogeneous intrinsic field distribution this TDLS occurs for low values of the modulation field [24], such as it is the case under our experimental conditions. In the temperature interval 40-190 K the spectra show a markedly different

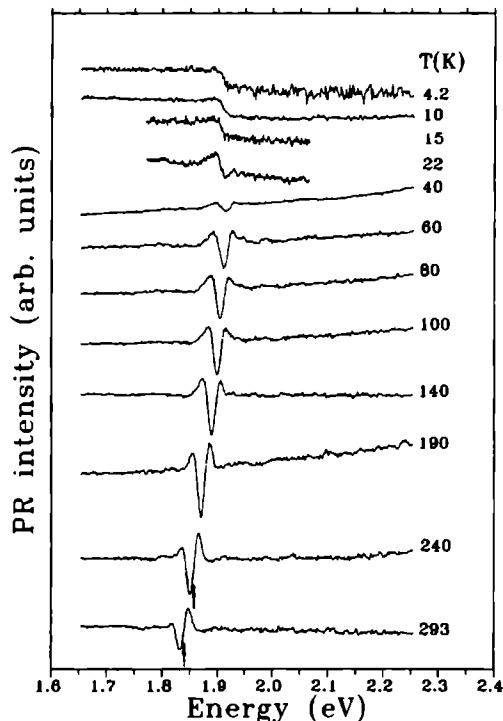


Figure 7.1 Photoreflectance spectra as a function of temperature. The arrows in the spectra with a third-derivative line shape correspond to the energy of the band gap.

PR line shape from those at higher T . This complex line shape corresponds nearly to that observed in the high-field limit [24,25]; the low energy side of the line shape may be affected by impurities. Because the value of the modulating field was not increased while lowering T [26], the high-field line shape can only be explained by field inhomogeneities in the sample. These inhomogeneities are presumably caused by confinement of electrons in the ordered domains, which have lower band gaps.

A second interesting change in PR line shape is observed in spectra recorded at temperatures between 4.2 K and 22 K: the spectra then clearly show a first-derivative line shape (FDLS). Recently, the effects of electric field modulation on the PR line shapes of isolated confined systems, such as quantum wells and superlattices, have been calculated by Glembocki and Shanabrook [27], and by Enderlein, Djiang and Tang [28,29]. In all cases a first-derivative line shape (FDLS) was found. For superlattices and quantum wells this line shape resulted from the Stark effect of minibands and sublevels, respectively. In the case of superlattices, tunneling through its barriers resulted in an additional TDLS, which is characteristic for the Franz-Keldysh effect [29]. Therefore, our observation of a pronounced FDLS with PR shows that at low T the carriers are strongly localized.

From the PR line shapes the band gap was calculated using Aspnes and Rowe's three-point method [24]. For the TDLS's these energies are shown by arrows in the lower spectra of Fig.7.1; they will be discussed below in conjunction with results from PL.

7.3.2 Hall-van der Pauw measurements

Fig.7.2 shows the Hall mobility μ_H as a function of T . Below $T = 100$ K the $\mu_H \propto T^{1.5}$, which is characteristic of the dominance of ionized impurity scattering; between 150-200 K the $\mu_H \propto T^{-0.3}$, showing that scattering of electrons by optical phonons through the polar interaction plays an important role [30,31]. Above $T = 200$ K μ_H depends only little on T , which shows that a third scattering mechanism predominates. By treating spherically ordered domains as clusters Friedman, Kibbler and Olson [32] calculated that scattering at ordered clusters in GaInP₂ strongly affected μ_H . Their model predicts that, for samples with large cluster radius r_c , the μ_H should even increase with increasing T . However, experimental verification of the effect of cluster scattering on μ_H at high T could not be made from their measurements on ordered Ga_xIn_{1-x}P samples; they could only conclude that $r_c < 20$ Å. We believe that the behaviour of μ_H above $T = 200$ K, shown in Fig.7.2, is the first experimental observation of the pronounced effect that cluster scattering can have on the mobility of GaInP₂ samples. The temperature at which electrons in the disordered regions show pronounced scattering at ordered domains corresponds with the temperature above which PR spectra show a uniform carrier distribution in the entire sample. According to the model of Ref.[32], the influence of cluster scattering should become more pronounced if r_c is larger. For sample 2, which has a larger degree of ordering, larger effects of cluster scattering were indeed observed: the mobility decreased only by 15% upon increasing T from 200 to 450 K. This result and further data obtained from magnetotransport measurements will be published separately [33].

Before proceeding, a brief reminder will be given on impurity conduction in semi-

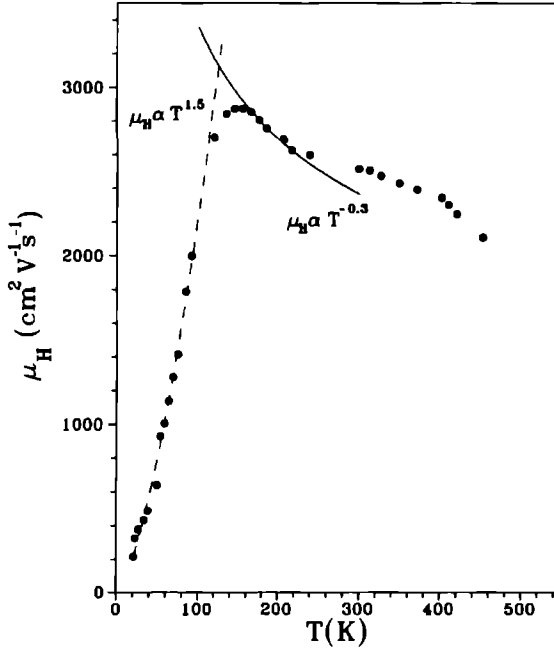


Figure 7.2 Temperature dependence of the dc Hall mobility.

conductors, valid for not too high temperatures; n -type terminology is used. The dc conductivity can be expressed as a sum of three terms [34,35]:

$$\sigma(T) = \sigma_1 e^{-\epsilon_1/kT} + \sigma_2 e^{-\epsilon_2/kT} + \sigma_3 e^{-\epsilon_3/kT} \quad , \quad (7.1)$$

where ϵ_1 is the donor ionization energy, which can always be observed provided the donor concentration n_D does not give rise to metallic conduction ($n_D < 10^{18} \text{cm}^{-3}$ for GaInP_2). The second term in the conductivity can only be observed at intermediate concentrations in a certain temperature range intermediate between the high- T regime where ϵ_1 conduction dominates, and the low- T regime where ϵ_3 conduction dominates [36]. This ϵ_2 conduction is associated with conduction in an impurity band that is believed to arise from a resonance between negatively charged donors, the D^- ions. The D^- band is intermediate between the bottom of the conduction band and the donor level. The activation energy ϵ_2 is known to be half of the energy gap from the donor ground state to the bottom of the D^- band [37]. Owing to the great spatial extent of these D^- states [37], the interaction between them is strong, which results in a large D^- band width. Upon increasing n_D this width increases and ϵ_2 is consequently reduced. The third term in the conductivity is observed most prominently in the low impurity concentration region and dominates at the lowest

temperatures. Charge transport is explained in terms of hopping conduction: phonon-induced tunneling of electrons from occupied to unoccupied donor states [34,38,39]. Its small activation energy ϵ_3 is attributed to the potential difference between impurity sites owing to Coulomb fields of compensating impurity ions.

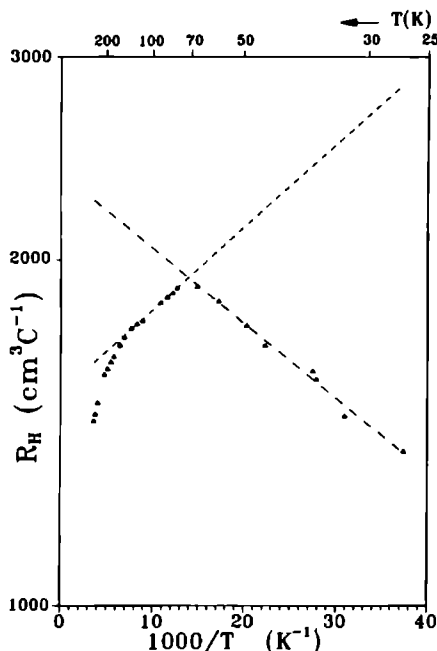


Figure 7.3 Hall coefficient R_H versus T^{-1} .

Changes in the dominant conductivity mechanism can be observed by a maximum in the relationship between the Hall coefficient $R_H = [n(T)e]^{-1}$ and T^{-1} , where $n(T)$ is the carrier concentration and e the electron charge [40]. Fig.7.3 shows such a plot for sample 1 above $T = 25$ K; the clear maximum shows that the dominant conduction mechanism changes at $T \approx 70$ K. A maximum was found for sample 2 at $T \approx 85$ K. In order to determine whether ϵ_3 conduction or ϵ_2 conduction occurs below the transition point, we performed magnetotransport measurements on sample 2 in the High-Field Magnet Laboratory, Nijmegen. From the behaviour of activation energies in a magnetic field we found ϵ_2 conduction for temperatures in the range 30-70 K and ϵ_3 conduction below 30 K; the results from these measurements will be published separately [33]. Because neutral donors are required for both impurity conduction mechanisms, the remarkably high temperatures at which the changes in conduction mechanisms occurred suggest a large donor binding energy. From the T -region where carrier freeze-out determined the

resistivity in the magnetotransport measurements, a donor binding energy ϵ_1 of 36 meV was found [33]. This value is large compared with the ionization energy E_D of a hydrogenlike donor in GaInP₂. On the basis of effective mass theory this energy is expected to be 11.1 meV because $E_D = (m_0^*/\epsilon_r^2)Ry$, where $m_0^* = 0.108$ is the effective electron mass in units of the free electron mass [41], $\epsilon_r = 11.49$ is the dielectric constant [42] and $Ry = 13.6$ eV is the Rydberg energy. The ordered domains are, at least in the direction of growth, expected to be smaller than the effective Bohr radius of the hydrogenlike donor. By analogy with quantum wells, the conduction-band offset between the ordered (well) and disordered (barrier) alloy then acts as a potential barrier and constricts the donor wave-function to the ordered domains, which results in a large overlap with the donor core. An accompanying enhancement of E_D by up to a factor of four was calculated for quantum wells [43].

Although all nominally undoped Ga_xIn_{1-x}P samples grown in our group were *n*-type at 10¹⁵ - 10¹⁶ cm⁻³ (at room temperature), ϵ_2 and ϵ_3 conduction from donors in the ordered domains was only observed in those samples with long-range ordering; this implies large film-like domains. Clearly interdomain distances are relatively small in these epilayers otherwise it would not be possible to measure conduction through the ordered domains.

7.3.3 Photoluminescence

The low-excitation-density PL and PR spectra at $T = 4.2$ K are compared in Fig.7.4. The dominant PL peak is accompanied by a low-energy shoulder that increased sublinearly with increasing excitation density. This shoulder is probably acceptor related or results from intrinsic recombination with large spatial separation and small recombination probability. The most important feature of Fig.7.4 is that the dominant PL signal is emitted at the same energy as the step in the PR signal. This is a remarkable result because PR more strongly reflects the band structure and PL comes preferentially from impurity states in the band gap. Therefore, the absence of Franz-Keldysh oscillations and the clear first-derivative line shape at the impurity edge shows that the PR line shape is entirely determined by electron localization at these impurities in our samples. On the basis of Hall data and the long lifetimes, we attribute the low- T PL to spatially separated recombination between electrons at donors in the ordered regions and photoexcited holes, *i.e.* (D_{ord}^0, h).

Fig. 7.5 shows PL spectra for temperatures below 45 K recorded at $P = 1$ Wcm⁻². A second low-energy shoulder is now observed in the lowest T spectra separated 47 meV from the dominant PL (labelled 'A'). On the basis of the energy difference we attribute this shoulder to an LO phonon replica, for which an energy separation of 46.8 meV was reported [44]. According to selection rules for scattering of excitons by LO phonons, the first LO replica is forbidden owing to momentum conservation [45]. However, this selection rule is relaxed in cases of strong spatial localization, for which the uncertainty in momentum is comparable with the phonon momentum. Our observation of an LO phonon replica below $T = 25$ K is therefore further evidence for the strong localization that appears in GaInP₂ alloys at low temperatures. At the high-energy side another shoulder (labelled 'B') is present, which dominates the spectrum above $T > 25$ K. Peak

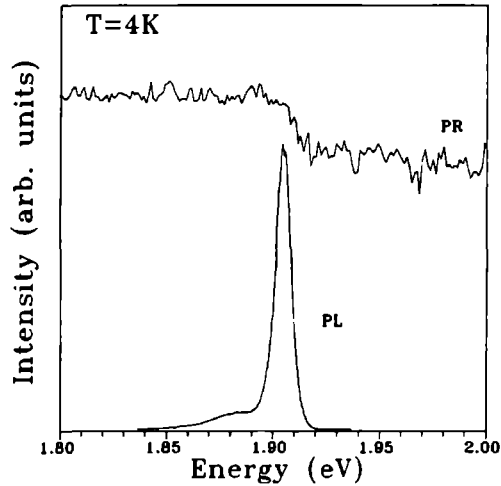


Figure 7.4 Photoreflectance and photoluminescence spectra at $T = 4.2$ K.

TABLE I: Rates of emission shift dE/dP and exponents x in $I \propto P^x$ for peaks A and B at different temperatures.

$T(K)$	Peak A		Peak B	
	dE/dP	x	dE/dP	x
4.2	4.7	0.98	†	†
25	5.2	1.01	0	1.45
40	7.2	1.08	0	1.49
70	†	†	0	1.61

†not observable

B is not accompanied by a phonon replica, indicating a nonlocalized nature of that PL.

Table I summarizes the rate of emission shift dE/dP and the dependence of PL intensity I upon P for peaks A and B at various temperatures. The I of peak 'A' depends virtually linearly on P . This behaviour is in accordance with the expected behaviour of ($D_{ord,h}^0$): I proportional to the hole density [h], which in turn depends linearly on P . The I of peak 'B' depends superlinearly on P . An exponent between 1 and 2 is typical for PL processes in which both electrons and holes are photocreated (e.g. bound-excitons, free excitons and band-to-band recombination), and in which parallel radiationless processes

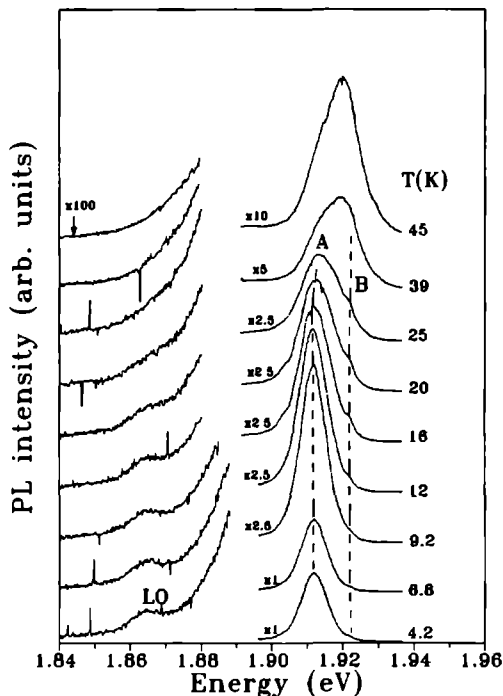


Figure 7.5 Temperature dependence of the photoluminescence spectra from 4.2-45 K.

participate. The dE/dP was found to be zero for peak 'B' which shows that electrons and holes are not spatially separated. The rate at which the PL energy of peak 'A' shifts is seen to increase if peak 'B' increases. This can be rationalized by assuming that peak 'B' has a short lifetime, which results in a reduction of the valence band filling. The accompanying reduction in band flattening will then cause a larger dE/dP for peak 'A'.

The anomalous behaviour of photon energy as a function of temperature in ordered GaInP_2 [16,17] is shown in Fig.7.6 for sample 1; where possible, energies of the moving and nonmoving components are shown separately. The dashed curve visualizes the energy of the PL maximum. With increasing temperature (4-20 K) an initial small decrease in energy was observed, followed by an increase in energy (T from 20-45 K) and finally a decrease again: the so-called inverted-S shape [46]. The energies of the band gap E_0 as deduced from PR are also shown in Fig.7.6 by squares. At the highest temperatures these energies could be precisely determined using Aspnes and Rowe's formalism [24]. The more complex line shape between $T = 40$ and 190 K hindered the precise determination

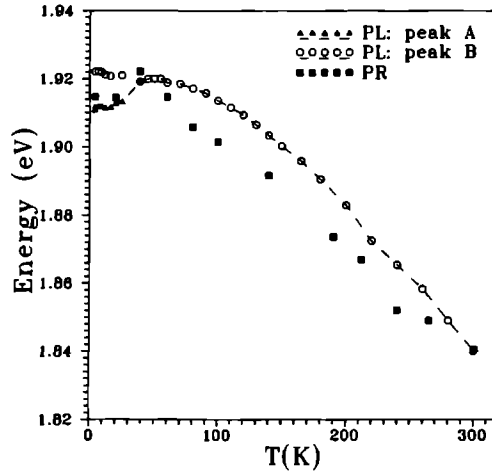


Figure 7.6 Energy of photoluminescence emissions as a function of T ; the dashed curve visualized the energy of the PL maximum. The values of the band gap as determined by photoreflectance are shown by squares.

of E_0 . The E_0 determined using Ref.[24] corresponded virtually to the energies of the dips in the spectra for $40 < T < 190$ K and merged with the FDLS at lower temperatures. At $T = 293$ K E_0 coincides with the energy of the PL emission, from which the PL process at $T = 293$ K is identified as band-to-band recombination. For $40 < T < 190$ K E_0 is of lower energy than that of the PL emissions. Kondow *et al.* [16] also reported lower E_0 values obtained from the dips in their PR spectra (recorded below 150 K) for GaInP₂ epilayers with smaller degree of ordering (V/III ratio of 160 and growth temperature of 700 K). They attributed this effect to an inhomogeneous band gap distribution in their sample. However, our data points at 300 K and below 22 K show that PR and PL features appear at the same energy. Therefore, we believe that the energy of the dip in the PR spectrum gives an unreliable value for the band gap for such a complex PR line shape.

A similar inverted-S-shaped temperature dependence of PL energy E was also reported recently in so-called disordered superlattices, *i.e.* those in which disorder is introduced by random variations of the well and/or barrier widths [47]. It was also observed for Al_xIn_{1-x}As epilayers [48]. For both the disordered superlattices [49,50] and the Al_xIn_{1-x}As, strong carrier localization was reported. Therefore, it appears that the inverted S-shaped behaviour occurs only together with carrier localization. For our sample the anomalous increase of PL energy starts if T exceeds 25 K, which is virtually the same temperature below which PR spectra showed evidence for strong localization through a FDLS. Furthermore, the conduction mechanism changed from ϵ_3 conduction

to ϵ_2 conduction at this temperature. The origin of the inverted-S-shaped dependence of photon energy on temperature may therefore be the following. At low temperature confined donor-to-band transitions occur (peak 'A'). Because the gap between the bottom of the D^- band and the donor states is small, the lowest lying states in the D^- band can be occupied at relatively low temperature and this wide band will then be filled. The observed increase in PL energy upon increasing temperature may therefore be due to PL from the D^- band, which in the spectra of Fig.7.5 is observed as peak 'B' (note its consistent superlinear relationship between I and P). The additional, usual band gap reduction [51] upon increasing temperature leads to a decrease in PL energy at higher temperatures.

Yamamoto *et al.* [50] also reported the PL intensity as a function of temperature for their disordered superlattices $(\text{AlAs})_m(\text{GaAs})_n$ (m and n randomly chosen between one and three with an average value of two), and found that their behaviour was strongly determined by the presence of localized states. In comparison with ordered superlattices and a random $\text{Al}_{0.5}\text{Ga}_{0.5}\text{As}$ alloy, which both also contained 50 % of Al for the group III component, the PL intensity of the disordered superlattices showed a more gradual reduction upon increasing temperature [47,50]. It appeared that the data could be well fitted to a relationship valid for amorphous semiconductors because of the existence of localized states therein [52]:

$$I_{\text{PL}}(T) = \frac{I_0}{1 + A \exp(T/T_0)} \quad (7.2)$$

where I_{PL} is the PL intensity, T is the measured temperature, T_0 is a characteristic temperature corresponding to the energy depth of localized states, A is the tunneling factor, and I_0 scales the PL intensity at the low-temperature limit.

In Fig.7.7 we show the numerically-integrated PL intensity of the GaInP_2 PL as a function of temperature. A discontinuity is seen around 200 K. Above this temperature PR data indicated a homogeneous electron distribution, and Hall data showed cluster scattering. Therefore, the discontinuity in the PL intensity will most likely be caused by the onset of luminescence from the disordered regions above 200 K. Below this discontinuity two regions can be distinguished in Fig.7.7. The data could be well described by equation 7.2 for $T < 30$ K; the solid curve represents a best fit yielding $T_0 = 7.5$ K, $A = 0.01$ and $I_0 = 753.1$. The fit became less good if data points above $T = 30$ K were added showing this data was not consistent with equation 7.2. However, an Arrhenius equation $I_{\text{PL}}(T) = I_0 \exp(-T/T_0)$, with $T_0 = 32.0$ K, described these data perfectly, as is shown by the broken curve in Fig.7.7.

7.4 Conclusions

We have performed PR, PL and Hall-van der Pauw measurements as a function of temperature on long-range ordered GaInP_2 obtained by metalorganic vapour-phase epitaxy. The data provide information on the origin of the "anomalous" optical and transport properties of the ordered alloy. Below $T = 200$ K we found that optical and transport properties were strongly influenced by a donor state which, owing to confinement in the ordered domains,

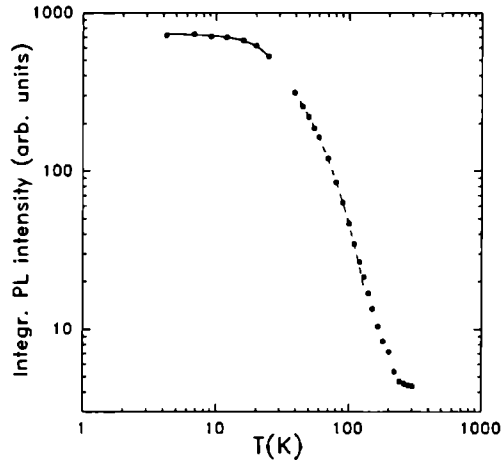


Figure 7.7 Numerically-integrated photoluminescence intensity versus T . The solid and broken curves are computer-calculated best fits described in the text.

had a high binding energy of 36 meV. Evidence for strong localization was obtained for $T < 30$ K: the PR spectra showed a pronounced first-derivative line shape, the conductivity was dominated by ϵ_3 conduction (hopping), the relationship between PL intensity and temperature could be well fitted assuming localized states, and an LO phonon replica was observed. Energies of the PL and PR features were found to be identical at these low temperatures. On the basis of transport data the low- T PL transition was attributed to recombination between a photoexcited hole and an electron that is localized on a donor in an ordered superlattice domain. Between 30 and 70 K the dominating conduction mechanism was identified as ϵ_2 conduction via negatively charged donors: the D^- band. At 70 K, Hall data showed a changeover from ϵ_2 to band conduction. It is proposed that the origin of the inverted-S shape of PL energy as a function of temperature is connected with thermal population of the D^- band. In the temperature interval 30-200 K the PR showed a complex line shape owing to the absence of carriers in the disordered regions. Furthermore, the conduction mechanism changed at $T = 70$ K from band-conduction (ϵ_1) to ϵ_2 conduction via negatively charged donors.

Above $T \approx 200$ K the PR showed third-derivative line shapes, which indicates a uniform electric-field distribution. Hall-mobility data showed unprecedentedly strong effects of cluster scattering on ordered domains above $T = 200$ K. These two observations show that a finite carrier concentration will then be present in the disordered regions of GaInP₂. The discontinuity in the PL intensity at 200 K therefore indicates that additional recombination from randomly alloyed regions occurs above this temperature.

Acknowledgements

The authors are grateful to P.R. Hageman and A. van Geelen for growing the samples, to R.A.J. Thomeer for performing the time-resolved PL measurement, to A.J. Bons for performing the TEM measurements, and to D.M. Frigo for his critical reading of the manuscript.

References

1. J.M. Olson, S.R. Kurtz, A.E. Kibbler, and P. Faine, *Appl. Phys. Lett.* **56**, 623 (1990).
2. M. Ikeda, K. Nakano, Y. Mori, K. Kaneko, and N. Watanabe, *Appl. Phys. Lett.* **48**, 89 (1986).
3. J.P. André, E. Dupont-Nivet, D. Moroni, J.N. Patillon, M. Erman, and T. Ngo, *J. Cryst. Growth* **77**, 354 (1986).
4. A. Valster, C.T.H.F. Liedenbaum, M.N. Finke, A.L.G. Severens, M.J.B. Boermans, D.E.W. Vandenhoudt, and C.W.T. Bulle-Lieuwma, *J. Cryst. Growth* **107**, 403 (1991).
5. P. Roentgen, W. Heuberger, G.L. Bona, and P. Unger, *J. Cryst. Growth* **107**, 724 (1991).
6. J.M. Olson, R.K. Ahrenkiel, D.J. Dunlavy, B. Keyes and A.E. Kibbler, *Appl. Phys. Lett.* **55**, 1208 (1989).
7. P.M. Mooney, *J. Appl. Phys.* **67**, R1 (1990).
8. A. Mascarenhas, and J.M. Olson, *Phys. Rev. B* **41**, 9947 (1990).
9. S.-H. Wei, and A. Zunger, *Appl. Phys. Lett.* **56**, 662 (1990).
10. M.C. DeLong, P.C. Taylor, and J.M. Olson, *Appl. Phys. Lett.* **57**, 620 (1990)
11. M.C. DeLong, P.C. Taylor, and J.M. Olson, *J. Vac. Sci. Technol. B* **8**, 948 (1990).
12. B.T. McDermott, N.A. El-Masry, B.L. Jiang, F. Hyuga, S.M. Bedair, and W.M. Duncan, *J. Cryst. Growth* **107**, 96 (1991).
13. M.K. Lee, R.H. Horng, and L.C. Haung, *J. Cryst. Growth* *in press*.
14. J.B. Lee, S.D. Kwon, I. Kim, Y.H. Cho, and B.-D. Choe, *J. Appl. Phys. Lett.* **71**, 5016 (1992).
15. A. Gomyo, T. Suzuki, K. Kobayashi, S. Kawata, I. Hino, and T. Yuasa, *Appl. Phys. Lett.* **50**, 673 (1987).
16. M. Kondow, and S. Minagawa, *Appl. Phys. Lett.* **54**, 1760 (1989).
17. M. Kondow, and S. Minagawa, *J. Appl. Phys.* **64**, 793 (1988).
18. M.C. DeLong, W.D. Ohlsen, I. Viohl, P.C. Taylor, and J.M. Olson, *J. Appl. Phys.* **70**, 2780 (1991).
19. F.A.J.M. Driessen, H.G.M. Lochs, S.M. Olsthoorn, and L.J. Giling, *J. Appl. Phys.* **69**, 906 (1991).
20. J.L. Shay, *Phys. Rev. B* **2**, 803 (1970).
21. T. Nishino, *J. Cryst. Growth* **98**, 44 (1989).
22. T. Nishino, Y. Inoue, Y. Hamakawa, M. Kondow, and S. Minagawa, *Appl. Phys. Lett.* **53**, 583 (1988).

23. J.E. Fouquet, V.M. Robbins, J. Rosner, and O. Blum, *Appl. Phys. Lett.* **57**, 1566 (1990).
24. D.E. Aspnes, and J.E. Rowe, *Phys. Rev. Lett.* **27**, 188 (1971).
25. D.E. Aspnes, and A. Frova, *Solid State Commun.* **7**, 155 (1969).
26. In fact the laser power was occasionally *lowered* because of the increasing luminescence and its attendant noise at lower temperatures.
27. G.J. Glembocki, and B.V. Shanabrook, *Superlattices and Microstructures* **5**,603 (1989).
28. R. Enderlein, D. Jiang, and Y. Tang, *Phys. Stat. Sol. B* **145**, 167 (1988).
29. R. Enderlein, in *Proceedings of the 20th International Conference on the Physics of Semiconductors*, edited by E.M. Anastassakis and J.D. Joannopoulos (World Scientific, Singapore, 1990), p.1089.
30. C.M. Wolfe, G.E. Stillman, and W.T. Lindley, *J. Appl. Phys.* **41**, 3088 (1970).
31. H. Ehrenreich, *Phys. Rev.* **120**, 1951 (1960).
32. D.J. Friedman, A.E. Kibbler, and J.M. Olson, *Appl. Phys. Lett.* **59**, 2998 (1991).
33. G.J. Bauhuis, F.A.J.M. Driessen, S.M. Olsthoorn, and L.J. Giling, *to be published*
34. N.F. Mott and W.D. Twose, in *Advances in Physics*, edited by N.F. Mott (Taylor and Francis, Ltd., London, 1961), Vol.10, p.107.
35. E.A. Davis, and W.D. Compton, *Phys. Rev.* **140**, A2183 (1965).
36. G. Sadasiv, *Phys. Rev.* **128**, 1131 (1962).
37. H. Nishimura, *Phys. Rev.* **138**, A815 (1965).
38. T. Kasuya, and S. Koide, *J. Phys. Soc. Japan* **13**, 1287 (1958).
39. A. Miller and E. Abrahams, *Phys. Rev.* **120**, 745 (1960).
40. B.I. Shklovskii and A.L. Efros, *Electronic Properties of Doped Semiconductors*, (Springer, Berlin, 1984), chapter 4.
41. C.T.H.F. Liedenbaum, A. Valster, A.L.G.J. Severens, and G.W. 't Hooft, *Appl. Phys. Lett.* **57**, 2698 (1990).
42. Landolt-Bornstein, *Numerical Data and Functional Relationships in Science and Technology*, edited by O. Madelung (Springer, New York, 1982), Group III, Vol. 17a.
43. G. Bastard, *Phys. Rev. B* **24**, 4714 (1981).
44. D.J. As, S. Korf, Z.M. Wang, J. Windscheif, K.H. Bachem, and W. Jantz, *Semicond. Sci. Technol.* **7**, A27 (1992).
45. S. Permogorov in *Excitons*, edited by E.I. Rashba and M.D. Sturge (North-Holland, Amsterdam, 1982), p.177.
46. This behaviour significantly differs from that for randomly alloyed semiconductors, where PL lines follow the band gap that increases monotonically with decreasing temperature.
47. M. Kasu, T. Yamamoto, S. Noda, and A. Sasaki, *Jap. J. Appl. Phys.* **29**, 828 (1990).
48. S.M. Olsthoorn, F.A.J.M. Driessen, A.P.A.M. Eijkelenboom, and L.J. Giling, *submitted to J. Appl. Phys.*
49. A. Chomette, B. Deveaud, A. Regreny, and G. Bastard, *Phys. Rev. Lett.* **57**, 1464 (1986).
50. T. Yamamoto, M. Kasu, S. Noda, and A. Sasaki, *J. Appl. Phys.* **68**, 5318 (1990).

51. Y.P. Varshni, *Physica* **34**, 149 (1967).
52. R.A. Street, T.M. Searle, and I.G. Augustin in *Amorphous and Liquid Semiconductors*, edited by J. Stuke and W. Brenig (Taylor and Francis, London, 1974), p.953.

Chapter 8

Photoluminescence on high quality $\text{Al}_x\text{Ga}_{1-x}\text{As}$ grown by metalorganic vapour phase epitaxy using alane bis(dimethylethylamine)

S.M. Olsthoorn, F.A.J.M. Driessen and L.J. Giling

Department of Experimental Solid State Physics, RIM, Faculty of Science, University of Nijmegen, Toernooiveld, 6525 ED Nijmegen, The Netherlands

D.M. Frigo and C.J. Smit

Billiton Research B.V., P.O. Box 40, 6800 AA Arnhem, The Netherlands

Abstract

Photoluminescence (PL) spectra are reported of initial results of $\text{Al}_x\text{Ga}_{1-x}\text{As}$ grown by metalorganic vapour-phase epitaxy (MOVPE), using a new precursor, alane bis(dimethylethylamine), as the aluminum source. The advantage of this new precursor over other alane precursors used previously is that it is liquid at room temperature. Using this new precursor instead of trimethylaluminum (TMAI), we found a reduction by a factor 6 in carbon incorporation when it was used together with trimethylgallium (TMGa), whereas a reduction by a factor 50 was found when it was used in combination with triethylgallium (TEGa). At low excitation density the linewidth of the separate donor-bound exciton (D^0, X) was 2.6 meV at an Al fraction of 0.31. This is comparable with the smallest values ever reported in literature for MOVPE-grown $\text{Al}_x\text{Ga}_{1-x}\text{As}$ with an Al fraction higher than 0.2. This narrow linewidth indicates a very uniform aluminum composition.

Published in:

Applied Physics Letters, **60**, 82-84 (1992)

The growth of $\text{Al}_x\text{Ga}_{1-x}\text{As}$ by metalorganic vapour-phase epitaxy (MOVPE) has been conventionally carried out using trimethylaluminum (TMAI) as the aluminum precursor. Since the use of TMAI leads to high levels of carbon incorporation in $\text{Al}_x\text{Ga}_{1-x}\text{As}$ layers [1], there has been considerable recent interest in the development of alternative aluminum sources. Although reduced carbon incorporation has been demonstrated using triethylaluminum (TEAl) [2], this precursor suffers from low volatility, which limits the growth rate, and its lower thermal stability causes problems with both compositional and thickness uniformity over a wafer.

Recent publications have shown the successful MOVPE of $\text{Al}_x\text{Ga}_{1-x}\text{As}$ using trimethylamine alane (TMAAl), $\text{AlH}_3 \cdot (\text{CH}_3)_3\text{N}$, as the aluminum source. Roberts *et al.* [3] and Jones *et al.* [4] have reported MOVPE of $\text{Al}_x\text{Ga}_{1-x}\text{As}$ with TMAAl and trimethylgallium (TMGa) at atmospheric and reduced pressure, respectively. In both cases no significant reduction in the residual carbon contamination was found compared to growth with TMAI and TMGa. However, Jones *et al.* [5] found a strong reduction of the carbon acceptor-related emission in the 10 K photoluminescence (PL) spectrum using TMAAl in combination with triethylgallium (TEGa). They recorded a full width at half maximum (FWHM) of 4 meV for the bound exciton peak, at an Al fraction of 0.14. Similarly, Hobson *et al.* [6] also observed a strong carbon emission in $\text{Al}_x\text{Ga}_{1-x}\text{As}$ grown by low-pressure (40 mbar) MOVPE using TMAAl in conjunction with TMGa. However, their PL spectra of $\text{Al}_{0.24}\text{Ga}_{0.76}\text{As}$ grown with TMAAl in combination with TEGa showed a very low intensity for the carbon emission compared to that of the bound exciton, even at a very low excitation density. At 1.6 K they observed a FWHM of the bound-exciton peak of 6 meV at an Al fraction of 0.24. Linewidths of the bound-exciton peaks for samples grown with TMAAl plus TMGa were not specified in the papers mentioned above.

Although the results of MOVPE with TMAAl are promising, the melting point of this precursor is 77-78 °C, and being solid at room temperature it may suffer from problems with variable dosimetry similar to those encountered with trimethylindium [7,8]. In this letter we present PL results obtained from the first $\text{Al}_x\text{Ga}_{1-x}\text{As}$ layers successfully grown using a new liquid aluminum precursor, alane bis(dimethylethylamine), $\text{AlH}_3 \cdot [\text{N}(\text{CH}_3)_2(\text{C}_2\text{H}_5)]_2$. Since this is a liquid at ambient temperature (and at the temperature at which it is evaporated) dosimetry is expected to be much more reproducible. Its properties are otherwise very similar to those of TMAAl. A fuller account of these will be reported later. Relative to $\text{Al}_x\text{Ga}_{1-x}\text{As}$ grown using TMAI plus TMGa, a small reduction in carbon incorporation was observed when the new alane was used together with TMGa. A much greater reduction was obtained by using the alane in combination with TEGa. For the $\text{Al}_x\text{Ga}_{1-x}\text{As}$ layer grown with the new alane plus TMGa, the excitonic linewidth was 2.6 meV at an Al fraction of 0.31, which is comparable with the narrowest ever reported for MOVPE-grown material [9].

The $\text{Al}_x\text{Ga}_{1-x}\text{As}$ epilayers which were used in this study were grown on (100) 2° off towards (110) semi-insulating GaAs substrates. Both alane test samples were grown at 760 °C at a pressure of 200 mbar on a CVT-MOVPE 4000 reactor at EPI, Cardiff. Hall measurements at 77 K were used to determine the electrical properties of the $\text{Al}_x\text{Ga}_{1-x}\text{As}$ layers. Thicknesses of all $\text{Al}_x\text{Ga}_{1-x}\text{As}$ layers were about 4 μm.

The Al fractions x of the samples were calculated using Casey's relationship [10]:

$$E_g(\text{Al}_x\text{Ga}_{1-x}\text{As}) = E_g(\text{GaAs}) + 1.247x \quad (8.1)$$

where the bandgap (E_g) of $\text{Al}_x\text{Ga}_{1-x}\text{As}$ can be derived by the addition of the exciton binding energy as a function of Al fraction [11] to the energy of the free exciton peak. The photoluminescence measurements were performed at 4.3 K, with the sample in He exchange gas. Optical excitation was provided by the 2.41 eV (514.5 nm) line from an Ar^+ laser with excitation densities ranging from 2.6×10^{-3} to 2.6 W/cm^2 at a spotsize of $3.8 \times 10^{-2} \text{ cm}^2$. The luminescence was dispersed by a 0.6-m double monochromator and detected by a cooled photomultiplier tube with a GaAs photocathode.

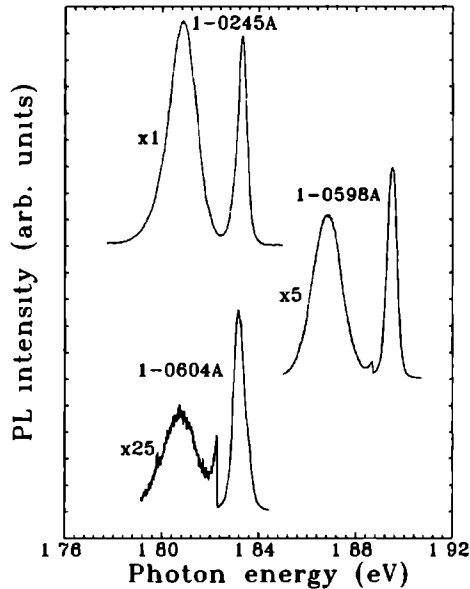


Figure 8.1 PL spectra of $\text{Al}_x\text{Ga}_{1-x}\text{As}$ grown at 760°C using TMAI and TMGa (sample 1-0245A, $x=0.26$), the new precursor together with TMGa (sample 1-0598A, $x=0.31$), and the new precursor with TE Ga (sample 1-0604A, $x=0.26$). The relative gain used to record each carbon peak with respect to the exciton peak is given to the left of the carbon peaks.

Figure 8.1 shows the 4.3-K PL spectra of three samples recorded at an excitation density of 0.26 W/cm^2 . The bound-exciton (BX) emissions are seen on the high-energy side of the spectra, whereas the carbon-related emissions are seen on the low-energy side. The uppermost spectrum is an earlier reference $\text{Al}_{0.26}\text{Ga}_{0.74}\text{As}$ sample [12] grown with

high-purity Billiton Precursors TMAI and TMGa at 760°C and 950 mbar. The 77-K n -type carrier concentration n_{77} , of this sample was $2.0 \times 10^{15} \text{cm}^{-3}$. The intensity ratio of the exciton to carbon-related peak is approximately unity for this spectrum. Sample 1-0598A (the middle spectrum), grown with the new alane precursor plus TMGa, had an Al fraction of 0.31 and its n_{77} was $5.1 \times 10^{15} \text{cm}^{-3}$. The exciton peak intensity here is 6 times higher than that of the carbon peak. The lowest spectrum is that of sample 1-0604, grown with the alane precursor in combination with TEGa, for which the Al fraction was 0.26, and n_{77} was $4.8 \times 10^{15} \text{cm}^{-3}$. The peak intensity ratio is 50 for this spectrum. So in comparison with growth using TMAI plus TMGa, using the new aluminum precursor together with TMGa gives a carbon reduction of at least a factor of 6, and in combination with TEGa, at least a factor of 50. The relatively high values of n_{77} for the alane-grown samples are consistent with the detection of 0.6 ppm of Si in the precursor by inductively-coupled plasma optical emission spectroscopy.

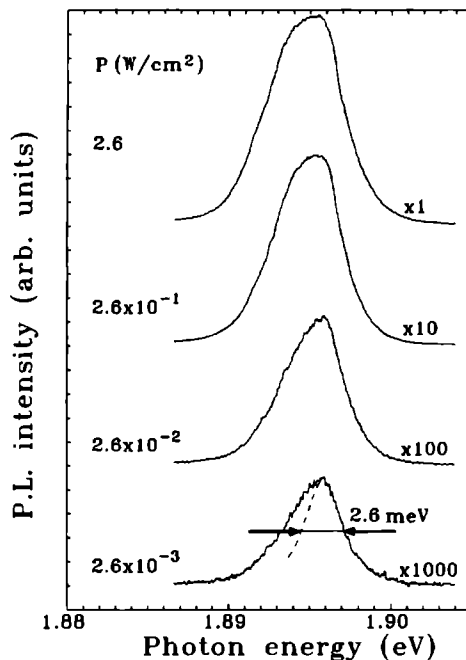


Figure 8.2 Exciton spectra of sample 1-0598A ($x=0.31$), grown with the new precursor and TMGa, recorded at various excitation densities (P). The relative gain used to record each spectrum is given to the right. The linewidth of the separate (D^0, X) peak (FWHM) of the spectrum recorded at the lowest excitation density is shown.

Figure 8.2 shows the excitonic part of the PL spectrum of sample 1-0598A (TMGa plus alane precursor), which had the narrowest excitonic linewidth, recorded at different excitation densities. At the lowest excitation density one peak at the high-energy side is shown with a shoulder on the low-energy side. The peak can be attributed to neutral donor-bound-exciton emission (D^0, X), whereas the shoulder can be attributed to ionized-donor-bound- (D^+, X) and acceptor-bound-exciton emission (A^0, X). The linewidth (FWHM) of the (D^0, X) peak is 2.6 meV at this low excitation density; this value is comparable to that of the reference sample [12].

The alloy broadening in a perfectly random alloy has been calculated by Singh and Bajaj [13] to be 1.4 meV at an Al fraction of 0.31. This means that for sample 1-0598A an additional 1.2 meV broadening in the exciton peak is caused by both ionized and nonionized impurities, and by local variations in the composition. Even if the broadening caused by impurities is ignored and it is assumed that the 1.2 meV broadening is caused only by variations in alloy composition (which is not very likely), then by equation 8.1 the maximum compositional deviation may be calculated. Thus the 1.2 meV broadening represents a deviation of less than 0.001 in the absolute value of the Al fraction, both laterally (over the area of the laser spot size) and, more significantly, throughout the entire 4 μm depth of the epilayer, since the excitons are known to diffuse easily over such a depth [14]. For sample 1-0604A (TEGa plus alane precursor), the excitonic linewidth was 3.7 meV at the lowest excitation density. Following the procedure mentioned above a slightly larger but still excellent upper limit of 0.002 in absolute compositional variation was calculated. Such extremely good compositional uniformity with depth for both samples indicates that the pick-up from both the group III precursors during epitaxy was very stable. It is very likely that this excellent uniformity is a direct result of using only group III precursors which are liquids at the temperature at which they are used, and consequently give very reproducible pick-up rates during a single growth experiment.

Comparing our results of the excitonic linewidths with the FWHM of other groups, it is necessary to compare the experimental conditions. As shown in Figure 8.2, the FWHM is very dependent upon excitation density. Since Jones *et al.* [5], who reported a FWHM of 4 meV at an Al fraction of 0.14, did not mention their excitation density, it is possible that their exciton peak is broadened with respect to ours because of a much higher excitation density. They also measured at 10 K which gives a small additional thermal broadening with respect to measurements at 4.3 K. These make it impossible to compare our results with theirs directly. The spectrum of Hobson *et al.* [6] with a FWHM of 6 meV was measured at an excitation density of 2.5 mW/cm^2 , which is the same as our lowest excitation density. The temperature at which their spectrum was obtained (1.6 K) would give less thermal broadening than ours (4.3 K); and furthermore, their lower Al fraction (0.24, as compared to 0.31 and 0.26 for samples 1-0598A and 1-0604A, respectively) would give less alloy broadening. Therefore, that the bound-excitonic linewidths were consistently narrower in our samples highlights the excellent composition uniformity in the grown layers.

In conclusion, we have demonstrated via low temperature PL spectroscopy that MOVPE of $\text{Al}_x\text{Ga}_{1-x}\text{As}$ using the liquid alane bis(dimethylethylamine) as the aluminum

source gives reduced levels of carbon relative to that grown with TMAI: a reduction by a factor of at least 50 was obtained when used with TEGa, whereas when used with TMGa, the reduction was by a factor of at least 6. Furthermore, an exciton linewidth (FWHM) of 2.6 meV was measured at an Al fraction of 0.31, which is as narrow as the values reported hitherto even using conventional precursors [9]. This very narrow linewidth compared to excitonic linewidths measured on material grown using TMAAl [6], is an indication that the compositional uniformity during the growth is better using the liquid precursor alane bis(dimethylethylamine) instead of a solid precursor TMAAl.

References

1. T.F. Kuech, D.J. Wolford, E. Veuhoff, V. Deline, P.M. Mooney, R. Potemski and J. Bradley, *J. Appl. Phys.* **62**, 632 (1987).
2. T.F. Kuech, E. Veuhoff, T.S. Kuan, V. Deline and R. Potemski, *J. Cryst. Growth* **77**, 257 (1986).
3. J.S. Roberts, C.C. Button, J.P.R. David, A.C. Jones and S.A. Rushworth, *J. Cryst. Growth* **104**, 857 (1990).
4. A.C. Jones, S.A. Rushworth, D.A. Bohling and G.T. Muhr, *J. Cryst. Growth* **106**, 246 (1990).
5. A.C. Jones and S.A. Rushworth, *J. Cryst. Growth* **106**, 253 (1990).
6. W.S. Hobson, T.D. Harris, C.R. Abernathy and S.J. Pearton, *Appl. Phys. Lett.* **58**, 77 (1991).
7. J. Knauf, D. Schmitz, G. Strauch, H. Jürgensen, M. Heyen and A. Melas, *J. Cryst. Growth* **93**, 34 (1988).
8. B.R. Butler and J.P. Stagg, *J. Cryst. Gr.* **94**, 481 (1989).
9. S.M. Olsthoorn, F.A.J.M. Driessen and L.J. Giling, *Appl. Phys. Lett.* **58**, 1274 (1991).
10. H.C. Casey, Jr., *J. Appl. Phys.* **49**, 3684 (1978).
11. P.J. Pearah, W.T. Masselink, J. Klem, T. Henderson, H. Morkoç, C.W. Litton and D.C. Reynolds, *Phys. Rev. B* **32**, 3857 (1985).
12. This sample, with an exciton linewidth of 2.8 meV at low excitation density, is from the same series of high-quality $\text{Al}_x\text{Ga}_{1-x}\text{As}$ samples reported in Ref.9.
13. J. Singh and K.K. Bajaj, *Appl. Phys. Lett.* **48**, 1077 (1986).
14. R.G. Ulbrich and G.W. Fehrenbach, *Phys. Rev. Lett.* **43**, 963 (1979).

Chapter 9

Excitonic photoluminescence spectra of $\text{Al}_x\text{Ga}_{1-x}\text{As}$ grown by metalorganic vapour-phase epitaxy

S.M. Olsthoorn, F.A.J.M. Driessen and L.J. Giling

Department of Experimental Solid State Physics, RIM, Faculty of Science, University of Nijmegen, Toernooiveld, 6525 ED Nijmegen, The Netherlands

Abstract

Excitonic transitions were measured in $\text{Al}_x\text{Ga}_{1-x}\text{As}$, grown by metalorganic vapour-phase epitaxy (MOVPE), at two different alloy compositions using high-resolution photoluminescence spectroscopy. The first observation is reported of an excitonic spectrum which is separated into neutral donor, ionized donor and neutral acceptor bound exciton transitions $[(D^0, X), (D^+, X) \text{ and } (A^0, X)]$ at an aluminum fraction higher than 20 %. A significant decrease in linewidth of the (D^0, X) peak is found by decreasing the excitation density and by decreasing the laser spot size. This means that the linewidths of the various excitonic transitions are, apart from alloy broadening, strongly dependent on both the long range Coulombic potentials of the ionized impurities in our samples, and on clustering effects. Finally, linewidths of 1.75 and 2.5 meV were measured for the (D^0, X) transition for samples with Al fractions of 0.12 and 0.244, respectively. These are the smallest values ever reported in literature for samples grown by MOVPE.

Published in:
Applied Physics Letters **58**, 1274-1276 (1991)

The ternary semiconductor $\text{Al}_x\text{Ga}_{1-x}\text{As}$ is an important material for the fabrication of optoelectronic and microwave devices. This material is commonly grown by liquid-phase epitaxy (LPE), molecular-beam epitaxy (MBE) or metalorganic vapour-phase epitaxy (MOVPE). Low-temperature photoluminescence spectroscopy is a useful technique to obtain information about this semiconductor. Especially the excitonic emission spectra give information about the quality of the alloy. Singh and Bajaj [1] and Schubert *et al.* [2] independently calculated the full width at half maximum (FWHM) of the excitonic lines as a function of alloy composition in perfectly random alloys, thereby treating the exciton as a classical system. In a later paper Singh and Bajaj [3] again calculated this FWHM for a perfectly random alloy, following a quantum mechanical approach. The result of these last calculations was a considerably smaller value for the FWHM as a function of alloy composition. The best experimental results of the excitonic linewidths observed for $\text{Al}_x\text{Ga}_{1-x}\text{As}$ samples grown with MOVPE, up to now, were reported by Shealy *et al.* [4] and Deschler *et al.* [5]. The best observed linewidths for MBE-grown samples were, however, roughly twice as narrow at the same aluminum fractions as reported by Reynolds and co-workers [6-8].

In this letter we report excitonic linewidths of MOVPE-grown samples which are comparable to MBE-grown samples and hence an improvement by a factor two is obtained in comparison to FWHM values for previously reported MOVPE-grown $\text{Al}_x\text{Ga}_{1-x}\text{As}$ samples. Furthermore, a linewidth reduction of almost 30% is obtained by decreasing the excitation density which means that the broadening effect due to residual ionized impurity centers is not negligible in our samples. Neither is clustering, as we concluded by reducing the spot size of the laser. However, this clustering effect does not enlarge the linewidth as much as the ionized impurities.

The $\text{Al}_x\text{Ga}_{1-x}\text{As}$ epilayers which were used in this study were grown on (100) 2° off towards (110) semi-insulating GaAs substrates. Sample 1 was grown at atmospheric pressure in a SPI-MOCVD 450 reactor at Spire Corporation. The growth temperature was 800 °C and the V/III ratio was 15. Sample 2 was grown at a pressure of 950 mbar in a CVT-MOVPE 4000 reactor at EPI. In this case the growth temperature was 760 °C and the V/III ratio was 50. In both runs high-quality trimethylaluminum grade M of Billiton Precursors was used. Hall measurements at 77 K showed *n*-type carrier concentrations of $1.7 \times 10^{15} \text{ cm}^{-3}$ and $1.8 \times 10^{15} \text{ cm}^{-3}$, respectively. Thicknesses of both $\text{Al}_x\text{Ga}_{1-x}\text{As}$ layers were about 4 μm .

The photoluminescence measurements were performed at 4.3 K, with the sample in He exchange gas. Optical excitation was provided by the 2.41 eV (514.5 nm) line from an Ar^+ laser with excitation densities ranging from 1.8×10^{-2} to 5.6 W/cm^2 . The luminescence was dispersed by a 0.6-m double monochromator and detected by a cooled photomultiplier tube with S1-response.

Two samples were investigated. The Al fractions x of the samples were calculated using Casey's relation [9]:

$$E_g(\text{Al}_x\text{Ga}_{1-x}\text{As}) = E_g(\text{GaAs}) + 1.247 \cdot x, \quad (9.1)$$

where the band gap (E_g) of $\text{Al}_x\text{Ga}_{1-x}\text{As}$ can be derived by the addition of the exciton binding energy as a function of Al fraction [10] to the energy of the free exciton peak. This leads to Al fractions of 0.120 and 0.244 for samples 1 and 2, respectively.

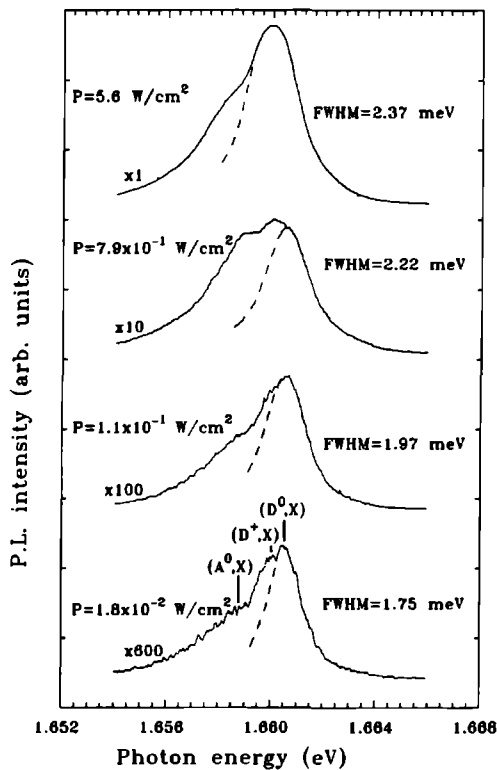


Figure 9.1 Exciton spectra of sample 1 ($x=0.12$) recorded at various excitation densities (P). The relative gain used to record each spectrum is given to the left. The linewidth of the individual (D^0,X) peak (FWHM) of each spectrum is given to the right.

Figure 9.1 shows the excitonic spectra of sample 1 recorded at different excitation densities. The excitation beam was focused to a spot size of $1.96 \times 10^{-3} \text{ cm}^2$. At the lowest excitation density the clearest separation between various bound-exciton peaks is observed; (D^0,X) , (D^+,X) and (A^0,X) transitions are resolved. Furthermore, the individual peakwidths get smaller at lower excitation densities. The linewidth of the (D^0,X) peak becomes as small as 1.75 meV at an excitation density of $1.8 \times 10^{-2} \text{ W/cm}^2$.

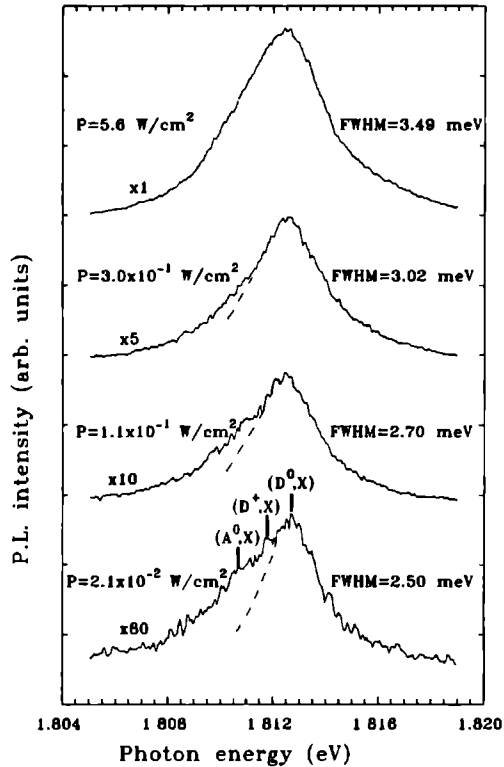


Figure 9.2 Exciton spectra of sample 2 ($x=0.244$) recorded at various excitation densities (P). The relative gain used to record each spectrum is given to the left. The linewidth of the separate (D^0, X) peak (FWHM) of each spectrum is given to the right.

Figure 9.2 shows the excitonic spectra of sample 2 recorded at various excitation densities. Although the separation of the peaks is not as clear as in sample 1, it is still possible to resolve the (A^0, X), (D^+, X) and (D^0, X) transitions. The smallest linewidth of the (D^0, X) peak in this figure is 2.5 meV at an excitation density of 2.1×10^{-2} W/cm².

In Figure 9.3 the linewidths of the (D^0, X) peaks of both samples are shown as a function of excitation density. For both samples a relatively large decrease in linewidth is obtained by decreasing the laser intensity. This was also found by Cunningham *et al.* [11]. From this figure it can be concluded that in our samples, apart from alloy broadening, the ionized impurities give rise to a broadening of the (D^0, X) peak. To make sure that the attribution of the peaks is correct, and none of these peaks is to be attributed to a free-

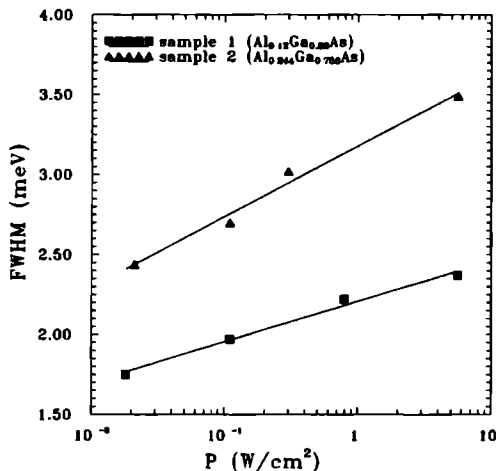


Figure 9.3 The linewidths (FWHM) of the (D^0,X) transitions of both samples as a function of excitation density.

exciton transition (FX), we performed PL measurements at higher temperatures (4.3–25 K). A shoulder appeared at the high-energy side of the other excitonic peaks. We attribute this shoulder to FX luminescence since free excitons have a larger activation energy than bound excitons [12]. This means that none of the peaks in Figures 9.1 or 9.2 is an FX transition.

From Figures 9.1 and 9.2 it is seen that the energy difference between the (A^0,X) and (D^0,X) peaks becomes slightly larger at higher Al fractions. It is known that the (D^0,X) peak follows the band gap because the localization energy of the exciton on the donor is proportional to the ionization energy of the donor (Haynes' rule [13]) which is independent of x at these composition values ($x < 0.3$) [14] as is known from effective mass theory. Therefore, the change in energy difference between the exciton peaks can be seen as a change in binding energy of the exciton on the acceptor. This is expected since the ionization energy of acceptors, which are not described as well by effective mass theory, is not independent of x in the direct band gap region. This behaviour was measured for C_{As} , the principal acceptor in MOVPE-grown $\text{Al}_x\text{Ga}_{1-x}\text{As}$, by Stringfellow and Linnebach [15]. Their values for the ionization energies as a function of x are roughly proportional to the binding energies of the excitons on the acceptor as measured from our spectra. This Haynes' rule indicates that the principal residual acceptor in our samples is C_{As} .

Furthermore, we investigated possible effects of clustering, *i.e.*, macroscopic deviations in Al fraction, by measuring smaller areas of the sample at the same excitation density. We observed a small reduction in linewidth (less than 10 %) by reducing the

excited area from 3.8×10^{-2} to 1.96×10^{-3} cm^2 . Hence, in comparison to the previously discussed linewidth reduction at smaller excitation densities, it is concluded that the effect of clustering on line broadening is of minor importance in our samples.

In Figure 9.4 we have plotted the values of the narrowest observed excitonic linewidths together with the theoretical variations of the FWHM for perfectly random alloys, using both classical [1,2] (dashed curve) and quantum mechanical [3] calculations (solid curve). Furthermore, the best experimental values of FWHM as found in the liter-

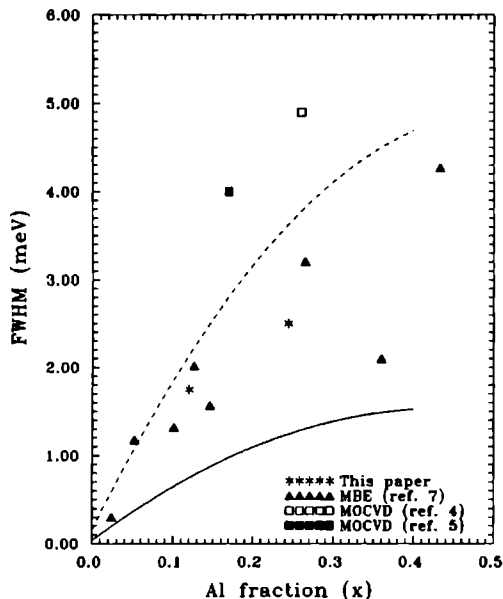


Figure 9.4 Experimental values of the linewidths of the bound-exciton peaks (FWHM) as a function of aluminum fraction x . The dashed and solid lines are theoretical curves using respectively classical and quantum mechanical calculations.

ature [4-8] are shown. We point out that the best reported experimental values obtained with MOVPE-grown samples so far [4,5], are a factor two larger than those observed in this study¹

In conclusion, we have measured the excitonic spectra of high-quality MOVPE-grown $\text{Al}_x\text{Ga}_{1-x}\text{As}$ at two different alloy compositions using photoluminescence spectroscopy. We found that the observed linewidths are a factor two smaller than reported

¹After publication of this paper a refinement of the theory on alloy broadening was published by Langer, Buczko and Stoneham [16]; their theoretical curve shows a remarkable correspondence to our experimental data.

ever before for MOVPE-grown samples. In both samples, with Al fractions of 0.120 and 0.244, the excitonic spectrum was split into various bound excitons; this is the first time that such a substructure is reported in samples with $x > 0.2$. A considerable reduction in linewidth was observed by decreasing the excitation density, whereas a smaller reduction was found by decreasing the spot size of the laser. Therefore, both broadening due to ionized impurity centers and clustering cannot be neglected.

The authors would like to thank Billiton Precursors B.V. for providing the samples and H.F. Pen, H.A. van der Linden and G. Bauhuis for valuable assistance with plotting the spectra.

References

1. J. Singh and K.K. Bajaj, *Appl. Phys. Lett.* **44**, 1075 (1984).
2. E.F. Schubert, E.O. Göbel, Y. Horikoshi, K. Ploog and H.J. Queisser, *Phys. Rev. B* **30**, 813 (1984).
3. J. Singh and K.K. Bajaj, *Appl. Phys. Lett.* **48**, 1077 (1986).
4. J.R. Shealy, V.H. Kreismanis, D.K. Wagner and J.M. Woodall, *Appl. Phys. Lett.* **42**, 83 (1983).
5. M.Deschler, M.Cuppers, A. Brauers, M. Heyen and P. Balk, *J. Cryst. Growth* **82**, 628 (1987).
6. D.C. Reynolds, C.W. Litton, K.K. Bajaj, P.W. Yu, J. Singh, P.J. Pearah, W.T. Masselink, T. Henderson, J. Klem and H. Morkoç, *J. Vac. Sci. Technol. B* **4**, 523 (1986).
7. D.C. Reynolds, K.K. Bajaj, C.W. Litton, P.W. Yu, J. Klem, C. K. Peng, H. Morkoç and J. Singh, *Appl. Phys. Lett.* **48**, 727 (1986).
8. D.C. Reynolds, K.K. Bajaj, C.W. Litton, J. Singh, P.W. Yu, T. Henderson, P. Pearah and H. Morkoç, *J. Appl. Phys.* **58**, 1643 (1985).
9. H.C. Casey, Jr., *J. Appl. Phys.* **49**, 3684 (1978).
10. P.J. Pearah, W.T. Masselink, J. Klem, T. Henderson, H. Morkoç, C.W. Litton and D.C. Reynolds, *Phys. Rev. B* **32**, 3857 (1985).
11. J.E. Cunningham, W.T. Tsang, T.H. Chiu and E.F. Schubert, *Appl. Phys. Lett.* **50**, 769 (1987).
12. D.D. Sell, S.E. Stokowski, R. Dingle and J.V. DiLorenzo, *Phys. Rev. B* **7**, 4568 (1973).
13. J.R. Haynes, *Phys. Rev. Letters* **4**, 361 (1960).
14. P.M. Mooney, *J. Appl. Phys.* **67**, R1 (1990).
15. G.B. Stringfellow and R. Linnebach, *J. Appl. Phys.* **51**, 2212 (1980).
16. J.M. Langer, R. Buczko, and A.M. Stoneham, *Semicond. Sci. Technol.* **7**, 547 (1992).

Chapter 10

The influence of impurity concentration on exciton PL in GaAs and InP

H.F. Pen, F.A.J.M. Driessen , S.M. Olsthoorn, and L.J. Giling

Department of Experimental Solid State Physics, Research Institute for Materials, University of Nijmegen, Toernooiveld, 6525 ED Nijmegen, The Netherlands

Abstract

We report an investigation of the exciton photoluminescence (PL) spectra of high-purity nominally n -type GaAs and InP layers, grown by metalorganic vapour-phase epitaxy. The results are discussed in terms of exciton-polariton kinetics. The ratio of the integrated emission intensities of neutral donor-bound exciton (D^0, X) transitions and free exciton-polariton (FX) transitions $r_{DF} = I(D^0, X)/I(FX)$ shows a sublinear dependence upon neutral donor concentration n_D^0 deduced from 77K Hall measurements. This relationship is particularly useful for estimating carrier concentrations in high-purity materials, which cannot be characterized by Hall measurements due to depletion.

Published in:
Semiconductor Science and Technology, 7, 1400-1406 (1992).

10.1 Introduction

Several attempts at quantitative impurity characterization in direct-gap semiconductors using PL have been reported in the literature. Morgan *et al.*[1] introduced a model by which the shape of the neutral donor to neutral acceptor (D^0, A^0) emission could be correlated with the distribution of donors and acceptors throughout the crystal, *i.e.* with the distance between isolated donor-acceptor pairs. For a low compensation ratio and a low excitation density, the (D^0, A^0) linewidth would then be determined by the donor concentration n_D in n -type material. This model was refined by Kamiya *et al.*[2], who took into account recombination of free electrons at neutral acceptors (e, A^0) and nonradiative recombination, and were thus able to estimate both donor and acceptor concentrations. The results, however, did not agree with electrical measurements. According to Skromme *et al.* [3], this discrepancy was due to the fact that excited donor states had been neglected. Golka [4,5], however, stated that the use of only an isolated pair model was incorrect and that multi-impurity complexes had to be taken into account. The recombination rates of these complexes are much higher than those of isolated pairs, making their contribution particularly important in cases of high impurity concentrations. In summary, it would seem impossible to determine impurity concentrations routinely from PL measurements of the (D^0, A^0) pairs, owing to the complexity of the (D^0, A^0) recombination process.

Nam *et al.*[6] determined n_D and n_A for one sample from the relative intensities of neutral donor to free hole (D^0, h), free electron to neutral acceptor (e, A^0) and (D^0, A^0) lines at low temperature (8K) and very high excitation densities ($4.4 \times 10^3 \text{Wcm}^{-2}$). Unfortunately, no comparison with Hall measurements was made.

Recently, Lu *et al.*[7] found an empirical relation $\Theta = 0.89r_x + 0.06$, where $\Theta = n_A/n_D$ is the compensation ratio and r_x the intensity ratio of the neutral acceptor-bound exciton line to the neutral donor-bound exciton line in their 10-K PL measurements. Almost simultaneously, Steiner *et al.*[8] also postulated that $\Theta = \kappa r_x$ in their study on semi-insulating GaAs samples and found 0.65 ± 0.1 for the constant κ . Lu *et al.* [7] also claimed that r_x did not depend on the excitation density P . At first sight this seems reasonable because in n -type material ionized acceptors are rather efficiently neutralized by laser excitation. Even strongly differing values of various bound-exciton properties might be incorporated in the numerical

constant κ . Amongst these are differing values for the cross sections for exciton capture, lifetimes of the respective bound-exciton complexes and localization energies of excitons on either donors or acceptors. However, the insensitivity of r_x upon P is very remarkable because thermal dissociation of bound excitons, especially the (D^0, X), depends on excitation density, and is therefore expected to affect the ratio r_x .

In this paper we present high-resolution PL measurements on a series of n -type GaAs and InP epilayers of differing purities grown in the same metalorganic vapour-phase epitaxy (MOVPE) reactor which had exclusively been used for growing nominally undoped material. The PL data are compared with donor concentrations n_D^0 which were obtained via 77-K Hall measurements. The laser excitation was chosen to be close to the band gap in order to minimize the quasi-population of the upper polariton branch

(UPB), which is enhanced by hot electron-exciton interaction [9]. We report a useful relationship between the low-temperature donor concentration n_D^0 and the intensity ratio of the donor-bound-exciton (D^0, X) line to that of the lower polariton branch (LPB). The use of polariton luminescence for quantitative PL characterization and its possible complications are discussed.

10.2 Experimental Details

TABLE I: Electrical and optical properties of the GaAs samples.

sample	$n_{77}(\times 10^{13}\text{cm}^{-3})^a$	$\mu_{77}(\times 10^5\text{cm}^2/\text{Vs})^a$	Θ^b	$n_D(\times 10^{13}\text{cm}^{-3})^c$	r_x^d
1-0209A	e	e			0.39
1-0210A	e	e			0.36
1-0212A	e	e			0.29
1-0207A	3.3	1.77	0.50	6.6	0.48
1-0163A	2.3	1.54	0.70	7.6	0.26
1-0196A	2.9	1.59	0.65	8.3	0.10
1-0204A	4.4	1.56	0.50	8.8	0.14
1-0192A	8.5	1.54	0.30	12.2	0.11
1-0155A	11	1.65	0.10	12.2	0.51
1-0151A	7.3	1.42	0.50	14.6	0.12
1-0132A	11	1.37	0.45	20	0.13
1-0135A	8.2	1.31	0.65	23.4	0.09
1-0062A	20	1.17	0.45	36.4	0.13
1-0061A	33	1.05	0.30	47.1	0.07

^aFrom 77-K Hall data.

^bCalculated according to Ref.[10]; uncertainty ± 0.05 .

^cCalculated from $n_D = n_{77}/(1 - \Theta)$.

^d $r_x = I(A^0, X)/I(D^0, X)$.

^eNot measurable owing to depletion.

The experiments were carried out on layers of GaAs and InP, homoepitaxially grown by metalorganic vapour-phase epitaxy (MOVPE). The layers were grown at 650 °C on (1 0 0) 2° off towards (1 1 0) oriented semi-insulating substrates, and were nominally undoped. All epilayers were relatively thick ($> 8\mu\text{m}$) to avoid total depletion. The 77-K majority carrier concentrations n_{77} and mobilities μ_{77} of the layers were obtained by Hall measurements and are given in tables I and II. The compensation ratios of the InP layers, as determined from the Hall data (where available) and the data of Lancefield *et al.*[10], are all very low, whereas the GaAs samples were partly compensated owing to the presence of the carbon acceptor in MOVPE-grown GaAs (as can be seen in tables I and II [11]). Three of the GaAs layers were found to be depleted on the basis of Hall data. However, because these three epilayers were relatively thick (10 – 21 μm), this depletion indicates that n_{77} is very low. The tables also contain the calculated donor concentration $n_D = n_{77}/(1 - \Theta)$.

TABLE II: Electrical and optical properties of the InP samples.

sample	$n_{77}(\times 10^{13}\text{cm}^{-3})^a$	$\mu_{77}(\times 10^5\text{cm}^2/\text{Vs})^a$	Θ^b	$n_D(\times 10^{13}\text{cm}^{-3})^c$	τ_z^d
1-0432A	1.8	2.29	0.03	1.8	1.05
1-0435A	7.7	1.78	0.05	8.1	0.24
1-0433A	11	1.89	0.20	13.8	0.15
1-0404A	14	1.44	0.05	14.7	0.16
1-0434A	16	1.54	0.01	16.1	0.19
1-0456A	18	1.77	0.05	18.9	0.0
1-0431A	17	1.11	0.30	24.3	0.06
1-0407A	27	1.22	0.00	27	0.0
1-0455A	28	1.47	0.03	28.8	0.0
1-0264A	29	0.99	0.08	31.5	0.09
1-0424A	74	0.92	0.00	74	0.0
1-0411A	270	0.47	0.10	300	0.0

^aFrom 77-K Hall data.

^bCalculated according to Ref.[10]; uncertainty ± 0.05 .

^cCalculated from $n_D = n_{77}/(1 - \Theta)$.

^d $\tau_z = I(A^0, X)/I(D^0, X)$.

The PL measurements were performed with the entire sample mounted in a strain-free way, immersed in superfluid He at 1.5 K. Optical excitation was provided by a ring dye laser using Styryl 9 dye, pumped by a 4 W all-lines Ar⁺ laser. The laser excitation density was controlled by using neutral density filters. The luminescence was dispersed by a 0.6-m double monochromator with 1200 lines/mm gratings, and detected by cooled photomultiplier tubes, one with a GaAs photocathode (GaAs samples) and one with an S1 characteristic (InP samples). The resolution was 0.1 meV for all measurements.

10.3 Results and Discussion

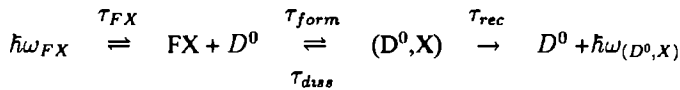
Figure 10.1 shows the exciton photoluminescence spectrum of the low-compensated GaAs sample 1-0155A at various excitation densities. In the experiments on the GaAs samples the excitation wavelength was kept at 1.5186 eV, which was high enough to ensure non-resonant excitation but below the band gap to minimize electron-exciton interactions [9]. At the lowest excitation density the excitons are well resolved into two neutral acceptor-bound excitons (A^0, X)_{J=5/2,3/2}, ionized donor-bound excitons (D^+, X) (which are nearly degenerate with neutral donor-to-band emissions (D^0, h)), neutral donor-bound excitons (D^0, X) and free exciton-polariton luminescence. It is known that the (D^+, X) emission has a smaller linewidth than (D^0, h) emission owing to the fairly large spread in k -space of the free holes in the latter emission, which in turn results from the relatively large effective heavy hole mass. The small width of the emission at 1.5133 eV involving

$(D^+, X)-(D^0, h)$ at the low excitation densities therefore implies that ionized donors are still present in the sample at these low P values. The presence of bound-exciton PL involving neutral acceptors (A^0, X) , which are created by photoexcitation, however, shows that even at the lowest excitation densities photoneutralization is very efficient and that $n_A^- < n_A$. Those donors that were initially compensating the acceptors are then also neutralized.

The $(D^+, X)-(D^0, h)$ PL shows a considerably larger broadening than the neutral bound excitons upon increasing excitation density. This shows that (D^0, h) PL then becomes the dominant process around 1.5133-1.5135 eV. The relative decrease in (D^+, X) signal upon increasing P is accompanied by a rise in the (A^0, X) signal. When the intensities of (A^0, X) and (D^0, X) are compared, it is seen that the relative contribution of (A^0, X) to the PL spectrum increases as a function of excitation density. The previously claimed insensitivity of the intensity ratio $r_x = I(A^0, X)/I(D^0, X)$ with respect to variations in excitation density by Lu *et al.* [7] is therefore not observed in our measurements. Figure 10.2 shows r_x as a function of excitation density for four different samples including the aforementioned. Intensities of (A^0, X) and (D^0, X) were obtained with a line fitting procedure and numerical integration.

The spectra of a number of GaAs samples of differing purities are shown in Figure 10.3. An excitation density of 80 mWcm^{-2} was used. The luminescence efficiencies of all samples were comparable. The r_x for every sample under identical excitation densities are added in Tables I and II. These data show no relationship between Θ and r_x . Before proceeding to the main results in this paper we shall discuss the above observations briefly.

The behaviour of r_x as a function of P can be rationalized by realizing that bound-exciton complexes can dissociate thermally. This dissociation is especially important in case of the weakly localized (D^0, X) complex [14] for which quenching of the bound exciton PL upon increasing temperature T shows that the activation energy for dissociation of (D^0, X) is approximately 1.0 meV in comparison to ~ 2.7 meV for that of (A^0, X) [15]. For the donor-bound exciton the recombination system is then given by:



where τ_{FX} is the free-exciton lifetime and the (D^0, X) -related timescales τ_i involve recombination, formation and dissociation of the (D^0, X) complex. The formation time τ_{form} is assumed to be much smaller than the radiative lifetimes of free or bound excitons [14, 16-18].

An enhancement of excitation density causes an increase of the quasi-Fermi level as a result of exciton-electron inelastic scattering [19]. Two competitive mechanisms influence the (D^0, X) dissociation-formation quasi-equilibrium: an increase in the effective exciton-polariton temperature causes an enhanced dissociation of the (D^0, X) complex, whereas

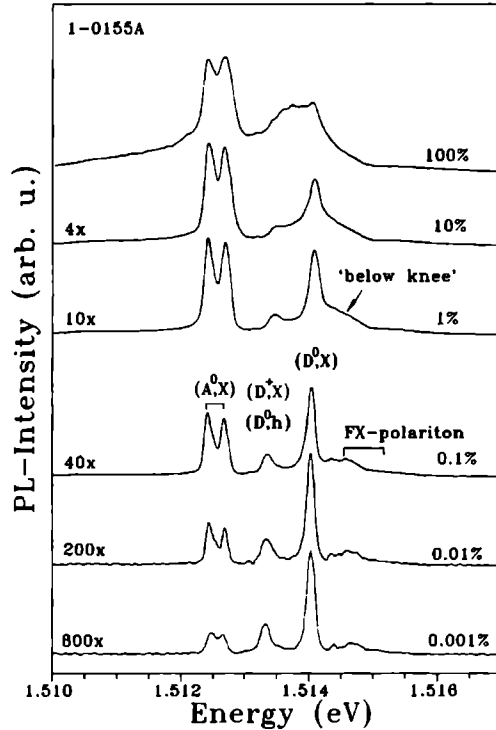


Figure 10.1 Exciton spectrum of the GaAs sample 1-0155A at various excitation densities (given to the right); an excitation density of 12Wcm^{-2} corresponds to 100%. Excitons bound to neutral acceptors (A^0,X), neutral donors (D^0,X), ionized donors (D^+,X), which are nearly degenerate with donor-to-band (D^0,h) emission, and exciton-polariton (UPB and LPB) emission are observed. The relative gain used to record each spectrum is given to the left.

an increase in the exciton-polariton density shifts the equilibrium to enhanced formation of the (D^0,X) complex. Owing to the significantly larger localization energy of excitons on acceptors, the first mechanism of enhanced dissociation is expected to be orders of magnitude smaller for (A^0,X) PL, whereas the second process will be similar. Furthermore, the relative increase of (A^0,X) signal upon increasing P is also caused by the suppression of the competitive channel for exciton capture via neutral donors. Hence the relative increase of (A^0,X) PL seen in Figure 10.1 can be understood by thermal dissociation of (D^0,X).

Now, will be considered the relationship between neutral donor concentration n_D^0

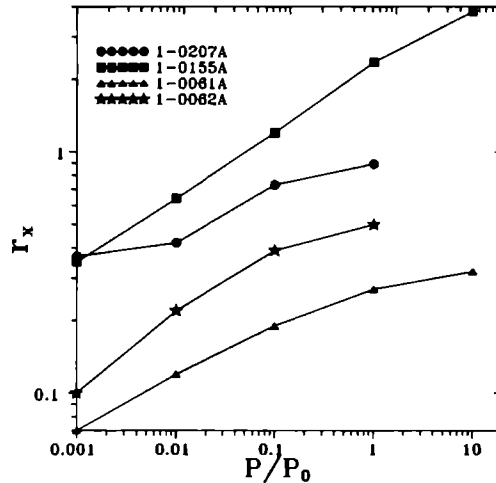


Figure 10.2 Intensity ratio r_x of the integrated (A^0, X) and (D^0, X) emissions as a function of excitation density P for the GaAs samples 1-0207A, 1-0155A, 1-0161A and 1-0162A; $P_0 = 12 \text{ W cm}^{-2}$.

and the ratio of (D^0, X) and free exciton-polariton luminescence τ_{DF} and the dependence of τ_{DF} on excitation density for both the GaAs and the InP samples. Figure 10.3 shows a considerable overlap between the (D^0, X) and the FX-polariton peaks. Although free-exciton luminescence has a Lorentzian lineshape in indirect semiconductors [20], this is no longer the case in direct band gap semiconductors where coupling between free excitons with photons of the same energy occurs: the so-called polariton effect [21,22]. This coupling results in a two-branch polariton dispersion curve: the upper (UPB) and lower (LPB) polariton branches. Both branches have an excitonlike and a photonlike component. Excitonlike LPB polaritons can be inelastically scattered to the lower energy photon-like region, and are then able to exit the crystal as photons, as illustrated in Figure 10.4. A low concentration of photons with suitably small wave vectors, however, hinders further inelastic scattering to lower energy and causes a “bottleneck” in the “knee”-region of the LPB dispersion curve. This bottleneck leads to a quasi-thermal equilibrium distribution of polaritons with energies above the “knee”.

Increasing excitation density leads to an increase of the quasi-Fermi energy (or alternatively the effective exciton-polariton temperature) [19]. In the PL spectrum this results in a red shift of LPB emission and a stronger rise in LPB than in UPB emission [19, 23]. In Figure 10.1 the red shift of LPB can be clearly observed. Recently, Aaviksoo *et al.* [9] showed that electrons that were created by above band gap excitation scattered low energy polaritons into states with higher energies, thereby increasing the population above

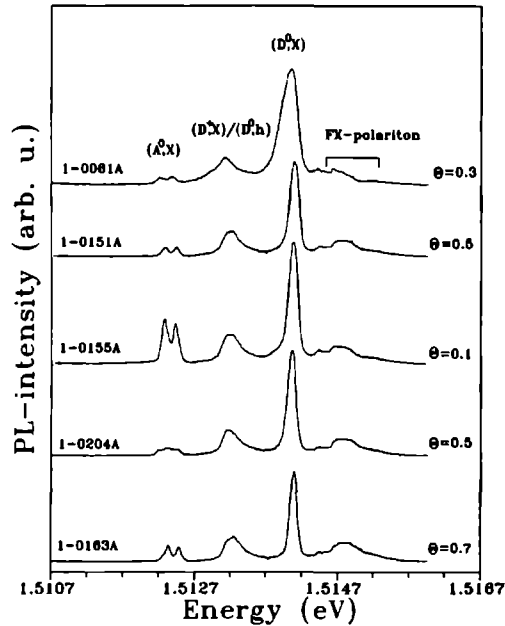


Figure 10.3 A selection of PL spectra corresponding to GaAs epilayers of varying purity presented in descending order of n_D^0 . The same units of PL intensity were used; compensation ratios are given to the right.

the “knee”. In the case of excitation below the band gap no such polariton heating occurs. As already mentioned, we used below-band-gap excitation at low excitation densities in the GaAs samples to minimize the above-knee polariton distribution. In spite of the fact that the polariton luminescence is more complex than that of free excitons, a fit using a Lorentzian line shape, as also used by Steiner *et al.* [8], gave a good description of the polariton PL at low excitation densities, as can be seen in Figure 10.5. Hence this fitting procedure was used to determine the polariton contribution to the spectrum. The fit was subtracted from the spectrum after which the intensity of the (D^0, X) PL was calculated by numerical integration. Figure 10.5A shows the spectrum of the GaAs sample 1-0163A and the fit which, in Figure 10.5B, has been subtracted from the spectrum. At the high-energy side the latter figure still shows a fraction of the above-knee polariton distribution, whereas rotational states of the donor-bound exciton, labeled $(D^0, X)_{rot}$ [24], are the remainders in the low-energy polariton region.

An important point to note is that the polariton PL reflects both the flux of polaritons reaching the surface and the probability that these polaritons exit the sample as photons (as mentioned above). This probability depends on the surface conditions: surface damage

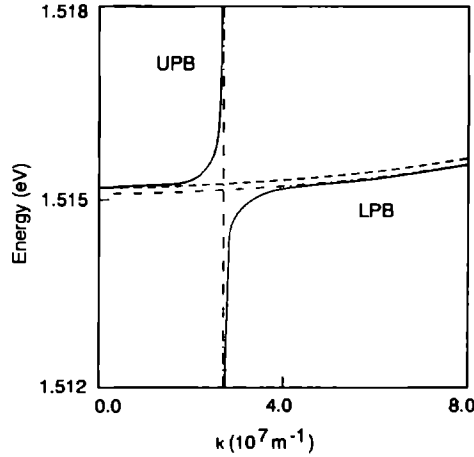


Figure 10.4 The polariton dispersion curves for GaAs calculated using the parameters that are summarized in Ref.[28]. The upper (UPB) and lower (LPB) polaron branches are labelled. Dashed lines indicate the unperturbed exciton and photon dispersion curves.

decreases the polariton PL whereas surface passivation leads to an increase [25]. Because our samples were all grown in the same reactor under the same conditions and have not been subject to any surface treatments such as etching, annealing or passivation, we do not expect that surface conditions lead to significant variations in the polariton PL in our samples.

Finally, the effect of defects on the exciton spectrum will be discussed. Szafraniek *et al.* [14] showed that a large concentration of the “A”-defect, which is accompanied by the “g”-defect bound exciton at 1.5112 eV, reduces the (D^0, X) PL and changes the polariton doublet structure into a singlet structure. This “A”-defect is commonly observed in samples grown by molecular-beam epitaxy (MBE) under conditions of slow growth rates (see Ref.[14] and references therein). In our MOVPE epilayers no detectable “g”-emission was observed (see *e.g.* Figure 10.3); therefore, an influence on the exciton spectrum can be ruled out.

Figure 10.6 shows the ratio $\tau_{DF} = I(D^0, X)/I(FX)$ as a function of neutral donor concentration n_D^0 for the GaAs samples in the two cases $P = 80$ and 320 mW cm^{-2} . Owing to the high efficiency of photoneutralization almost all donors are neutralized such that $n_D^0 \approx n_D = n_{\mathcal{N}}/(1 - \Theta)$. The τ_{DF} is seen to decrease if n_D^0 decreases. From this figure and the fact that the origin should always be a part of the relationship for samples with compensation ratios ≤ 1 , it is clear that τ_{DF} increases sublinearly with increasing n_D^0 . The exact functional relationship is not known, however; the broken curve

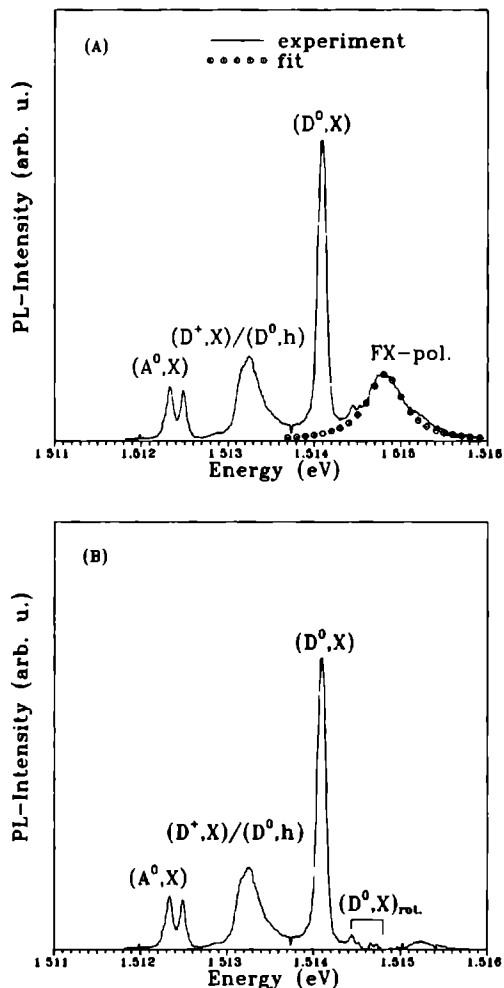


Figure 10.5 (A) Exciton luminescence of the GaAs sample 1-0163A and the Lorentzian fit (• • •) of the FX-LPB line, (B) spectrum after subtraction of the fit.

in Figure 10.6 is therefore only meant to guide the eye. The τ_{DF} values of the depleted GaAs samples 1-0209A, 1-0210A and 1-0212A were 0.72, 0.77 and 0.93, respectively. These values are shown by arrows at the vertical axis in Figure 10.6. In the case of these depleted samples no quantitative reference could be made to Hall measurements.

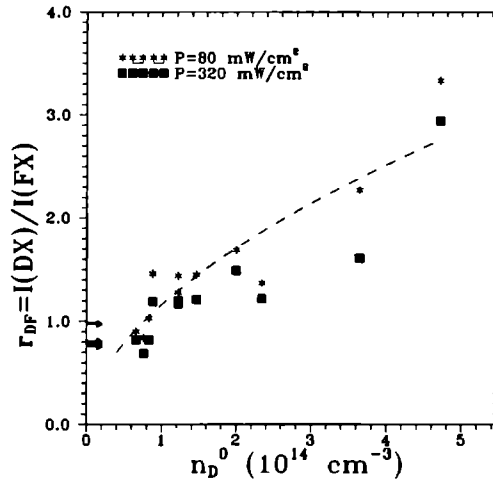


Figure 10.6 Intensity ratios $r_{DF} = I(D^0,X)/I(FX)$ as a function of n_D^0 for the GaAs samples, recorded at $P = 80 \text{ mW/cm}^2$ and 320 mW/cm^2 . The broken curve is a guide to the eye for the lowest P data points. The r_{DF} values of the depleted samples are given by arrows on the vertical axis; see the text for their values.

However, if the observed relationship between r_{DF} and n_D^0 holds, r_{DF} can be used as an indirect quantitative measure of n_D^0 in this range. This would yield values which fit well in the $n < 10^{14} \text{ cm}^{-3}$ regime for these three samples. The relationship is also of use for quantitative characterization of thinner epilayers than those studied here, since in these thin epilayers total depletion occurs at higher impurity concentrations.

The explanation of the observed behaviour in Figure 10.6 is not as straightforward as in Si. In that case, no polariton effect is present and the phonon-assisted FX luminescence accurately reflects the number and momentum distribution of free excitons in the bulk of the sample, therefore resulting in a linear relationship between r_{DF} and n_D^0 [26]. For the interpretation of the results presented in Figure 10.6 kinetic processes of the polariton PL have to be included.

First, it is known that the energy relaxation rate of polaritons in samples with lower impurity concentrations is decreased as a result of decreasing inelastic impurity scattering [9]. Secondly, Gross *et al.* [27] showed that the exciton trapping probability decreases with increasing polariton energy. Therefore, upon decreasing n_D^0 the decrease in inelastic impurity scattering leads to a shift of the polariton distribution towards higher energy. The high-energy polaritons have a smaller probability of being trapped by neutral donors, which explains the deviations from the linear behaviour shown in Figures 10.6 and 10.8 for the GaAs and InP samples, respectively.

We now consider changes in the relationship between τ_{DF} and n_D^0 caused by variations in excitation density. Every sample shows a decrease of τ_{DF} upon increasing P ; the effect becomes most pronounced in samples with higher n_D^0 . Samples with the highest impurity concentrations have the highest effective temperature of the exciton-polariton distribution because the exciton-polariton lifetime decreases [16,28]. This exciton temperature increases if the excitation density increases, and this enhances dissociation of (D^0, X) complexes. An increase in exciton-polariton temperature has the greatest impact on (D^0, X) dissociation in samples with high n_D , which explains the observed behaviour in Figure 10.6.

Excitation below the band gap was not possible for the InP samples because of the limited tuning range of the Styryl-9 dye laser; therefore $E_l=1.525$ eV was used. The exciton luminescence efficiency of the InP samples, however, was considerably larger than that of the GaAs samples, so that we were able to use lower excitation densities in the measurements. A selection of the InP PL spectra, which were recorded at an excitation density $P = 2.4$ mW cm⁻², is shown in Figure 10.7 (n_D^0 increases from bottom to top spectrum). It can be seen that the luminescence efficiencies of all samples were comparable, and furthermore, that under these experimental conditions above-knee polariton PL is virtually absent. The peak assignment is similar to that for the GaAs samples. In comparison with the GaAs spectra the energy differences between the various exciton peaks in the InP spectra are slightly larger, so that (D^0, X) and exciton-polariton emissions are easier separated. The (A^0, X) luminescence is relatively reduced in comparison to GaAs because the carbon acceptor is essentially absent in InP epilayers grown by MOVPE [3]. We observed small residual amounts of the acceptors Zn and 'A₁' [29] in all samples. Although the compensation ratios of all samples depicted in Figure 10.7 are approximately equal, the ratio $r_x = I(A^0, X)/I(D^0, X)$ is seen to increase with increasing purity. Therefore, as for the GaAs samples, our data show no relationship between Θ and r_x .

The τ_{DF} values of the InP samples are given in Figure 10.8 for the excitation densities $P = 2.4$ and 10 mW cm⁻². The InP data show greater spread than the GaAs data in Figure 10.6. Unfortunately, samples with n_D in the region $(8 - 25) \times 10^{14}$ cm⁻³ were unavailable. The FX luminescence intensity of sample 1-0411A (see also Fig.10.8) was extremely low, and so its intensity could not be determined very accurately, therefore leading to a large uncertainty in τ_{DF} . In spite of this, a sublinear relationship between τ_{DF} and n_D^0 appears to be present for these low compensated samples similar to the case of the GaAs samples. The broken curve in Figure 10.8 is again merely meant to guide the eye.

10.4 Conclusions

The relationship between compensation ratio Θ and r_x (the intensity ratio of the neutral acceptor-bound exciton line to the neutral donor bound exciton line) as presented by Lu *et al.* [7] and Steiner *et al.* [8] was not observed in our high-resolution photoluminescence measurements on series of GaAs and InP epilayers. In contrast to their claims, r_x was

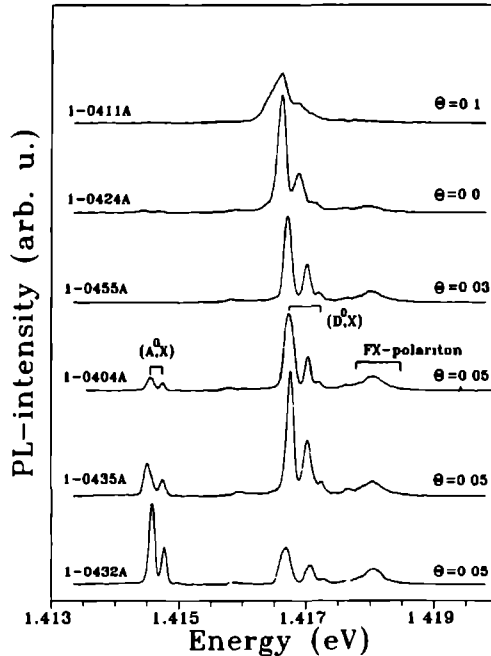


Figure 10.7 A selection of PL spectra corresponding to InP epilayers of varying purity presented in descending order of n_D^0 . The same units of PL intensity were used.

found to be very sensitive to changes in excitation density. The latter relationship can be explained by dissociation of the (D^0, X) complex.

We observed a sublinear dependence of the (D^0, X) to FX-polariton PL intensity ratio τ_{DF} on the neutral donor concentration n_D^0 in both high-purity GaAs and InP MOVPE-grown epilayers. These relationships offer the possibility of quantitative determination of the n_D^0 in high quality, nominally n -type III-V semiconductors in a non-destructive and contactless way. This technique may be particularly useful for the characterization of very pure samples, for which no Hall measurements are possible owing to large depletion fields. However, the relationships are neither applicable to samples which are known to contain large concentrations of defects nor to samples which were subject to intentional damage or passivation. The τ_{DF} values cannot be determined accurately in samples with $n_D \geq 5 \times 10^{15} \text{cm}^{-3}$, due to line broadening (which leads to enhanced (D^0, X) -FX overlap) and low FX intensities.

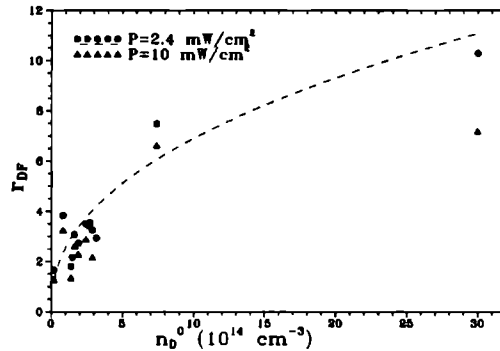


Figure 10.8 Intensity ratios $\tau_{DF} = I(D^0, X)/I(FX)$ as a function of n_D^0 for the InP samples, recorded at two excitation densities: $P = 2.4 \text{ mW/cm}^2$ and $P = 10 \text{ mW/cm}^2$. The broken curve is a guide to the eye for the lowest P data points.

Acknowledgements

The authors would like to thank Billiton Precursors B.V. for providing samples and Hall data (which were obtained by EPI Ltd., Cardiff, United Kingdom). We gratefully acknowledge Sir D.M. Frigo for his critical reading of the manuscript.

References

1. T.N. Morgan, T.S. Plaskett, and G.D. Pettit, *Phys. Rev.* **180**, 845 (1969)
2. T. Kamiya and E. Wagner, *J. Appl. Phys.* **48**, 1928 (1977)
3. B.J. Skromme, G.E. Stillman, J.D. Oberstar and S.S. Chan, *J. El. Mat.* **13**, 463 (1984)
4. J. Golka, *Solid State Commun.* **28**, 401 (1978)
5. J. Golka and H. Stoll, *Solid State Commun.* **32**, 479 (1979)
6. S.B. Nam, D.W. Langer, D.L. Kingston, and M.J. Luciano, *Appl. Phys. Lett.* **31**, 652 (1977)
7. Z.H. Lu, M.C. Hanna, D.M. Szmyd, E.G. Oh, and A. Majerfeld, *Appl. Phys. Lett.* **56**, 177 (1990)
8. T.W. Steiner, Yu Zhang, M.L.W. Thewalt, M. Maciaszek and R.P. Bult, *Appl. Phys. Lett.* **56**, 647 (1990)
9. J. Aaviksoo, I. Reimand, V.V. Rossin and V.V. Travnikov, *Phys. Rev. B* **45**, 1473 (1992)
10. D. Lancefield, A.R. Adams and M.A. Fisher, *J. Appl. Phys.* **62**, 2342 (1987)
11. The papers of Walukiewicz [12,13], which are conventionally used to determine the compensation ratio Θ from n_{77} and μ_{77} , did not yield realistic values (*i.e.* $\Theta < 0$) for

our high-purity InP samples, in contrast to the relationships reported by Lancefield *et al.* [10], who included additional scattering mechanisms in their calculations. Therefore, the latter work was also used to determine the compensation ratios of our GaAs samples.

12. W. Walukiewicz, J. Lagowski, and H.C. Gatos, *J. Appl. Phys.* **53**, 769 (1982)
13. W. Walukiewicz, J. Lagowski, L. Jastrzebski, P. Rava, M. Lichtensteiger, C.H. Gatos and H.C. Gatos, *J. Appl. Phys.* **51**, 2659 (1980)
14. I. Szafranek, M.A. Plano, M.J. McCollum, S.A. Stockman, S.L. Jackson, K.Y. Cheng and G.E. Stillman, *J. Appl. Phys.* **68**, 741 (1990).
15. E.W. Williams and H.B. Bebb, in *Semiconductors and Semimetals*, edited by R.K. Willardson and A.C. Beer, Vol. 8 (Academic, New York, 1972), p.321.
16. C.J. Hwang, *Phys. Rev. B* **8**, 646 (1973).
17. C.J. Hwang and L.R. Dawson, *Solid State Commun.* **10**, 443 (1972).
18. C.H. Henry and K. Nassau, *Phys. Rev. B* **1**, 1628 (1970).
19. K. Aoki, T. Kinugasa and K. Yamamoto, *Phys. Lett.* **72A**, 63 (1979).
20. Y. Toyozawa, *Progr. Theor. Phys.* **20**, 53 (1958).
21. J.J. Hopfield, *Phys. Rev.* **112**, 1555 (1958).
22. T. Steiner, M.L.W. Thewalt, E.S. Koteles and J.P. Salerno, *Phys. Rev. B* **34**, 1006 (1986).
23. C. Weisbuch, *Solid State Electron.* **21**, 179 (1978).
24. W. Rühle and W. Klingenstein, *Phys. Rev. B* **18**, 7011 (1978).
25. T. Steiner, Yu Zhang, S. Charbonneau, A. Villemaire, M.L.W Thewalt, M. Maciaszek and R.P. Bult, *Can. J. Phys.* **67**, 242 (1989).
26. M. Tajima, *Appl. Phys. Lett.* **32**, 719 (1978).
27. E.F. Gross, S.A. Permogorov, V.V. Travnikov and A.V. Sel'kin, *Fiz. Tverd. Tela* **14**, 1547 (1972) [*Sov. Phys.-Solid State* **14**, 1331 (1972)].
28. W.J. Rappel, L.F. Feiner and M.F.H. Schuurmans, *Phys. Rev. B* **38**, 7874 (1988).
29. Skromme *et al.* [3] showed that the unknown acceptor 'A₁' is most likely to be attributed to Mg.

Summary

The work described in this thesis is mainly concerned with magneto-optical studies on III-V semiconductor materials. The techniques employed were selectively-pumped photoluminescence (PL) and photorefectance (PR) spectroscopy. Chapter 2 describes these techniques as well as intrinsic and extrinsic electronic states in semiconductors and the optical transitions they give rise to.

In Chapter 3 we report the observation of $2p_{0,-1}$, $2s_0$, $3d_{-1,-2}$, $3p_{-1}$ and $4f_{-3}$ structures in the “two-electron” satellite photoluminescence of excitons bound to the (hydrogenic) shallow donors Ge and Se/Sn in high-purity metalorganic vapour-phase epitaxy (MOVPE) grown GaAs. The attribution is based upon selective excitation of the different principal donor-bound-exciton (D^0, X) lines at magnetic fields of 7 T at $T=1.5$ K, combined with a careful analysis of the behaviour of the hydrogen atom in a magnetic field. The results are interpreted in terms of high-magnetic-field quantum numbers and in terms of shapes of hydrogen wavefunctions in strong magnetic fields. One of the samples used in this work is so pure that for the first time donors have been identified from the relatively broad $n=2$ two-electron satellite involving the (D^0, X) ground state at zero field. Strong indications for exciton-acoustic phonon coupling and the appearance of a new donor are found.

Chapters 4-6 deal with a magneto-optical study of two-dimensional electron gases (2DEG) without -the for PL essential- holes being confined. Chapter 4 treats high-resolution magnetophotoluminescence measurements on a GaAs- $Al_xGa_{1-x}As$ heterojunction which contains a 2DEG with two occupied subbands at zero magnetic field. A very efficient, extremely narrow band luminescence involving the 2DEG is observed above a certain critical field strength in spite of the large built-in electric field acting on the photoexcited holes. The PL peak shows pronounced magneto-oscillations in peak energy, as well as in luminescence intensity and peakwidth. The luminescence is attributed to the exciton of the second subband which hybridizes with the Landau level of the first subband in which the Fermi level resides. This many-body interaction is most efficient at odd filling factors, *i.e.*, if the Fermi level lies in the extended states. The oscillations in photon energy and full width at half maximum originate from $n_c = 1$ Landau-level crossings with the lowest $n_c = 2$ Landau level. The optical data show that the exciton of the second subband is consecutively populated and de-populated. Tilted field measurements enable the determination of the intrasubband diamagnetic shift in a parallel field $\delta E_{12}/\delta B$.

In Chapter 5 a more extensive study of this PL is reported in high-carrier-density GaAs/ $Al_xGa_{1-x}As$ single heterojunctions for two-dimensional carrier densities in the range $(6.6 - 16.2) \times 10^{15} m^{-2}$. The MPL shows magneto-oscillatory behaviour of intensity, photon energy and peak width. Furthermore, $n_c = 2$ subband recombination with light holes $X(n_c = 2, l)$ is reported. A splitting of the $X(n_c = 2, h)$ is reported at low carrier

density, which results from the separate interaction of the two spin-split states of the $n_c = 1$ Landau level in which the Fermi level resides, on the second subband. The dependence of the spectra both on excitation density and temperature, indicates strongly that PL from the $n_c = 3$ subband occurs PL originating from the 2DEG and that from the GaAs buffer layer could be distinguished by excitation below and above the GaAs band gap. In the highest-carrier-density sample evidence is found for the formation of a band of localized states between the spin components of a Landau level. Recombination occurs between the exponentially decaying tails of the photoexcited holes, which relax to the flat-band region of the GaAs.

Additional information on the 2DEG was obtained via resonant-excitation experiments. Phonon replicas of both the second subband exciton and the *unpopulated* third subband are observed. The latter very sharp replica appears if a nonequilibrium electron concentration is created in the resonantly-excited third subband. Resonant excitation also reveals the recombination of electrons in the $n_c = 2$ subband with holes located at neutral acceptors. Strong indications were found for PL of the $n_c = 1$ lowest Landau level upon resonantly exciting the $X(n_c = 2, h)$ transition in the lowest-carrier-density sample.

This magneto-optical characterization is applied to detect unintended 2DEG's in Chapter 6. We report the observation of a magneto-exciton in undoped GaAs/Al_xGa_{1-x}As-heterojunctions by PL. The exciton originates from photoexcited holes and two-dimensional electrons, which are confined in the shallow potential at the heterointerface. The observation of this exciton is particularly useful for identification of unintended 2DEG's in cases where detection by temperature-dependent Hall measurements is difficult.

A study of the ordered alloy GaInP₂ (lattice matched to GaAs) is presented in Chapter 7. So far, little was understood of its electrical and optical behaviour. We report properties of long-range ordered GaInP₂ alloys as a function of temperature by a combination of PR, PL, Hall-van der Pauw measurements and magneto-transport measurements. Below $T = 200$ K optical and transport properties are strongly influenced by a donor state which, owing to confinement in the ordered domains, has a large binding energy of 36 meV. Evidence for strong localization was obtained for $T < 30$ K: the PR spectra showed a pronounced first-derivative line shape at the same energy where PL emission occurs, the conductivity was dominated by hopping (ϵ_3) conduction, and the temperature dependence of the PL intensity was consistent with localized states. Between 30 and 70 K the dominating conduction mechanism was identified as ϵ_2 conduction via negatively charged donors - the D^- band. At 70 K, Hall data showed a changeover from ϵ_2 to band conduction. It is proposed that the origin of the inverted-S shape of PL energy as a function of temperature is connected with thermal population of the D^- band. In the entire T interval between 30 and 200 K, the PR spectra showed a complex line shape owing to the absence of carriers in the disordered regions. Above $T = 200$ K pronounced effects of cluster scattering are observed in the Hall mobility. Supported by data from PR and PL, this shows that carriers are then present in both ordered and disordered regions of the epilayer.

Results on high-quality Al_xGa_{1-x}As are presented in Chapters 8 and 9. In Chapter 8, initial results are reported of Al_xGa_{1-x}As grown by using a new precursor, alane

bis(dimethylethylamine), as the aluminum source. The advantage of this new precursor over other alane precursors used previously, is that it is liquid at room temperature. Using this new precursor instead of trimethylaluminum (TMAI), we found a reduction by a factor 6 in carbon incorporation when it was used together with trimethylgallium (TMGa), whereas a reduction by a factor 50 was found when it was used in combination with triethylgallium (TEGa). At low excitation density the linewidth of the separate donor bound exciton (D^0, X) was 2.6 meV at an Al fraction of 0.31. This is comparable with the smallest values ever reported in literature for MOVPE grown $Al_xGa_{1-x}As$ with an Al fraction higher than 0.2. This narrow linewidth indicates a very uniform aluminum composition.

Excitonic transitions were measured in $Al_xGa_{1-x}As$, grown by MOVPE, at two different alloy compositions using high-resolution PL spectroscopy in Chapter 9. The first observation is reported of an excitonic spectrum which is separated into neutral donor, ionized donor and neutral acceptor-bound exciton transitions ((D^0, X) , (D^+, X) and (A^0, X)) at an aluminum fraction higher than 20 %. A significant decrease in linewidth of the (D^0, X) peak is found by decreasing the excitation density and by decreasing the laser spot size. This means that the linewidths of the various excitonic transitions are, apart from alloy broadening, strongly dependent on both the long range Coulombic potentials of the ionized impurities in our samples, and on clustering effects. Finally, linewidths of 1.75 and 2.5 meV were measured for the (D^0, X) transition for samples with Al fractions of 0.12 and 0.244, respectively. These are the smallest values ever reported in literature for samples grown by MOVPE.

Finally, the relationship between optical and electrical measurements is central in Chapter 10. We report an investigation of the exciton PL spectra of high-purity nominally n -type GaAs and InP layers, grown by MOVPE. The results are discussed in terms of exciton-polariton kinetics. The ratio of the integrated emission intensities of neutral donor bound exciton (D^0, X) transitions and free exciton-polariton (FX) transitions $\tau_{DF} = I(D^0, X)/I(FX)$ shows a sublinear dependence upon neutral donor concentration n_D^0 deduced from 77-K Hall measurements. This relationship is particularly useful for estimating carrier concentrations in high-purity materials, which cannot be characterized by Hall measurements due to depletion.

Samenvatting

Dit proefschrift behandelt magneto-optische studies van III-V halfgeleidermaterialen. De gebruikte technieken zijn selectief-gepompte fotoluminescentie (PL) en fotoreflectie (PR) spectroscopie. Hoofdstuk 2 behandelt deze technieken evenals intrinsieke en extrinsieke elektronische toestanden in halfgeleiders en de daaraan gecorreleerde optische overgangen.

In hoofdstuk 3 wordt de aanwezigheid gerapporteerd van $2p_{0,-1}$, $2s_0$, $3d_{-1,-2}$, $3p_{-1}$ en $4f_{-3}$ structuur in "twee-electron" satelliet (TES) fotoluminescentie van excitonen gebonden aan de waterstofachtige ondiepe donoren Ge en Se/Sn in hoog-zuiver GaAs gegroeid met metaal-organische damp-fase epitaxie (MOVPE). De toekenning is gedaan op grond van selectieve excitatie van de verschillende donor-gebonden exciton (D^0, X) lijnen bij een magneetveld van 7 T en $T=1.5$ K, gecombineerd met een nauwkeurige analyse van het gedrag van het waterstof atoom in magneetveld. De resultaten zijn geïnterpreteerd in termen van quantum getallen die gelden in de hoge-veld limiet en in termen van vormen van waterstof golffuncties in sterke magneetvelden. Eén van de preparaten waarover wordt gerapporteerd is zo zuiver dat voor de eerste keer donoren konden worden geïdentificeerd uit de relatief brede $n = 2$ TES van de (D^0, X) grond toestand zonder dat daarbij een magneetveld hoefde te worden aangelegd. Verder zijn indicaties gevonden voor koppeling tussen excitonen en akoestische fononen en voor de aanwezigheid van een nieuwe donor.

Hoofdstukken 4 t/m 6 gaan over magneto-optische studies van twee-dimensionale elektronen gassen (2DEG) zonder dat hierbij, voor PL essentiële, gaten zitten opgesloten. Hoofdstuk 4 behandelt hoge-resolutie magneto-PL metingen aan een GaAs- $Al_xGa_{1-x}As$ heterojunctie die een 2DEG bevat met twee bezette subbanden bij $B=0$ T. Een zeer efficiënte, extreem smalle luminescentie piek afkomstig van het 2DEG, wordt waargenomen boven een zekere kritische waarde van het magneetveld, ondanks het feit dat een sterk intern elektrisch veld de gaten van het 2D gebied wegtrekt. Zowel de piek energie, de PL intensiteit als ook de piek breedte van de 2D overgang tonen uitgesproken magneto-oscillaties. De luminescentie wordt toegeschreven aan het exciton van de tweede subband, $X(n_c = 2, h)$, dat mengt met het Landau nivo van de eerste subband waarin het Fermi-nivo is gelegen. Deze veel-deeltjes interactie is het meest efficiënt bij oneven vulfactoren, d.w.z. als het Fermi-nivo in de uitgebreide toestanden ligt. De oscillaties in foton energie en breedte-ter-halve-hoogte ontstaan door kruisingen van $n_c = 1$ Landau nivo's met het laagste $n_c = 2$ Landau nivo. De optische data laten zien dat de tweede subband opeenvolgend wordt bevolkt en ontvolkt. Met metingen in schuin magneetveld kan de intra-subband diamagnetische verschuiving in een parallel veld, $\delta E_{12}/\delta B$, worden bepaald.

In hoofdstuk 5 is een uitgebreidere studie van bovenstaande luminescentie uitgevoerd aan hoge-dichtheids GaAs- $Al_xGa_{1-x}As$ enkele heterojuncties met 2D ladingsdrager dichtheden in het gebied $(6.6 - 16.2) \times 10^{15} \text{ m}^{-2}$. De $X(n_c = 2, h)$ PL toont in alle gevallen

magneto-oscillerend gedrag van intensiteit, foton energie en piekbreedte. Verder word $n_c = 2$ subband recombinatie met lichte gaten gerapporteerd, $X(n_c = 2, l)$. Een splitsing van het $X(n_c = 2, h)$ treedt op bij lage ladingsdrager dichtheid en is het gevolg van afzonderlijke interactie van de tweede subband met de twee spin-gesplitste toestanden van het $n_c = 1$ Landau nivo waarin het Fermi-nivo zich bevindt. De spectrale afhankelijkheid van excitatie dichtheid en temperatuur tonen het optreden van $n_c = 3$ subband PL. De PL afkomstig van het 2DEG en vanuit de GaAs bufferlaag konden van elkaar worden gescheiden door excitatie zowel onder als boven de "band-gap". In de junctie met de hoogste ladingsdrager dichtheid is bewijs gevonden voor vorming van een band van gelocaliseerde toestanden tussen de spin componenten van een $n_c = 1$ Landau nivo. Als laatste wordt aangetoond dat bij dit alles recombinatie optreedt tussen exponentieel afvallende staarten van de gefotoexciteerde gaten, die relaxeren naar het vlakke-band gebied van het GaAs.

Extra informatie over het 2DEG wordt verkregen via resonante-excitatie experimenten. Foon replica's van zowel $X(n_c = 2, h)$ als ook van de onbezette derde subband zijn waargenomen. Het laatstgenoemde, zeer scherpe fonon replica treedt op als een niet-evenwichts electronen concentratie wordt gecreëerd in de resonant geëxciteerde derde subband. Met resonante excitatie wordt verder ook recombinatie waargenomen van electronen in de $n_c = 2$ subband met gaten, gelocaliseerd bij neutrale acceptoren. In de heterojunctie met de laagste electronen dichtheid zijn sterke aanwijzingen gevonden voor PL van het laagste Landau nivo van de $n_c = 1$ subband wanneer de $X(n_c = 2, h)$ overgang werd aangeslagen.

Deze magneto-optische techniek is in hoofdstuk 6 toegepast om de aanwezigheid van niet-opzettelijk gemaakt 2DEG's aan te tonen. In ongedoteerde GaAs-Al_xGa_{1-x}As heterojuncties wordt met PL een magneto-exciton gedetecteerd dat bestaat uit gefotoexciteerde gaten en twee-dimensionale electronen, die zich in een ondiepe potentiaalput aan het grensvlak bevinden. De observatie van dit exciton is m.n. van belang voor de detectie van onbedoelde 2DEG's in gevallen waarin dit met temperatuur-afhankelijke Hall metingen moeilijk of zelfs onmogelijk is.

In hoofdstuk 7 wordt een studie gepresenteerd van geordend GaInP₂, waarvan de roosterconstante gelijk is aan die van GaAs. Tot nu toe was weinig begrepen van het elektrische en optische gedrag van deze halfgeleider. Wij rapporteren hier eigenschappen van sterk-geordend GaInP₂ door combinatie van temperatuur-afhankelijke PR, PL, Hall- en Pauw metingen en magneto-transport metingen. Beneden $T=200$ K worden optische en transport eigenschappen sterk beïnvloed door een donor toestand die, a.g.v. opsluiting in de geordende domeinen, een zeer grote bindingsenergie van 36 meV heeft. Bewijs voor sterke localisatie is verkregen wanneer $T < 30$ K: de PR spectra toonden een duidelijke eerste-afgeleide lijnvorm bij dezelfde energie waar PL emissie optreedt; de geleiding wordt bepaald door hopping (ϵ_3) geleiding en de temperatuur-afhankelijkheid van de PL intensiteit wordt consistent beschreven door een formule die geldt voor gelocaliseerde toestanden.

Tussen 30 en 70 K is het dominante geleidingsmechanisme geïdentificeerd als ϵ_2 geleiding via negatief geladen donoren: de D^- band. Bij 70 K lieten Hall data een

overgang van ϵ_2 - naar bandgeleiding zien. Dit alles leidt tot de veronderstelling dat de oorsprong van de omgekeerde-S vorm van PL energie versus temperatuur ontstaat door thermische bevolking van de D^- band. In het gehele T interval van 30 tot 200 K lieten de PR spectra een complexe lijnvorm zien die ontstaat door afwezigheid van ladingsdragers in de ongeordende gebieden. Boven $T = 200$ K worden uitgesproken effecten van verstrooiing aan de geordende clusters waargenomen in de Hall mobiliteit. Gesteund door data van PR en PL, toont dit aan dat ladingsdragers dan aanwezig zijn in zowel de geordende als de ongeordende gebieden van de epitaxiale laag.

Resultaten aan $\text{Al}_x\text{Ga}_{1-x}\text{As}$ van hoge kwaliteit worden gegeven in hoofdstukken 8 en 9. In hoofdstuk 8 worden de eerste gegevens gerapporteerd van $\text{Al}_x\text{Ga}_{1-x}\text{As}$ gegroeid met een nieuwe precursor (groeigas) als aluminium bron: alaan bis(dimethylethylamine). Het grote voordeel van deze nieuwe precursor boven andere alaan precursors die voorheen zijn gebruikt, is dat het vloeibaar is bij kamertemperatuur. Door deze nieuwe precursor te gebruiken i.p.v. trimethylaluminium (TMAI) vonden wij een afname in koolstof-inbouw met een factor 6 wanneer het werd gebruikt in combinatie met trimethylgallium (TMGa) en zelfs een afname met een factor 50 wanneer het werd gecombineerd met triethylgallium (TEGa). Bij lage excitatiedichtheid was de lijnbreedte van het afzonderlijke donor-gebonden exciton, (D^0, X) , 2.6 meV bij een Al-fractie van 0.31. Dit is vergelijkbaar met de kleinste waarden ooit gerapporteerd in de literatuur voor MOVPE gegroeid $\text{Al}_x\text{Ga}_{1-x}\text{As}$ met Al-fracties hoger dan 0.2. Dit duidt op een zeer uniforme Al-compositie. In hoofdstuk 9 zijn exciton overgangen gemeten in MOVPE-gegroeid $\text{Al}_x\text{Ga}_{1-x}\text{As}$ met twee verschillende Al-fracties m.b.v. hoge-resolutie PL spectroscopie. Voor de eerste keer wordt een exciton spectrum getoond dat is opgesplitst in neutrale-donor-, geïoniseerde-donor en neutrale-acceptor gebonden exciton overgangen $((D^0, X), (D^+, X)$ en $(A^0, X))$ voor een Al-fractie hoger dan 20%. Een significante afname in lijnbreedte van de (D^0, X) piek wordt gevonden bij afname van zowel excitatie dichtheid als spot grootte. Dit betekent dat de lijnbreedtes van de afzonderlijke exciton overgangen naast "meng-verbreding", sterk afhangen van zowel de lange-afstands Coulomb potentialen van de geïoniseerde onzuiverheden als van cluster effecten. Voor $\text{Al}_x\text{Ga}_{1-x}\text{As}$ met $x=0.12$ en 0.244 werden respectievelijk lijnbreedtes van 1.75 en 2.5 meV gemeten voor de (D^0, X) overgang. Dit zijn de kleinste waarden ooit gerapporteerd voor $\text{Al}_x\text{Ga}_{1-x}\text{As}$ epilagen gegroeid met MOVPE.

Als laatste staat, in hoofdstuk 10, de relatie tussen optische en elektrische metingen centraal. Wij rapporteren een onderzoek van de exciton PL spectra van hoog-zuivere, nominaal n -type GaAs en InP lagen gegroeid met MOVPE. De resultaten worden besproken in termen van exciton-polariton kinetiek. De verhouding van de geïntegreerde emissie intensiteit van (D^0, X) overgangen en vrij-exciton polariton (FX) overgangen $\tau_{DF} = I(D^0, X)/I(FX)$ toont een sublineaire afhankelijkheid van de neutrale donor concentratie, die werd bepaald via 77-K Hall metingen. De relatie is bijzonder bruikbaar om ladingsdrager concentraties af te schatten in extreem-zuivere materialen die, a.g.v. depletie, niet kunnen worden vastgesteld met Hall metingen.

List of Publications

1. F.A.J.M. Driessen, H.G.M. Lochs, S.M. Olsthoorn, and L.J. Giling, *An analysis of the two electron satellite spectrum of GaAs in high magnetic fields*, J. Appl. Phys. **69**, 906-912 (1991).
2. F.A.J.M. Driessen, S.M. Olsthoorn, H.G.M. Lochs, and L.J. Giling, *Stress effects in GaAs-AlGaAs heterojunctions studied by magnetophotoluminescence*, in *Proceedings of the 20th International Conference on the Physics of Semiconductors*, edited by E.M. Anastassakis and J.D. Joannopoulos (World Scientific, Singapore, 1990), 1301-1304.
3. F.A.J.M. Driessen, S.M. Olsthoorn, T.T.J.M. Berendschot, H.F. Pen, L.J. Giling, G.A.C. Jones, D.A Ritchie, and J.E.F. Frost, *Influence of magnetic fields on an extremely narrow exciton line in a high-carrier-density heterojunction*, Phys. Rev. B **45**, 11823-11828 (1992).
4. F.A.J.M. Driessen, S.M. Olsthoorn, T.T.J.M. Berendschot, L.J. Giling, D.M. Frigo, G.A.C. Jones, D.A Ritchie, and J.E.F. Frost, *Fermi-edge-induced magnetophotoluminescence in high-carrier-density heterojunctions*, Phys. Rev. B. **47**, 1282-1291 (1993).
5. H.F. Pen, F.A.J.M. Driessen, S.M. Olsthoorn, and L.J. Giling, *The influence of impurity concentration on exciton photoluminescence in GaAs and InP*, Semicond. Sci. Technol. **7**, 1400-1406 (1992).
6. F.A.J.M. Driessen, S.M. Olsthoorn, G.J. Bauhuis and L.J. Giling, *Effects of confined donor states on optical and transport properties of ordered GaInP alloys*, Phys. Rev. B *submitted*.
7. G.J. Bauhuis, F.A.J.M. Driessen, S.M. Olsthoorn and L.J. Giling, *to be submitted*.
8. F.A.J.M. Driessen, S.M. Olsthoorn and L.J. Giling, *Detection of two-dimensional electron gases in undoped heterojunctions with magnetophotoluminescence*, Appl. Phys. Lett. *accepted*.
9. H.G.M. Lochs, S.M. Olsthoorn, T.P. Huijgen, F.L.M. Spijkers, F.A.J.M. Driessen, and L.J. Giling, *Photoluminescence properties of AlGaAs and an investigation of a new 1.951 eV transition*, J.Phys.: Condens. Matter **3**, 7179-7191 (1991).
10. S.M. Olsthoorn, F.A.J.M. Driessen, and L.J. Giling, *Photoluminescence properties of a new 1.951 eV transition in III-V semiconductors*, J. Appl. Phys. **71**, 2423-2427 (1992).
11. S.M. Olsthoorn, F.A.J.M. Driessen, L.J. Giling, D.M.Frigo, and C.J. Smit, *Photoluminescence on high-quality AlGaAs grown by metalorganic vapour-phase epitaxy*

- using *alane bis(dimethylethylamine)*, Appl. Phys. Lett. **60**, 82-84 (1992).
12. S.M. Olsthoorn, F.A.J.M. Driessen, and L.J. Giling *Excitonic photoluminescence spectra of AlGaAs grown by metalorganic vapour-phase epitaxy*, Appl. Phys. Lett. **58**, 1274-1276 (1991).
 13. S.M. Olsthoorn, F.A.J.M. Driessen, A.P.A.M. Eijkelenboom and L.J. Giling, *Photoluminescence and photoluminescence excitation spectroscopy on AlInAs*, J. Appl. Phys. *submitted*.
 14. S.M. Olsthoorn, F.A.J.M. Driessen, and L.J. Giling *Photoluminescence properties of the Al_{0.48}In_{0.52}As/InP interface and the diffusion of carriers thereto*, J. Appl. Phys. *submitted*.
 15. J.H. Wilkie, G.J.M. v Eyden, D.M. Frigo, C.J. Smit, P.J. Reuvers, S.M. Olsthoorn and F.A.J.M. Driessen, *Organometallic vapour-phase epitaxial growth of low carbon content Al_xGa_{1-x}As (x=0.2-0.6) to compare mono- and bis-dimethylethylamine alane as liquid Al precursors*, GaAs and related compounds, Japan (1992).
 16. P.F. Fontein, J.A. Kleinen, P. Hendriks, F.A.P. Blom, J.H. Wolter, H.G.M. Lochs, F.A.J.M. Driessen, L.J. Giling and C.W.J. Beenakker, *Spatially-resolved potential measurements under quantum Hall conditions by application of the linear electro-optic effect*, in *Proceedings of the 20th International Conference on the Physics of Semiconductors*, edited by E.M. Anastassakis and J.D. Joannopoulos (World Scientific, Singapore, 1990), 833-836.
 17. P.F. Fontein, J.A. Kleinen, P. Hendriks, F.A.P. Blom, J.H. Wolter, H.G.M. Lochs, F.A.J.M. Driessen, L.J. Giling and C.W.J. Beenakker, *Spatial potential distribution in GaAs-AlGaAs heterostructures under quantum Hall conditions studied with the linear electro-optic effect*, Phys. Rev. B **43**, 12090-12093 (1991).
 18. P.F. Fontein, J.A. Kleinen, P. Hendriks, F.A.P. Blom, J.H. Wolter, H.G.M. Lochs, F.A.J.M. Driessen and L.J. Giling, *The spatial potential distribution of GaAs-AlGaAs heterostructures under quantum Hall conditions studied with the linear electro-optic effect*, in *Localization and Confinement of Electrons in Semiconductors*, edited by F. Kuchar, H. Heinrich and G. Bauer, Springer series of Solid State Sciences Vol.97, pp. 162-167, (Springer, Heidelberg, 1990).
 19. L.E.C. van de Leemput, P.J.M. van Bentum, F.A.J.M. Driessen, J.W. Gerritsen, H. van Kempen, and L.W.M. Schreurs, *Morphology and surface topology of YBa₂Cu₃O_{7-x} crystals; theory and STM observations*, J. Cryst. Growth **98**, 551-560 (1989).
 20. L.E.C. van de Leemput, P.J.M. van Bentum, F.A.J.M. Driessen, J.W. Gerritsen, H. van Kempen, L.W.M. Schreurs, and P. Bennema, *Topography of YBa₂Cu₃O_{7-x} single crystals, spectroscopy of thin films and sintered YBa₂Cu₃O_{7-x}: theory and STM observations*, J. of Microscopy **152**, 103-115 (1988).

Curriculum Vitae

Frank A.J.M. Driessen
geboren op 13 april 1966 te Groesbeek

- 1978-1984 : VWO, Nijmeegse Scholengemeenschap.
- 1984-1988 : Studie Natuurkunde aan de Katholiek Universiteit Nijmegen.
Propaedeutisch examen: 30 augustus 1985.
Doctoraal examen: 8 december 1988.
Afstudeerrichting: Vaste Stof Fysica,
Scanning Tunneling Microscopy.
- 1989-1993 : Aanstelling als A.i.O. door NOVEM op de afdeling
Experimentele Vaste Stof Fysica III van de KUN.
Thema van onderzoek: Magneto-optica aan III-V halfgeleiders.

Stellingen behorende bij het proefschrift:
Magnetophotoluminescence on III-V semiconductors:
high-purity bulk material and low dimensional systems

I

GaInP is een model halfgeleider om hopping-processen te onderzoeken.

Dit proefschrift, hoofdstuk 7 en referentie 9 hiervan.

II

De door Koteles *et al.* gegeven verklaring voor de aard van vrij-exciton recombinatie is gebaseerd op een foute analyse van fotoluminescentie spectra.

E.S. Koteles, J. Lee, J.P. Salerno, and M.O. Vassell, Phys. Rev. Lett. 55, 867 (1985).

I. Szafranek, M.A. Plano, M.J. McCollum, S.A. Stockman, S.L. Jackson, K.Y. Cheng, and G.E. Stillman, J. Appl. Phys. 68, 741 (1990).

III

De door Lu *et al.* gegeven relatie tussen compensatiegraad en verhouding in de intensiteiten van acceptor- en donor-gebonden exciton luminescentie moet sterk gewantwoord worden. Verder is het uitvoeren van het experiment bij $T = 10$ K niet logisch.

Z.H. Lu, M.C. Hanna, D.M. Szymd, E.G. Oh, and A. Majerfeld, Appl. Phys. Lett. 56, 177 (1990).

Dit proefschrift, hoofdstuk 10.

IV

Licht met een golflengte van 880 nm is zichtbaar voor de geoefende waarnemer.

Eigen waarneming.

V

Het verschil in resultaten volgend uit de fotoreflectie- fotoluminescentie metingen van Kondow en Minagawa is het gevolg van een verkeerde interpretatie van fotoreflectie spectra en niet van legeringsfluctuaties.

M. Kondow, and S. Minagawa, Appl. Phys. Lett. 54, 1760 (1989).

Dit proefschrift, hoofdstuk 7.

VI

De electronica van een Jobin-Yvon monochromator zegt ons dat er 65 seconden in een minuut zitten. Wij werken derhalve $65/60=13/12$ keer zo hard als ieder ander en hebben jaarlijks dus recht op een extra maandsalaris.

VII

De grootte van een land is omgekeerd evenredig met de belangenverstrengeling binnen de wetenschap.

VIII

De inwerkfase in een onderzoeksterrein is vergelijkbaar met het ademen van rode wijn.

